

MS  
MAT  
1047

# Development and analysis of stretched flows with nanoparticles



*By*

*Rizwan Ul Haq*

Department of Mathematics  
Quaid-i-Azam University  
Islamabad, Pakistan  
2015



# Development and analysis of stretched flows with nanoparticles



By

*Rizwan Ul Haq*

Supervised By

*Dr. Sohail Nadeem*

Department of Mathematics  
Quaid-i-Azam University  
Islamabad, Pakistan  
2015

# Development and analysis of stretched flows with nanoparticles



By  
*Rizwan Ul Haq*

*\*Dissertation Submitted in the Partial Fulfillment of the Requirements*

*for the Degree of*

DOCTOR OF PHILOSOPHY

IN

MATHEMATICS

Supervised By

*Dr. Sohail Nadeem*

Department of Mathematics

Quaid-i-Azam University

Islamabad, Pakistan

2015

# Development and analysis of stretched flows with nanoparticles

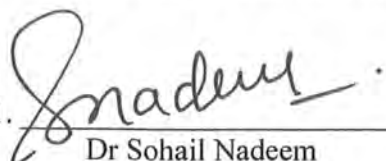
By

*Rizwan Ul Haq*

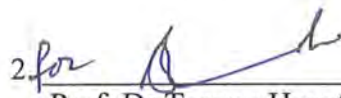
## CERTIFICATE

A THESIS SUBMITTED IN THE PARTIAL FULFILLMENT OF THE REQUIREMENTS FOR THE DEGREE OF THE DOCTOR OF PHILOSOPHY

We accept this dissertation as conforming to the required standard

1. 

Dr Sohail Nadeem  
(Supervisor)

2. 

Prof. Dr Tasawr Hayat  
(Chairman)

3. 

Prof. Dr Nazir Ahmad Mir  
(External Examiner)

4. 

Dr Muhammad Salahuddin  
(External Examiner)

**Department of Mathematics**  
**Quaid-i-Azam University**  
**Islamabad, Pakistan**  
**2015**

## *Dedication*

I dedicate this thesis to my parents because whatever I am is due to my parent's hard work, prays, and love.

I also dedicate this thesis to my respected supervisor Dr. Sohail Nadeem who always guide me during my research and impressed me by his hard working, sincerity and especially with his polite attitude.

All praise is to Allah, the Lord of the Creation, the Most Gracious and Merciful. Owner of the Day of Recompense. Who blessed us being the Ummah of His Beloved Prophet Muhammad (P.B.U.H), who blessed us with the most precious treasure of Iman (Faith). Countless Salutations, Peace and Blessings of Allah be upon the Cream of the Creation; Mercy for all Worlds; Seal of the Prophets Sayyiduna wa Mawlana Muhammadur Rasoolullah Sallallahu Alaihi wa Sallam, His Blessed Parents, His entire Family, His Progeny, His Companions and all those who Follow Him!!

I express my deepest and heart-felt gratitude to my supervisor, Dr. Sohail Nadeem for his knowledgeable discussions, valuable guidance and inexhaustible inspiration throughout my research time. His sympathetic attitude and encouragement prop up me to work harder with deep interest. Whatever I had learned and achieve today is all because of his splendid support. May Allah bless him with Long and Healthy life.

I am also grateful to the chairman, Department of Mathematics, Prof. Dr. Tasawar Hayat because he really inspires me to work hard and to follow his footsteps in research work. I also pay my special thanks to all respected teachers of mathematics departments those who morally support me during my research.

I am very thankful to my great Father and Mother. Their useful guidance helps me a lot throughout my life. May Allah give them long and healthy life and shower his blessings on them. I am thankful to my siblings: Ehsan bhai, Hafiz Fayyaz bhai, Imran Bhai and my younger sister for their prayers, encouragement and support. Special thanks to my friends Tayyab, Abbasi, Qasim, Z. H. Khan, Bilal, Sabir, Salaman, Aziz, Adeel Tahir, Sajjad, Ashfaq, Jamil, Afzal, Adnan, Rashid, Usman, Farhan, Atif, Muddasir, Malik Tariq, Haji Rabnawaz and I am sorry if someone is missing in above list. I am also thankful to my college's colleagues: Abid Majeed, Ali Raza, Shahid, Zia, Hamid, Murad, Zubair and those who always motivated me during my research.

At the end exceptional thanks to research colleagues Dr. Noreen Sher Akbar, Dr. Ehnber, Dr Noor Fadiya, Hina, Shagufta and Iqra for their moral support.

*Riswan Ul Haq*

# Contents

<b>Chapter 1</b>	<b>Introduction.....</b>	<b>4</b>
<b>Chapter 2</b>	<b>Convective heat transfer in MHD slip flow over a stretching surface in the presence of Carbon nanotubes.....</b>	<b>15</b>
	2.1 Introduction.....	15
	2.2 Mathematical formulation.....	15
	2.3 Numerical method for solution.....	19
	2.4 Result and discussion.....	20
	2.5 Concluding remarks.....	29
<b>Chapter 3</b>	<b>Thermophysical effects of carbon nanotubes on MHD flow over a stretching surface.....</b>	<b>30</b>
	3.1 Introduction.....	30
	3.2 Mathematical Model.....	30
	3.3 Numerical Procedure.....	35
	3.4 Result and discussion.....	35
	3.5 Conclusions.....	44
<b>Chapter 4</b>	<b>Three-dimensional flow of water-based nanofluid over an exponentially stretching sheet.....</b>	<b>45</b>
	4.1 Introduction.....	45
	4.2 Mathematical formulation.....	45
	4.3 Numerical Method.....	49
	4.4 Results and discussions.....	49
	4.5 Key findings.....	59

<b>Chapter 5</b>	<b>Convective heat transfer and MHD effects on Casson nanofluid flow over a stretching/shrinking Sheet.....60</b>
	5.1 Introduction.....60
	5.2 Fundamental equations of Buongiorno's Model.....61
	5.3 Mathematical model..... 61
	5.4 Numerical Technique..... 65
	5.5 Dual solutions.... ..67
	5.6 Results and discussions.....68
	5.7 Conclusion.....80
<b>Chapter 6</b>	<b>MHD three dimensional boundary layer flow of Casson nanofluid past a linearly stretching sheet with convective boundary condition..81</b>
	6.1 Introduction.....81
	6.2 Mathematical formulation..... 81
	6.3 Numerical Technique..... 85
	6.4 Results and discussions..... 86
	6.5 Final remarks..... 98
<b>Chapter 7</b>	<b>Numerical study of MHD boundary layer flow of a Maxwell fluid past a stretching sheet in the presence of nanoparticles.....99</b>
	7.1 Introduction.....99
	7.2 Problem Formulation..... 99
	7.3 Results and discussions.....102
	7.4 Closing remarks.....112
<b>Chapter 8</b>	<b>Numerical solution of Jeffrey nanofluid flow over a stretching Sheet.....113</b>
	8.1 Introduction.....113
	8.2 Problem Formulation..... 113
	8.3 Results and discussions.....116



	8.4	Concluding points.....	127
<b>Chapter 9</b>		<b>Numerical study of boundary layer flow and heat transfer of Oldroyd-B nanofluid towards a stretching sheet.....</b>	<b>128</b>
	9.1	Introduction.....	128
	9.2	Problem Formulation.....	128
	9.3	Results and discussions.....	131
	9.4	Conclusions.....	139
		<b>Bibliography.....</b>	<b>141</b>

## Chapter 1

---

### 1 Introduction

The recent development in the field of science and technology, nanotechnology has proven to be more moderate and beneficial option as an application to the following fields: electronics, fuel cells, batteries, solar cells, space, fuels, better air quality, medicine, food, cleaner water, chemical sensors, sporting goods and fabric. In the view of all these aspects and applications there is an important field known as nanofluid which has contributed significantly due to their enhanced thermal performance, potential benefits and applications in several important fields such as microelectronics, transportation, microfluidics, manufacturing, medical, saving in energy; all these aspects are reducing process time and raising thermal rating as well as lengthening the life span of equipment and so on. There are several countries around the globe that facilitate research centers for the development sake of nanofluid and heat transfer process. Recently, Choi [1] presented an article in which he declared that there is an exponential rise in the Science Citation Index (SCI) production as it is found that research scope of nanofluid has now, more than ever, the fastest growing rates in scientific papers in nanoscale science and technology.

There is an extensive range of industrial processes in which enhancement and transfer of heat energy is most commonly use at any industrial level. In fact it is a major task where heat must be removed, added, or transfer of process stream from one to another place and it has become an industrial necessity. So this processes required a huge source of energy to handle the process of fluid's heating/cooling and the transfer of heat.

The improvement in the progress of high thermal system to enhance its thermal conductivity and heat transfer rate has become a common issue. A vast amount of research has been accomplished to achieve the better heat transfer performance for its industrial applications. According to all this theories and research pretend that better heat transfer processes has a significant demand for advance technologies to enhance the heat transfer process.

There are several methods to improve the heat transfer efficiency. One of the ways to improve the efficiency of heat transfer is by increasing the thermal conductivity of the working fluid. Since very commonly used heat transfer base fluids such as water, engine oil and ethylene glycol have comparatively low thermal conductivities as compared to the thermal conductivity of solids. So those solids having high thermal conductivity can be used to enhance the thermal conductivity of the commonly used base fluid by incorporating very small solid particles to that fluid. This tiny solid particle is known as "nanoparticle" which ranges from 1-100nm in diameter and structure varies according to shape and size. The homogenous mixture of the base fluid and nanoparticle is known as "nanofluid". Main vision of incorporating the nanoparticles within the base fluid to enhance the thermal conductivity is introduced by Choi [2] in 1995. Before the development of nanofluids, it was found that heat transfer would be excellent but at the cost of higher pumping power. Through this vision Choi concluded that an effect of thermal conductivity of nanofluid is much better than highly cost pumping power for heat transfer. So the vision is not only beneficial for high thermal system but somehow it is cheap economically. Nanoparticles are created from different materials, such as oxide ceramics ( $Al_2O_3$ ,  $CuO$ ), metal nitrides ( $AlN$ ,  $SiN$ ), carbide ceramics ( $Sic$ ,  $Tic$ ), metals ( $Cu$ ,  $Ag$ ,  $Au$ ), carbons in various (e.g., diamond, graphite, carbon nanotubes, fullerene) and functionalized nanoparticles. Cheng [3] discussed the brief concept of nanofluid with heat transfer and the effects of thermal conductivity

of various materials like carbon, metallic solids, non-metallic solids, metallic liquids and many others.

The suspension of nanoparticles within the base fluid is not enough to enhance the thermal conductivity of base fluid so it is important to analyze the influence of shape and size of the particle within the base fluid. According to recent research of Elena et al. [4] in which they demonstrated the effect of particle shapes for thermal conductivity enhancement. They presented a comparison through performance of thermal conductivity among five different shapes of the particles namely: spheres shape particles, bricks shape particles, cylinders shape particle, platelets shape particles and blades shape particles. Through this study it is concluded that particle shape is like blades have higher thermal conductivity as compare to rest of the shapes. Apart of particles shape effects, contributions of nanoparticles materials also have dominant effects to enhance the thermal conductivity of base fluid. According to latest study of Murshed et al. [5], carbon nanotubes (CNT) provide round about six times better thermal conductivity as compared to other materials at the room temperature. The CNT are allotropes of carbon with a cylindrical nanostructure. There are three main characteristics of CNT namely single wall carbon nanotubes (SWCNT), double wall carbon nanotubes (DWCNT) and multiple-wall carbon nanotubes (MWCNT).

Currently there is no reliable theory to predict the anomalous thermal conductivity of nanofluids. From the experimental results of many researchers, it is known that the thermal conductivity of nanofluids depend on parameters including the thermal conductivities of base fluid and nanoparticles, the volume fraction, the surface area, shape of the nanoparticles and the temperature. There are no theoretical formulas currently available to predict the thermal

conductivity of nanofluids satisfactorily but here we have very common used expression for effective thermal conductivity:

**Table 1.1: Analytical models on effective thermal conductivity of nanofluids.**

Investigator	Expressions ( $k_{eff} / k_b$ )	Remarks
Maxwell [6]	$\frac{k_p + 2k_b + 2\phi(k_p - k_b)}{k_p + 2k_b - \phi(k_p - k_b)}$	relates the thermal conductivity of spherical particle base fluid and solid volume fraction
Hamilton and Crosser [7]	$\frac{k_p + (n-1)k_b - (n-1)(k_p - k_b)\phi}{k_p + (n-1)k_b + (k_p - k_b)\phi}$	For non-spherical particles, $k_p / k_b > 100$ , $n$ is an realistic spherical shape segment ( $n = 3 / \psi$ , $\psi$ is the sphericity)
Jeffrey [8]	$1 + 3\beta\phi + \phi^2 \left( \frac{3\beta^2 + \frac{3\beta^2}{4} + \frac{9\beta^3}{16}}{\frac{\alpha + 2}{2\alpha + 3} + \frac{3\beta^4}{2^6} + \dots} \right)$	Accurate to order $\phi^2$ ; high-order terms represent pair interactions of randomly dispersed spheres
Davis [9]	$1 + \frac{3(\alpha - 1)}{(\alpha + 2) - (\alpha - 1)\phi} \left( \frac{\phi + f(\alpha)\phi^2}{+O(\phi^3)} \right)$	1) Accurate to order $\phi^2$ ; high-order terms represent pair interactions of randomly dispersed spheres 2) $f(\alpha) = 2.50$ for $\alpha = 10$ ; $f(\alpha) = 0.50$ for $\alpha = \infty$ ;
Xue [10]	$\frac{1 - \phi + 2\phi \frac{k_{CNT}}{k_{CNT} - k_f} \ln \frac{k_{CNT} + k_f}{2k_f}}{1 - \phi + 2\phi \frac{k_f}{k_{CNT} - k_f} \ln \frac{k_{CNT} + k_f}{2k_f}}$	For CNTs-based nanofluids and including the axial ratio and the space distribution

Recently, Buongiorno [11] presented different approach to analyze the effects of nanoparticle dispersion with in the base fluid. Before presenting his model, numerous authors have attempted to improve convective transport models for nanofluids with two different ways

namely; Homogeneous flow models and Dispersion models. But the homogenous flow models are in conflict with the experimental observation. So as dispersion models are concerned, heat transfer enhancement from nanoparticle dispersion is completely negligible in nanofluids. In the view of Buongiorno's approach the effect of the nanoparticle/base-fluid, relative velocity is defined more mechanistically than in the dispersion models. Despite of slip mechanisms introduced in the literature Buongiorno proposed seven foremost slip mechanisms named as: inertia, Brownian diffusion, thermophoresis, diffusiophoresis, Magnus effect, fluid drainage and gravity settling. So constructing the governing equations for nanofluids, the major concern was to complete the transport model for nanofluids. It is important to note that all these effects are dominant for turbulence. However, in the absence of turbulent effects (in the laminar sublayer near the wall), the contribution of Brownian diffusion and thermophoresis effects are more important as slip mechanisms, while the gravitational effects may also be negligible. So according to the Buongiorno model, the constitutive equations are based on two major effects named as; Brownian motion and thermophoresis.

The interest in the boundary layer flow over a stretching surface for both Newtonian and non-Newtonian fluids is increasing substantially due to the large number of practical applications in industrial and manufacturing processes. Examples of such applications are drilling muds, polymer processing industries, environmental pollution, biological process, aerodynamic extrusion of plastic sheets, glass fiber production of the boundary layer along a liquid film and condensation process, plastic polymers, optical fibers, hot rolling paper production, metal spinning, cooling of metallic plates in cooling baths and many others fields. In the year of (1961), Sakiadis [12] was the first who discussed the boundary layer flow over a stretching surface. He governs the laminar boundary layer behavior over a moving continuous flat surface

and determines the numerical solution for the boundary layer equation. Experimental and analytical behavior of this problem was completed by Tsou et al. [13]. They showed that such a flow is physically possible by confirming the data from Sakiadis. Crane [14] extended the work of Sakiadis for both linear and exponentially stretching sheet. He discussed the problem of steady two dimensional boundary layer flow of an incompressible and viscous fluid caused by a stretching sheet whose velocity varies linearly with the distance from a fixed point on the sheet. Free convection on a vertical stretching surface was discussed by Wang [15]. Heat transfer analysis over an exponentially stretching continuous surface with suction was presented by Elbashbeshy [16]. He calculated similarity solutions for the laminar boundary layer equations describing heat and flow in a quiescent fluid driven by an exponentially stretching surface subject to suction and evaluated his problem numerically. Viscoelastic MHD flow in the presence of heat and mass transfer over a stretching sheet with dissipation of energy and stress work was discussed by Khan et al. [17]. Later on many authors extend this concept of stretching surfaces for both Newtonian and non-Newtonian fluids [18-30].

Initially, Khanafer et al. [31] presented the heat transfer enhancement in a two-dimensional flow utilizing nanofluids. The Cheng-Minkowycz problem for convection past along with the vertical plate through porous medium filled by a nanofluid is studied analytically by Nield and Kuznetsov [32]. They used the nanofluid model with the effects of Brownian motion and thermophoresis parameter. For the porous medium, the Darcy model is employed. The convection problem for boundary layer flow phenomena of a nanofluid along with the vertical plate has been studied analytically by Kuznetsov and Nield [33]. They found that the reduced Nusselt number is a decreasing function of thermophoresis parameter and Brownian motion parameter. Later on, Khan and Pop [34] discussed the steady boundary layer flow, heat

transfer and nanoparticle fraction over a stretching surface for a nanofluid. Makinde and Aziz [35] studied the influence of convective boundary condition on the flow of nanofluid past a stretching surface. After this Nadeem and Lee [36] presented the concept of nanofluid over an exponentially stretching surface. Recently, Khan et al. [37] presented an article related to fluid flow and heat transfer of carbon nanotubes along a flat plate with Navier slip boundary. More recently various authors have discussed various effects of nanoparticles for boundary layer flow over a stretching/shrinking surface [38-50].

In the understanding of all the above literature, main emphasis of the current thesis is to examine the Newtonian and non-Newtonian fluid flow over a stretched surface in the presence of nanoparticles. Throughout the analysis, all the mathematical models are constructed in the form of boundary value problem (BVP) for nanofluid flow over a stretched surface. To determine the solution of the coupled nonlinear ordinary differential equations, we first convert boundary value problem (BVP) into the initial value problem using shooting technique and then Runge-Kutta-Fehlberg method is applied to obtain the initial guesses. The detail description of this Runge-Kutta method along with the shooting technique can be found in [51-56] and the stability analyses of this method are mentioned in [57-60]. The thesis is divided into nine chapters in which first chapter consist of brief literature survey and other eight chapters are described as:

**Chapter 2** is devoted for the analysis of heat transfer rate for three commonly used base fluids (water, engine oil and ethylene glycol) in the presence of Single wall carbon nanotubes (SWCNT) and multiple wall carbon nanotubes (MWCNT), when the fluid is flowing over a two dimensional stretching surface. The viscous dissipation and magnetic field effects are also incorporated in the present phenomena. Slip effects are also considered at the upper surface of the wall while convective boundary conditions are considered at the lower surface of the wall.



The mathematical model of the problem is built in the form of partial differential equations which are reduced into the system of coupled ordinary differential equations through similarity transformations. These set of differential equations are tackled numerically and finally physical behavior for both SWCNT and MWCNT are shown graphically for each velocity, temperature, skin friction and local Nusselt numbers. Conclusion have been developed and it is found that engine oil-based SWCNT provides the better heat transfer rate as compared to the rest of the mixtures. **This chapter is published in: Physica B: Condensed Matter, Vol 457, pp. 40-47, (2015).**

**Chapter 3** is the further generalization of previous chapter. In this chapter, problem is model for three dimensional flow over a linear stretching surface in the presence of CNTs but the effects of slip and viscus dissipation are negligible. Moreover, we have made comparison among the effective thermal conductivity proposed by: Xue [10], Maxwell [6] and Hamilton & Crosser [7]. The dimensionless velocity and shear stress are obtained in both directions. The dimensionless heat transfer is determined on the surface and it is found that Xue model provides the higher heat transfer rate as compare to other two models. **These observations have been published in: Physica E: Low-dimensional Systems and Nanostructures, Vol. 63, pp. 215-222, (2014).**

In **Chapter 4**, results are investigated for the water based flow over a three dimensional exponential stretching surface in the presence of metallic particles. Effective thermal conductivity of three kind of metallic nanoparticles named as: copper ( $Cu$ ), alumina ( $Al_2O_3$ ) and titanium ( $TiO_2$ ) are incorporated. Three dimensional exponential type similarity transformations are applied for basic boundary layer equations for nanofluid and then transformed into the system of ordinary differential equations. Physical behavior of velocities and temperature

profiles are examined through graphs and discussed for both  $x$  –and  $y$  – directions. It is finally noticed that water-based Copper ( $Cu$ ) nanoparticle have higher thermal conductivity as compare to water- based alumina ( $Al_2O_3$ ) and titanium ( $TiO_2$ ) nanoparticles. **These results are published in: Alexandria Engineering Journal, Vol. 53(1), pp. 219-224, (2014).**

Two dimensional magnetohydrodynamic (MHD) boundary layer flow of a Casson nanofluid over an exponentially permeable shrinking sheet using Buongiorno's model are analyzed in **Chapter 5**. The convective boundary condition is also considered at the lower surface of the wall. Main emphasis of the present analysis is to discuss the two major slip mechanism presented by Buongiorno [11] named as: Brownian motion and thermophoresis for Casson fluid flow. Numerical results for velocity, temperature and nanoparticle volume concentration are presented through graphs for various values of dimensionless parameters. Effects of parameters for heat transfer at wall and nanoparticle volume concentration are also presented through graphs and tables. Results of dual nature solutions which exist for shrinking sheet is also examined. At the end, fluid flow behavior is examined through stream lines. **Results of present analysis are published in: Central European Journal of Physics, Vol. 12(12), pp. 862-871, (2014).**

**Chapter 6** deals the study of three dimensional flow of a Casson fluid in the presence of nanoparticle over a linearly stretching sheet. Here we have considered the magnetohydrodynamics (MHD) effect normal to the fluid flow and convective condition is defined at the lower surface of the sheet. Constructed mathematical model is reduced in to the set of nonlinear differential equation for BVP with the help of similarity variables. The reduced problem is then solved numerically. Variation of the reduced Nusselt and Sherwood numbers against physical parameters are presented graphically. It is found that the reduced Nusselt

number is a decreasing function and the reduced Sherwood number is an increasing function of Brownian parameter and thermophoresis parameter. **The contents of present chapter are published in: IEEE Transactions on Nanotechnology, Vol. 13, pp. 109-115, (2014).**

**Chapter 7** deals the study of two dimensional boundary-layer flow and heat transfer of Maxwell fluid past a stretching sheet. The effects of magnetohydrodynamic (MHD) and elasticity on the flow are considered. Moreover, effects of nanoparticles are also investigated within the Maxwell fluid model. Similarity transformations are defined to convert the governing nonlinear partial differential equation to ordinary differential equations. The reduced boundary layer equations of Maxwell nanofluid model are solved numerically. The effects of emerging parameters namely: Hartmann number, elastic parameter, Prandtl number, Brownian motion, thermophoresis and Lewis number on temperature and concentration profile are discussed. Interesting results are shown graphically. The skin friction coefficient, dimensionless heat transfer rate and concentration rate are also plotted against the flow control parameters. **Results of this chapter are published in: Journal of the Taiwan Institute of Chemical Engineers, Vol. 45(1), pp. 121-126, (2014).**

In **chapter 8**, Jeffrey fluid model in the presence of nanoparticles is studied numerically. Boundary layer equations are transformed into the set of coupled nonlinear ordinary differential equations with the help of similarity transformations. Results are constructed through Runge-Kutta method. Behavior of emerging parameters are presented graphically and discussed for velocity, temperature and nanoparticles volume concentration. Variation of the reduced Nusselt and Sherwood number against physical parameters are presented graphically. In conclusion section it is found that the reduced Nusselt number is a decreasing function while the reduced

Sherwood number is increasing function of Brownian parameter and thermophoresis parameter.

**This chapter is published in: Applied Nanoscience, Vol. 4(5), pp. 625-631, (2014).**

In the **chapter 9**, we have considered two-dimensional steady incompressible Oldroyd-B fluid past a stretching sheet saturated with nanoparticles. The similarity transformation, reduce the system of nonlinear partial differential equations into the system of nonlinear ordinary differential equations. The coupled governing nonlinear equations are then solved numerically. Numerical results are presented graphically to see the physical behaviors of the involved fluid parameters namely Deborah numbers, Prandtl number, Brownian motion, thermophoresis parameter and Lewis number on velocity, temperature and nanoparticle volume concentration profile are discussed. Interesting results are shown graphically. To see the validity of the present results, we have made the comparison of present results with the existing literatures through tables. **Contents of this chapter are published in: Plos One, Vol. 8 (8), pp. e69811, (2013).**

# Convective Heat Transfer in MHD Slip Flow over a Stretching Surface in the presence of Carbon nanotubes

## 2.1 Introduction

In the present chapter, thermal conductivity and viscosity of both single-wall and multiple-wall Carbon Nanotubes (CNT) within the base fluids (water, engine oil and ethylene glycol) of similar volume have been investigated when the fluid is flowing over a stretching surface. The magnetohydrodynamic (MHD) and viscous dissipation effects are also incorporated in the present phenomena. Experimental data consists of thermo-physical properties of each base fluid and CNT have been considered. The mathematical model has been constructed and by employing similarity transformation, system of partial differential equations are rehabilitated into the system of non-linear ordinary differential equations. The results of local skin friction and local Nusselt number are plotted for each base fluid by considering both Single Wall Carbon Nanotube (SWCNT) and Multiple-Wall Carbon Nanotubes (MWCNT). The behavior of fluid flow for water based-SWCNT and MWCNT are analyzed through streamlines. Concluding remarks have been developed on behalf of the whole analysis and it is found that engine oil-based CNT have higher skin friction and heat transfer rate as compared to water and ethylene glycol-based CNT.

## 2.2 Mathematical formulation

Consider two dimensional (2D) steady boundary layer flow past a stretching sheet in the presence of carbon nanotubes. It is considered that the sheet is stretched along the  $x$ -axis. Moreover, fluid is placed on the half plane  $y > 0$ . It is also considered that the sheet is stretched with the velocity  $U_w = cx$ , with  $c > 0$  (see Fig. 1). The hot base fluid without incorporating the nanoparticles effects is also fixed along with the lower surface of the wall in such a way that temperature of the hot fluid,  $T_f$  is greater than the ambient fluid temperature,  $T_\infty$ . We considered a uniform magnetic field  $B_0$  applied parallel to  $y$ -axis to access the motion of the CNT uniformly while the induced magnetic field is assumed to be negligible. The base fluids and the CNT are assumed to be in thermal equilibrium and viscous dissipation effect is also considered in the energy equation. By using the order analysis, the proposed boundary layer equations are defined as,

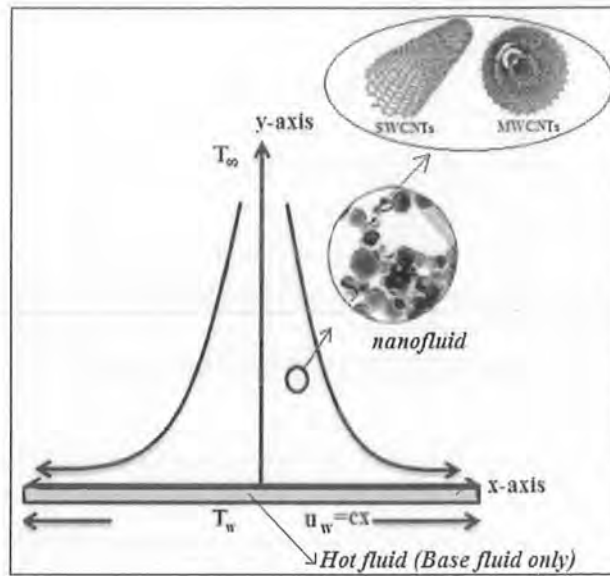


Fig 2.1: Geometry of the problem.

$$\frac{\partial u}{\partial x} + \frac{\partial v}{\partial y} = 0, \quad (2.1)$$

$$u \frac{\partial u}{\partial x} + v \frac{\partial u}{\partial y} = \nu_{nf} \frac{\partial^2 u}{\partial y^2} - \frac{\sigma B_0^2}{\rho_{nf}} u, \quad (2.2)$$

$$u \frac{\partial T}{\partial x} + v \frac{\partial T}{\partial y} = \alpha_{nf} \frac{\partial^2 T}{\partial y^2} + \frac{\nu_{nf}}{(\rho C_p)_{nf}} \left( \frac{\partial u}{\partial y} \right)^2. \quad (2.3)$$

In above expressions,  $u$  and  $v$  are the velocity components along the  $x$  and  $y$  –axes, respectively,  $T$  is the temperature of the base fluid,  $\rho_{nf}$  is the density of nanofluid,  $\mu_{nf}$  is the viscosity of nanofluid and  $\alpha_{nf}$  is the thermal diffusivity of nanofluid defined as,

$$\left. \begin{aligned} \nu_{nf} &= \frac{\mu_{nf}}{\rho_{nf}}, & \mu_{nf} &= \frac{\mu_f}{(1-\phi)^{2.5}}, \\ \alpha_{nf} &= \frac{k_{nf}}{\rho_{nf}(C_p)_{nf}}, & \rho_{nf} &= (1-\phi)\rho_f + \phi\rho_{CNT}, \\ (\rho C_p)_{nf} &= (1-\phi)(\rho C_p)_f + \phi(\rho C_p)_{CNT}, \\ \frac{k_{nf}}{k_f} &= \frac{1-\phi+2\phi\left(\frac{k_{CNT}}{k_{CNT}-k_f}\right)\ln\left(\frac{k_{CNT}+k_f}{2k_f}\right)}{1-\phi+2\phi\left(\frac{k_f}{k_{CNT}-k_f}\right)\ln\left(\frac{k_{CNT}+k_f}{2k_f}\right)}, \end{aligned} \right\} \quad (2.4)$$

where  $\mu_f$  is the viscosity of base fluid,  $\phi$  is the nanoparticle volume fraction,  $(\rho C_p)_{nf}$  is the effective heat capacity of a CNT,  $k_{nf}$  is the thermal conductivity of nanofluid,  $k_f$  and  $k_{CNT}$  are the thermal conductivities of the base fluid and CNT respectively while  $\rho_f$  and  $\rho_{CNT}$  are the thermal conductivities of the base fluid and CNT respectively. The corresponding boundary conditions are stated as

$$\left. \begin{aligned} u &= U_w(x) + \gamma \frac{\partial u}{\partial y}, \quad v = 0, \quad -k_f \frac{\partial T}{\partial y} = h_f(T_f - T) \text{ at } y = 0, \\ u &\rightarrow 0, \quad v \rightarrow 0, \quad T \rightarrow T_\infty \text{ as } y \rightarrow \infty. \end{aligned} \right\} \quad (2.5)$$

In the above expressions,  $U_w(x) = cx$  is the stretching velocity with  $c$  is a stretching constant,  $\gamma$  is the slip parameter,  $k_f$  is the thermal conductivity of the hot fluid,  $h_f$  is the convective heat transfer coefficient and  $T_f$  is the convective fluid temperature below the stretching sheet. Introducing the following similarity transformations,

$$\left. \begin{aligned} f(\eta) &= \frac{\psi}{x\sqrt{av_f}}, \quad \eta = \sqrt{\frac{c}{v_f}}y, \quad u = \frac{\partial\psi}{\partial y} = cx f'(\eta), \\ v &= -\frac{\partial\psi}{\partial x} = \sqrt{cv_f}f(\eta), \quad \theta(\eta) = \frac{T-T_\infty}{T_w-T_\infty} \end{aligned} \right\} \quad (2.6)$$

Making use of Eq. (2.6) into Eqs. (2.1)-(2.3), we get

$$f'''' + (1-\phi)^{2.5}[(1-\phi + \phi(\rho_{CNT}/\rho_f))\{ff'' - (f')^2\} - M^2 f'] = 0, \quad (2.7)$$

$$\frac{(K_{nf}/k_f)}{[1-\phi + \phi((\rho C_p)_{CNT}/(\rho C_p)_f)] Pr} \theta'' + f\theta' + \frac{Ec}{(1-\phi)^{2.5}} f'^2 = 0, \quad (2.8)$$

subject to the boundary conditions (2.5) which transformed to

$$\left. \begin{aligned} f(0) &= 0, \quad f'(0) = 1 + \frac{\beta}{(1-\phi)^{2.5}}, \quad \theta'(0) = -Bi(1 - \theta(0)) \\ f'(\eta) &\rightarrow 0, \quad \theta(\eta) \rightarrow 0 \quad \text{as } \eta \rightarrow \infty. \end{aligned} \right\} \quad (2.9)$$

Primes denote derivative with respect to  $\eta$ . Here,  $Pr = \frac{(\mu C_p)_f}{k_f}$  is the Prandtl number of base fluid,  $\beta = \gamma\sqrt{c/v_f}$  is dimensionless slip parameter and  $Bi = (h_f/k_f)\sqrt{v_f/c}$  is the Biot number. Expressions for the local skin friction coefficient  $C_f$  and the local Nusselt number  $Nu$  are

$$C_f = \frac{\tau_{wx}}{\rho_f U_w^2}, \quad Nu = \frac{xq_w}{k_f(T_w - T_\infty)}, \quad (2.10)$$



where  $\tau_{wx}$  is the surface shear stress along the  $x$ -direction and  $q_w$  is the heat flux which are given by

$$\tau_{wx} = \mu_{nf} \left( \frac{\partial u}{\partial y} \right)_{y=0}, \quad q_w = -k_{nf} \left( \frac{\partial T}{\partial y} \right)_{y=0}. \quad (2.11)$$

Reduced dimensionless expressions of Eq. (2.10) take the following form after fixing  $Re = \frac{U_w x}{\nu_f}$ ,

$$C_f Re_x^{1/2} = \frac{f''(0)}{(1-\phi)^{2.5}}, \quad (2.12)$$

$$Re_x^{-1/2} Nu = -\frac{K_{nf}}{K_f} \theta'(0). \quad (2.13)$$

### 2.3 Numerical method for solution

Equations (2.7)–(2.8) combined with the boundary conditions (2.9) are solved numerically using a shooting technique with a Runge-Kutta (RK) method. The step size is taken as  $\Delta\eta = 0.01$  and the convergence criteria is set to  $10^{-6}$ . The following system is established:

$$\left. \begin{aligned} f' &= p, \\ f'' &= p' = q, \\ f''' &= q' = -(1-\phi)^{2.5} \left\{ \left( 1 - \phi + \phi \frac{\rho_{CNT}}{\rho_f} \right) \{fq - (p)^2\} - M^2 p \right\}, \end{aligned} \right\} \quad (2.14)$$

$$\left. \begin{aligned} \theta' &= z, \\ \theta'' &= z' = -Pr \frac{\left[ 1 - \phi + \phi \left( \frac{\rho C_p}{\rho C_p} \right)_{CNT} \right]}{(K_{nf}/k_f)} \left\{ fz + \frac{Ec}{(1-\phi)^{2.5}} q^2 \right\}, \end{aligned} \right\} \quad (2.15)$$

with the initial conditions

$$f(0) = 0, \quad p(0) = 1 + \frac{\beta}{(1-\phi)^{2.5}}, \quad z(0) = -Bi(1 - \theta(0)). \quad (2.16)$$

In order to integrate Eq. (2.14) and (2.15) with initial condition (2.16), the values of  $q(0) = f''(0)$  and  $z(0) = \theta'(0)$  are required but no such values are given in the boundary conditions. The suitable guess value for  $f''(0)$  and  $\theta'(0)$  are chosen and then integration is performed. The calculated values for  $f'(\eta_{max})$  and  $\theta'(\eta_{max})$  at  $\eta_{max} = 12$  (say) are compared with the given boundary conditions as  $f'(12) = 0$  and  $\theta(12) = 0$  while the estimated values  $f''(0)$  and  $\theta'(0)$  are adjusted to give a better approximation for the solution. We take the series of values for  $f''(0)$  and  $\theta'(0)$ , and further apply the fourth order classical Runge-Kutta method with step-size  $\Delta\eta = 0.01$ . The above procedure is repeated until we get the asymptotically converged results within a tolerance level of  $10^{-6}$ .

## 2.4 Result and discussion

Before going to discuss the behavior of fluid flow and its heat transfer characteristics, it is worthwhile to provide the comparison among the base fluids (water, engine oil and ethylene glycol) in the presence of both multiple and single wall carbon nanotubes (CNT) for absolute values of reduced skin friction coefficient  $-Re_x^{1/2}C_{fx}$  and reduced Nusselt number  $Re_x^{-1/2}Nu_x$ . In fact, each base fluid and carbon nanotubes have their own thermo-physical properties (See Table. 2.1) so it will be more effective for heat transfer. Table 2.1 presents the thermo-physical properties of each base fluid and nanoparticles. Based on collective analysis, results have been drawn for reduced skin friction and reduced Nusselt number as depicted in Fig. 2.2. It is evidenced that due to more viscosity and density of engine-oil-based nanoparticle, it should have higher friction and heat transfer rate near the wall as compared to other mixtures. Moreover it can be observed that although the base fluids did not provide a difference in the skin friction coefficient and Nusselt number, CNT have dominant contribution in the nanofluid flow motion and in the heat transfer phenomenon. Table 2.2 and Table 2.3 present the numerical results of the

reduced skin friction coefficient and the reduced Nusselt number for various values of emerging parameters.

**Table 2.1:** Thermophysical properties of different base fluids and CNTs [37].

Physical properties	Base fluids			Nanoparticles	
	Water	Ethylene glycol	Engine oil	SWCNT	MWCNT
$\rho$ (kg/m <sup>3</sup> )	997	1115	884	2,600	1,600
$C_p$ (J/kg K)	4,179	2,430	1,910	425	796
$k$ (W/m K)	0.613	0.253	0.144	6,600	3,000
$Pr$	6.2	206.63	6450		

**Table 2.2:** Variation of reduced skin friction coefficient  $-C_f Re_x^{1/2}$  for various values of emerging parameter.

	$\phi \downarrow$	$\beta = 0.5$		M = 0.5	
		M=0	M=0.5	$\beta=0$	$\beta=0.5$
Water					
SWCNT's	0	0.5912	0.6495	1.1180	0.6495
	0.1	0.6680	0.7242	1.3549	0.7242
	0.2	0.7504	0.8051	1.6569	0.8051
MWCNT's	0	0.5912	0.6495	1.1180	0.6495
	0.1	0.6508	0.7106	1.3058	0.7106
	0.2	0.71808	0.7795	1.5475	0.7795
Ethylene glycol					
SWCNT's	0	0.59119	0.64951	1.1180	0.64951
	0.1	0.66342	0.72056	1.3416	0.72056
	0.2	0.74199	0.79838	1.6275	0.79838
MWCNT's	0	0.59119	0.64951	1.1180	0.6495
	0.1	0.64781	0.70823	1.2974	0.7082
	0.2	0.71208	0.77484	1.5282	0.7748
Engine Oil					

SWCNT's	0	0.5911	0.6495	1.1180	0.6495
	0.1	0.6734	0.7285	1.3708	0.7285
	0.2	0.7601	0.8129	1.6917	0.8129
MWCNT's	0	0.5911	0.6495	1.1180	0.6495
	0.1	0.6544	0.7134	1.3161	0.7134
	0.2	0.7251	0.7850	1.5705	0.7850

**Table 2.3:** Variation of reduced Nusselt number  $Re_x^{1/2} Nu_x$  for various values of emerging parameters.

	$\beta=Bi=Ec=0.5$			$M=Bi=Ec=0.5$		$\beta=M=Bi=0.5$		$\beta=M=Ec=0.5$	
	$\phi \downarrow$	$M=0$	$M=0.5$	$\beta = 0$	$\beta=0.5$	$Ec=0$	$Ec=0.5$	$Bi=\infty$	$Bi=0.5$
Water									
SWCNT 's	0	0.2703	0.2507	0.1318	0.2506	0.3701	0.2506	0.1318	0.2506
	0.1	0.6779	0.6350	0.3913	0.6351	0.8515	0.6350	0.3913	0.6351
	0.2	1.0426	0.9738	0.6067	0.9738	1.2530	0.9738	0.6067	0.9738
MWCN T's	0	0.2703	0.2507	0.1318	0.2507	0.3701	0.2506	0.1318	0.2506
	0.1	0.6562	0.6138	0.3945	0.6138	0.8186	0.6138	0.3945	0.6138
	0.2	1.0232	0.9542	0.6474	0.9542	1.2151	0.9542	0.6473	0.9542
Ethylene glycol									
SWCN T's	0	0.1892	0.1354	-0.2172	0.1354	0.4740	0.13546	2.6148	0.1354
	0.1	0.7056	0.5927	-0.4449	0.5927	1.4070	0.59273	6.3154	0.5927
	0.2	1.3868	1.2282	-0.7583	1.2283	2.4908	1.2282	4.3270	1.2282
MWCN T's	0	0.1892	0.1354	-0.2172	0.1354	0.4741	0.1354	2.6148	0.1354
	0.1	0.6873	0.5743	-0.3522	0.5742	1.3324	0.5743	6.3422	0.5742
	0.2	1.3562	1.1917	-0.4721	1.1917	2.3364	1.1917	4.5114	1.1917
Engine Oil									
SWCN T's	0	-0.002	-0.1070	-0.7248	-0.1070	0.4952	-0.1070	-11.335	-0.1070
	0.1	0.1264	-0.1273	-2.3318	-0.1273	1.5868	-0.1273	-2.1937	-0.1273
	0.2	0.3838	0.0039	-4.7355	0.0039	2.9334	0.0039	0.1579	0.0039
MWCN T's	0	-0.002	-0.1070	-0.7248	-0.1070	0.4952	-0.1070	-11.335	-0.1070
	0.1	0.1855	-0.0671	-1.9862	-0.0671	1.5017	-0.0671	-6.9427	-0.0671
	0.2	0.5516	0.1616	-6.6550	0.1616	2.7449	0.1616	6.7515	0.1616

In order to investigate the impact of emerging parameters namely: Hartmann number  $M$ , slip parameter  $\beta$ , Biot number  $Bi$  and Eckert number  $Ec$  on the absolute reduced skin friction

coefficient  $-Re_x^{1/2} C_{fx}$  and the reduced Nusselt number  $Re_x^{-1/2} Nu_x$ , graphical results are constructed (See Fig. 2.3 – 2.5). These results are only plotted for water-based CNT to analyze the variation of skin friction and heat transfer difference at the wall. Fig. 2.3 depicts the variation of local skin friction for various values of Hartmann number  $M$  and slip parameter  $\beta$  when the nanoparticle volumetric fraction is in the range of  $0 \leq \phi \leq 0.2$ . Since there is a random motion of the particles within the base fluid and for the sake of uniform motion of the particles, a constant Hartmann number  $M$  is applied normal to the fluid. Ultimately these nanoparticles move along with the magnetic field and slow down the motion of the nanofluid flow. The consequences of Hartmann number  $M$  towards the nanofluid flow can be observed through Fig 2.3(a). We can see that near the wall,  $M = 0$  provides lower friction as compared to non-zero values of MHD ( $M = 0.5, 1.0$ ). Contribution of slip effects on the skin friction coefficient are plotted in Fig. 2.3(b). As concern to the present study, it is found that slip effect reduces the friction near the wall whereas the evidence of this phenomenon can be observed through Fig. 2.3(b). It is clearly seen through Fig. 2.3(b), for no slip effects ( $\beta = 0$ ), higher friction is achieved along with the wall as compared to  $\beta = 0.5$  and  $\beta = 1$ . Finally, it is concluded that both the MHD and the slip parameter show the opposite effects in the fluid motion near the wall.

Another contribution of MHD on the local Nusselt number is plotted in Fig. 2.4(a). We can see through Fig. 2.4(a), where the local heat transfer rate is plotted for both cases when  $M = 0$  and  $M = 0.5, 1$ . It is found that for  $M = 0$ , higher heat transfer rate is attained at the wall as compared to nonzero values of Hartmann number  $M$ . It is found that simultaneous increase in the nanoparticle volume fraction and Hartmann number provide enhancement in the heat transfer rate while opposite impact on the local Nusselt number has been found for increasing values of Eckert number  $Ec$  (see Fig. 2.4(b)). Effect of slip parameter on local Nusselt number has been

plotted in Fig 2.5(a). It is found that an increase in the slip parameter leads to decreasing effect in the heat transfer rate. It is also noticed that when the effect of the slip parameter is negligible ( $\beta = 0$ ), the heat transfer rate becomes higher while non-zero values of the slip parameter ( $\beta = 0.5, 1$ ) provide decreasing effects on the heat transfer rate. Convective heat transfer coefficient  $Bi$  shows a dominant contribution on the local Nusselt number. It is found that in the case of infinitely large value of Biot number, the present model reduces to uniform temperature at the wall. It is also concluded that in the case of uniform temperature ( $Bi = \infty$ ), higher heat transfer rate is initiated as compared to the case of non-zero values of convective heat transfer parameter  $Bi$  (see Fig. 2.5(b)).

Although behavior of the fluid motion remains the same, a slight difference should appear between the base fluid (water) and the water based CNT (SWCNT, MWCNT) due to difference in densities (See Fig. 2.6). It can be observed through Fig. 2.6(a) that the stream lines of the base fluid (water) remain much closer to each other however in the case of water based CNT, behavior of the stream lines remains isolated to each other.

Variation of profiles of the velocity  $f'(\eta)$  and temperature  $\theta(\eta)$  against the emerging parameters is plotted in Figs. 2.7 and 2.8, respectively only for water based SWCNT. From Fig. 2.7, we can observe that the velocity profile increases with an increase in the nanoparticle volume fraction while in the absence of both slip and Hartmann number, the velocity profile remains higher as compared to their non-zero values. Simultaneous effects of nanoparticle volume fraction  $\phi$  along with the Hartmann number  $M$ , Eckert number  $Ec$  and Biot number  $Bi$  against the temperature profile  $\theta(\eta)$  are plotted in Fig. 2.6. For each parameter, an increase in the nanoparticle volume fraction provides enhancement to the temperature profile. Moreover, it is found that for non-zero values of both Hartmann number and Eckert number, the

temperature profile remains higher as compared to absence of both magnetic and viscous dissipation effects (see Fig. 2.8(a) and 2.8(b)). It is also highlighted that for infinitely large value of Biot number, the present model reduces to uniform wall temperature while for small values of Biot number, the results obtained signify weak convection near the wall (see Fig. 2.8(c)). Finally, the numerical values against each physical parameter are calculated for local skin friction coefficient and local Nusselt number (see Table. 2.2 and 2.3).

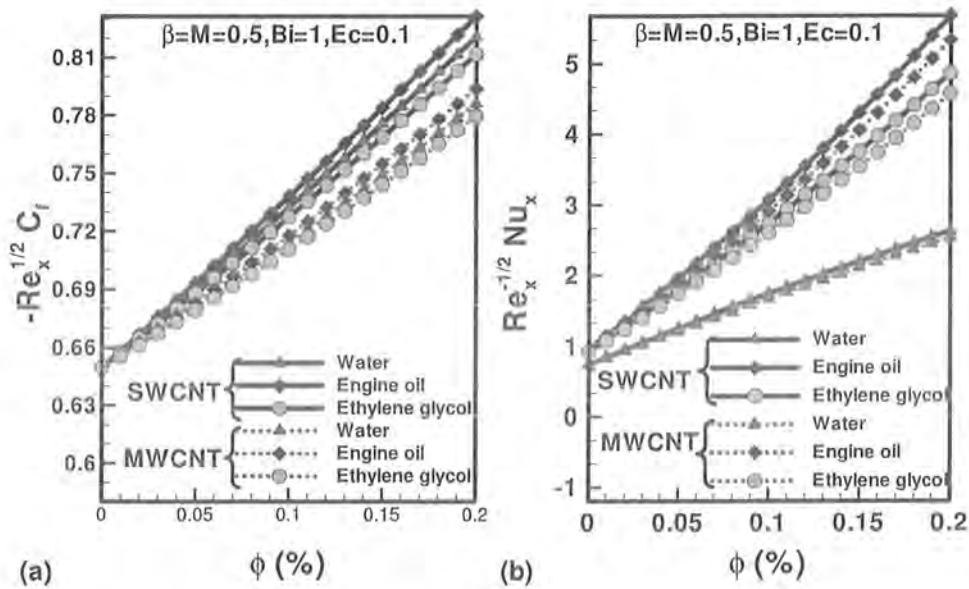


Fig 2.2: Comparison among the different base fluids for skin friction and reduced Nusselt number in the presence of SWCNTs and MWCNTs.

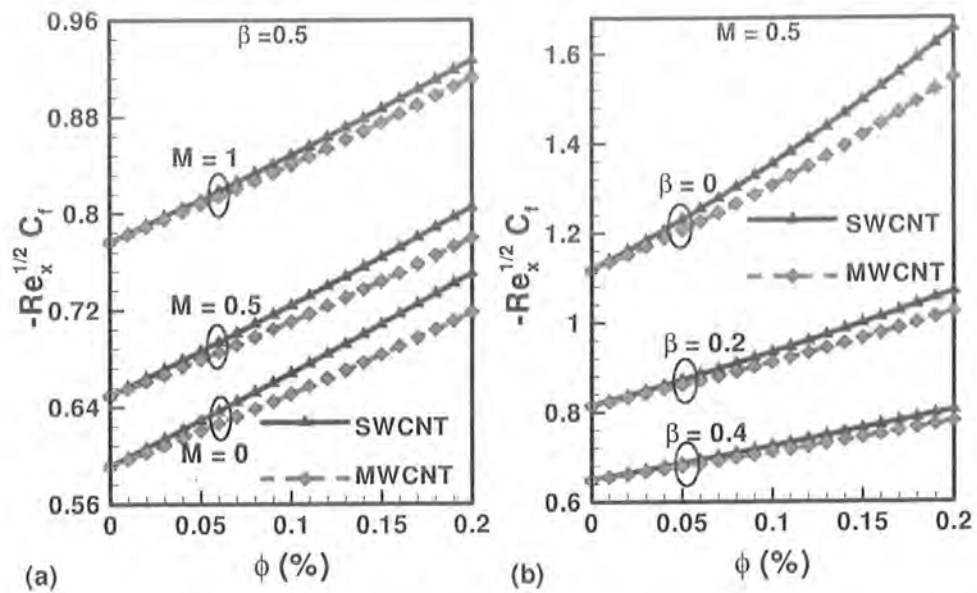


Fig 2.3: Variation of reduced skin friction coefficient for various values of  $M$  and  $\beta$  for water-based CNTs.

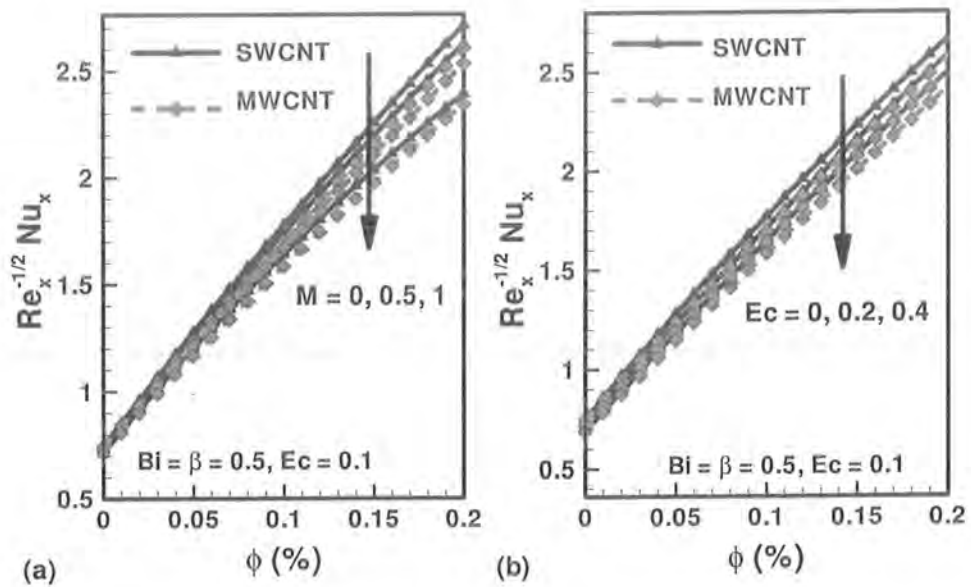


Fig 2.4: Variation of reduced Nusselt Number for various values of  $M$  and  $\text{Ec}$  for water-based CNTs.



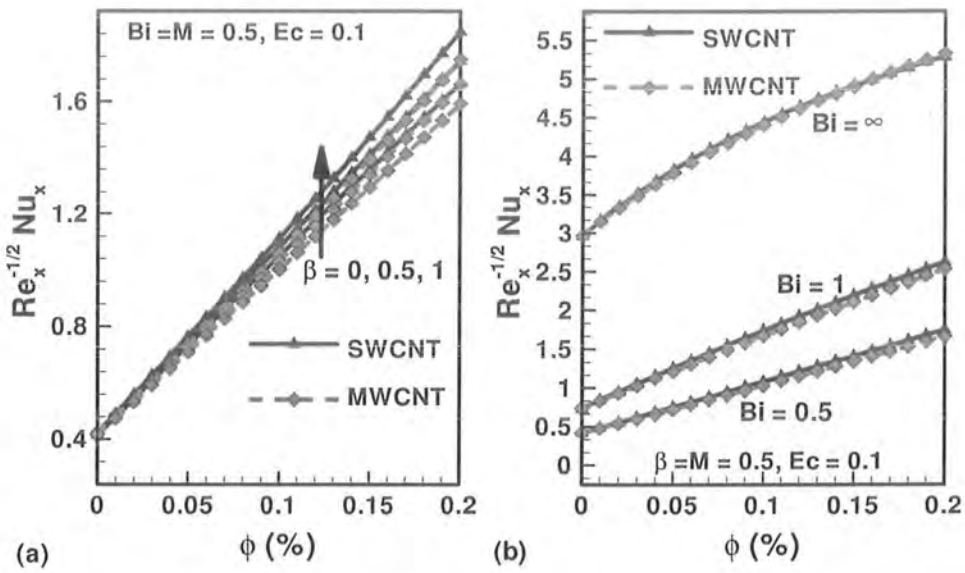


Fig 2.5: Variation of reduced Nusselt Number for various values of  $M$  and  $Ec$  for water-based CNTs.

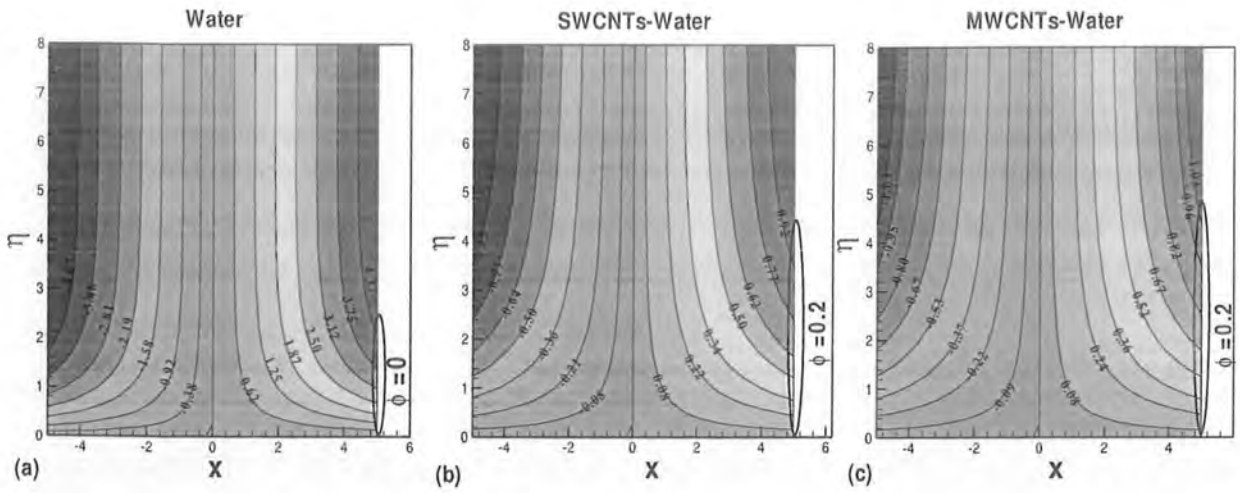


Fig 2.6: Comparison among the stream lines for base fluid and water based CNTs.

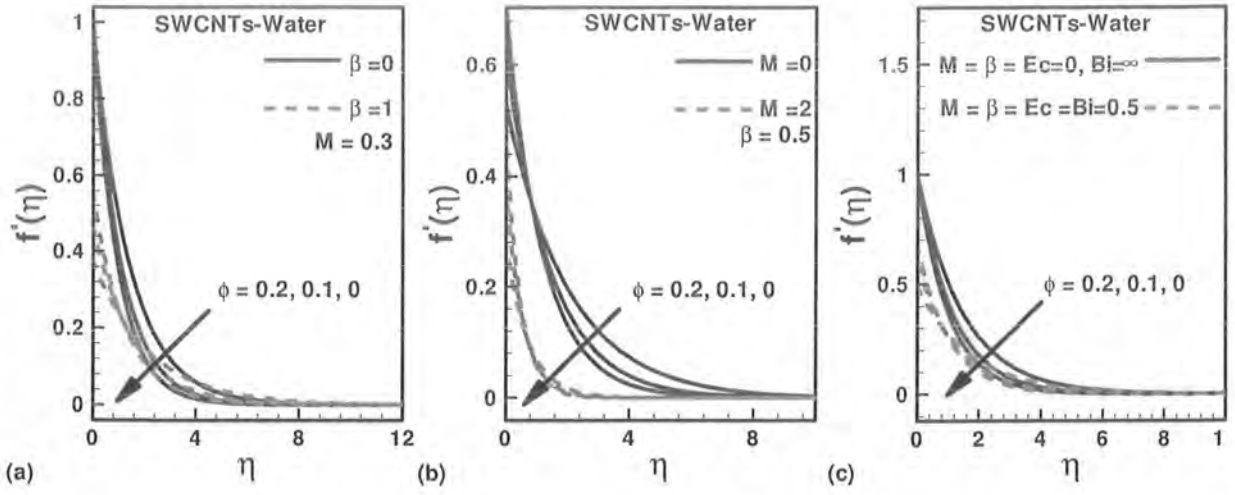


Fig 2.7: Variation of velocity profile for various values of nanoparticle volume fraction.

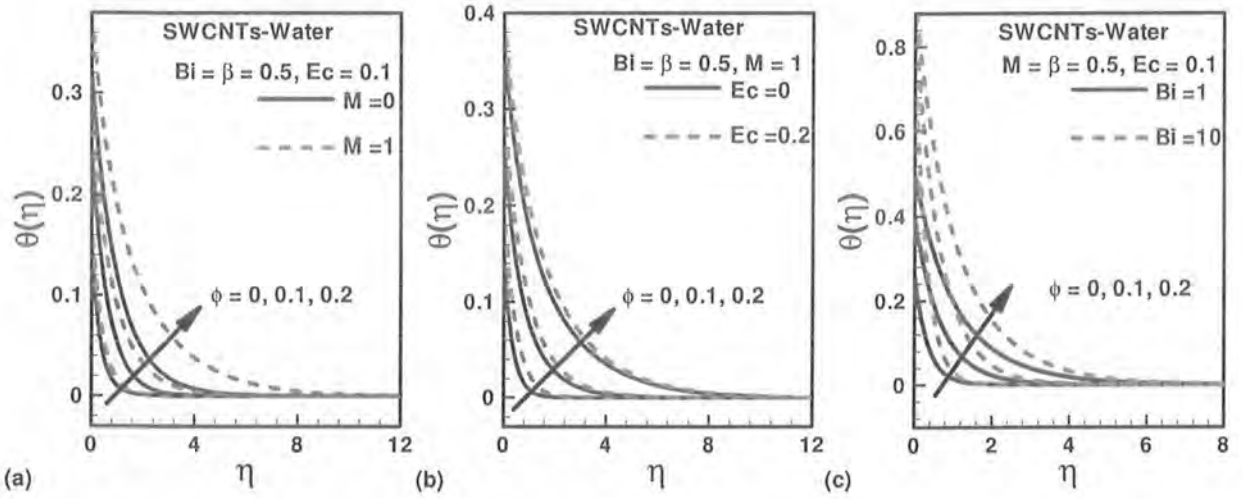


Fig 2.8: Variation of temperature profile for various values of nanoparticle volume fraction.

## 2.5 Concluding remarks

MHD boundary layer flow of a nanofluid over a linearly stretching sheet for Xue [10] model subject to the convective boundary condition is solved numerically. Moreover, effects for various values of existing parameters are discussed for velocity, temperature, reduced skin friction and reduced Nusselt number. The main results of present analysis are listed below:

- Both Hartmann number and slip parameter have opposite effects on the local skin friction coefficient.
- Influence of Hartmann number and Eckert number caused similar decreasing effects on the local Nusselt number.
- An increase in the slip parameter enhances the heat transfer rate while dominant effect on heat transfer is for the case of constant wall temperature ( $Bi = \infty$ ) as compared to ( $Bi = 0.5, 1$ ).
- The trend of velocity is fluctuating for the slip parameter while increasing value of each parameter involved in the momentum equation decreases the velocity profile.
- The temperature profile is enhanced with increasing values of each physical parameter.
- Engine oil-based CNT have higher skin friction and heat transfer rate as compared to water-based and ethylene glycol-based CNT.
- Base fluid SWCNT provides better heat transfer as compared to MWCNTs.

# Thermophysical effects of carbon nanotubes on MHD flow over a stretching surface

## 3.1 Introduction

This chapter is intended for investigating the effects of magnetohydrodynamics (MHD) and volume fraction of carbon nanotubes (CNTs) on the flow and heat transfer in two lateral directions over a stretching sheet. For this purpose, three types of base fluids specifically water, ethylene glycol and engine oil with single and multi-walled carbon nanotubes are used in the analysis. The convective boundary condition in the presence of CNTs is presented for the first time and has not been explored so far. The transformed nonlinear differential equations are solved by Runge-Kutta-Fehlberg method with a shooting technique. The dimensionless velocity and shear stress are obtained in both directions. The dimensionless heat transfer is determined on the surface. Three different models of thermal conductivity are comparable for both CNTs and it is found that the Xue [10] model gives the best approach to gain the superb thermal conductivity in comparison with the Maxwell [6] and Hamilton & Crosser [7] models. Finally, another finding suggests the engine oil provides the highest skin friction and heat transfer rates.

## 3.2 Mathematical model

We considered a steady and incompressible flow of CNTs with three different base fluids past a stretching sheet coinciding with the plane  $z=0$ . The flow has taken place at above the surface which is convectively heated by a fluid at temperature  $T_f$  and heat transfer coefficient  $h_f$ . The mainstream flow has the temperature  $T_\infty (> T_f)$  (See Fig. 1). The sheet is assumed to stretch

continuously along  $x$ - and  $y$ -directions with linear velocities  $ax$  and  $by$ , respectively. Correspondingly, a uniform magnetic field  $B_0$  is applied parallel to  $z$ -axis and the induced magnetic field is assumed to be negligible. The base fluids and the CNTs are assumed to be in thermal equilibrium. The viscous dissipation and radiation effects are neglected in the energy equation. The ambient temperature is assumed to be constant. Using the order of magnitude analysis, the standard boundary layer equations for this problem can be written as follow:

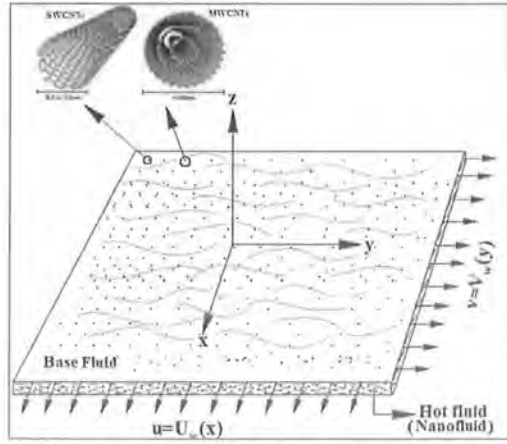


Fig 3.1: Geometry of the problem.

$$\frac{\partial u}{\partial x} + \frac{\partial v}{\partial y} + \frac{\partial w}{\partial z} = 0, \quad (3.1)$$

$$u \frac{\partial u}{\partial x} + v \frac{\partial v}{\partial y} + w \frac{\partial w}{\partial z} = \nu_{nf} \frac{\partial^2 u}{\partial z^2} - \frac{\sigma B^2}{\rho_{nf}} u, \quad (3.2)$$

$$u \frac{\partial v}{\partial x} + v \frac{\partial v}{\partial y} + w \frac{\partial v}{\partial z} = \nu_{nf} \frac{\partial^2 v}{\partial z^2} - \frac{\sigma B^2}{\rho_{nf}} v, \quad (3.3)$$

$$u \frac{\partial T}{\partial x} + v \frac{\partial T}{\partial y} + w \frac{\partial T}{\partial z} = \alpha_{nf} \frac{\partial^2 T}{\partial z^2}, \quad (3.4)$$

where  $u$ ,  $v$  and  $w$  are the velocity components along the  $x$ -,  $y$ - and  $z$ -axes,  $T$  is the temperature,  $\nu_{nf}$  and  $\alpha_{nf}$  are the effective kinematic viscosity and thermal diffusivity of nanofluids respectively. The effective properties of carbon nanotubes may be expressed in terms of the properties of base fluid and carbon nanotubes and the solid volume fraction of carbon nanotubes in the base fluids as follows:

$$\left. \begin{aligned} \mu_{nf} &= \frac{\mu_f}{(1-\phi)^{2.5}}, \quad \rho_{nf} = (1-\phi)\rho_f + \phi\rho_{CNT} \\ (\rho c_p)_{nf} &= (1-\phi)(\rho c_p)_f + \phi(\rho c_p)_{CNT}, \\ \nu_{nf} &= \frac{\mu_{nf}}{\rho_{nf}}, \quad \alpha_{nf} = \frac{k_{nf}}{(\rho c_p)_{nf}}, \\ \frac{k_{nf}}{k_f} &= \frac{1-\phi + 2\phi \frac{k_{CNT}}{k_{CNT}-k_f} \ln \frac{k_{CNT}+k_f}{2k_f}}{1-\phi + 2\phi \frac{k_f}{k_{CNT}-k_f} \ln \frac{k_{CNT}+k_f}{2k_f}} \end{aligned} \right\} \quad (3.5)$$

where  $k_{nf}$  is the thermal conductivity of the carbon nanotubes proposed by Xue [10],  $(\rho c_p)_{CNT}$  is the heat capacity of carbon nanotubes and  $\phi$  is the solid volume fraction of CNTs. Furthermore, these models do not account for the effect of the space distribution of the CNTs on thermal conductivity.

The hydrodynamic and thermal boundary conditions for the problem are given by

$$\left. \begin{aligned} v = V_w(x) = by, \quad u = U_w(x) = ax, \quad -k_{nf} \frac{\partial T}{\partial z} = h_{nf} (T_f - T), \quad \text{at } z = 0 \\ u \rightarrow 0, \quad v \rightarrow 0, \quad T \rightarrow T_\infty, \quad \text{as } z \rightarrow \infty \end{aligned} \right\} \quad (3.6)$$

where  $a$  and  $b$  are constants,  $U_w(x)$  and  $V_w(x)$  are stretching velocities in the  $x$ - and  $y$ -directions, respectively.

We look for a similar solution of Eqs. (3.1)-( 3.6) of the following form

$$\left. \begin{aligned} u = axf'(\eta), \quad v = byg'(\eta), \quad \theta(\eta) = \frac{T - T_\infty}{T_f - T_\infty}, \\ \eta = \left(\frac{a}{\nu_f}\right)^{1/2} z, \quad w = -\left(\frac{\nu_f}{a}\right)^{1/2} \{af(\eta) + bg(\eta)\} \end{aligned} \right\} \quad (3.7)$$

where  $\eta$  is the similarity variable. Employing the similarity variables (3.7), Eqs (3.1)-( 3.4) reduce to the following nonlinear system of ordinary differential equations:

$$\frac{1}{(1-\phi)^{2.5} (1-\phi + \phi\rho_{CNT} / \rho_f)} f''' + (f + \lambda g) f'' - f'^2 - \frac{M^2}{(1-\phi + \phi\rho_{CNT} / \rho_f)} f' = 0, \quad (3.8)$$

$$\frac{1}{(1-\phi)^{2.5} (1-\phi + \phi\rho_{CNT} / \rho_f)} g''' + (f + \lambda g) g'' - g'^2 - \frac{M^2}{(1-\phi + \phi\rho_{CNT} / \rho_f)} g' = 0, \quad (3.9)$$

$$\frac{1}{Pr \left\{ 1 - \phi + \phi(\rho_{C_p})_{CNT} / (\rho_{C_p})_f \right\}} \frac{k_{nf} / k_f}{\left\{ 1 - \phi + \phi(\rho_{C_p})_{CNT} / (\rho_{C_p})_f \right\}} \theta'' + (f + \lambda g) \theta' = 0, \quad (3.10)$$

Subject to the boundary conditions

$$\left. \begin{aligned} f(0) = 0, \quad f'(0) = 1, \quad g(0) = 0, \quad g'(0) = \lambda, \\ \theta'(0) = -Bi \frac{1 - \phi + 2\phi \frac{k_f}{k_{CNT} - k_f} \ln \frac{k_{CNT} + k_f}{2k_f}}{1 - \phi + 2\phi \frac{k_{CNT}}{k_{CNT} - k_f} \ln \frac{k_{CNT} + k_f}{2k_f}} (1 - \theta(0)) \\ f' \rightarrow 0, \quad g' \rightarrow 0, \quad \theta \rightarrow 0, \quad \text{as } \eta \rightarrow \infty \end{aligned} \right\} \quad (3.11)$$

Here, primes denote derivative with respect to  $\eta$ ,  $M^2 = \sigma B_0^2 / \rho_f a$  is the magnet parameter,

$Pr = \nu_f / \alpha_f$  is the Prandtl number of the base fluid,  $Bi = h_f / k_f \sqrt{\nu_f / a}$  is the convective

parameter and  $\lambda = b/a$  is the stretching ratio of velocities in the  $y$ - and  $x$ -directions. The physical quantities of interest are the skin friction coefficients  $C_{fx}$  and  $C_{fy}$  along  $x$ - and  $y$ -directions, respectively, and the local Nusselt number  $Nu_x$ , which are defined as

$$C_{fx} = \frac{\tau_{wx}}{\rho_f u_w^2}, \quad C_{fy} = \frac{\tau_{wy}}{\rho_f u_w^2}, \quad Nu_x = \frac{xq_w}{k_f \Delta T} \quad (3.12)$$

Where  $\tau_{wx}$  and  $\tau_{wy}$  are the surface shear stresses along the  $x$ - and  $y$ -directions, and  $q_w$  is the wall heat flux, and are defined as

$$\tau_{wx} = \mu_{nf} \left( \frac{\partial u}{\partial z} \right)_{z=0}, \quad \tau_{wy} = \mu_{nf} \left( \frac{\partial v}{\partial z} \right)_{z=0}, \quad q_w = -k_{nf} \left( \frac{\partial T}{\partial z} \right)_{z=0} \quad (3.13)$$

with  $\mu_{nf}$  and  $k_{nf}$  being the dynamic viscosity and the thermal conductivity of the nanofluids, respectively. Using the similarity variables (3.7), we obtain

$$\begin{aligned} \text{Re}_x^{1/2} C_{fx} &= \frac{1}{(1-\phi)^{2.5}} f''(0) \\ \text{Re}_y^{1/2} C_{fy} &= \lambda(y/x) \frac{1}{(1-\phi)^{2.5}} g''(0) \\ \text{Re}_x^{-1/2} Nu_x &= -\frac{k_{nf}}{k_f} \theta'(0) \end{aligned} \quad (3.14)$$

where  $\text{Re}_x$  is the local Reynolds number.

### 3.3 Numerical Procedure

System of Coupled nonlinear ordinary differential Eqs. (3.8)–(3.10) subjected to the



boundary conditions (3.11) are solved numerically using the Runge-Kutta-Fehlberg method with a shooting technique for different values of governing parameters. Such includes magnetic parameter  $M$ , stretching parameter  $\lambda$ , Prandtl number  $Pr$ , convective parameter  $Bi$  and CNTs volume fraction  $\phi$ . The boundary value problem is initially transformed into an initial value problem (IVP). Then the IVP is solved by a systematic guessing for,  $g''(0)$  and  $\theta'(0)$  until the far field boundary condition is achieved. The step size  $\Delta\eta = 0.01$  is used to obtain the numerical solution with  $\eta_{\max} = 12$ , where  $\eta_{\max}$  is the finite value of the similarity variable  $\eta$  for the far field boundary conditions. The convergence is assured by taking error  $10^{-6}$  in all cases. For pure fluid ( $\phi = 0$ ) and isothermal boundary condition ( $Bi \rightarrow \infty$ ), the results for skin friction (with  $Pr=0.7$ ) and Nusselt number (with  $Pr=10$ ) are compared with those obtained by Ahmad and Nazar [18] and Wang [29] for different values of magnetic parameter  $M$  in Table 3.1. We notice that the comparison shows good agreement for each value of  $M$ . Therefore, we are confident that the present results are very accurate.

### 3.4 Results and discussion

The effects of the solid volume fraction  $\phi$  of CNTs, magnetic parameter  $M$ , stretching ratio of velocities  $\lambda$  as well as the the convective parameter  $Bi$  on the dimensionless velocities with temperature are analyzed for both CNTs with water as base fluid. The skin friction coefficients and heat transfer rates are analyzed along  $x$ -direction and  $y$ -direction for three different base fluids. The solid volume fraction  $\phi$  is used in the range of  $0 \leq \phi \leq 0.5$ . The thermo-physical properties of base fluids and CNTs are presented in Table 3.5. Figures 3.2(a) and 3.2(b) show the effects of CNTs volume fraction of both SWCNT and MWCNT on the dimensionless velocities for different values of magnetic parameter. In the absence of magnetic

field, the dimensionless velocities are found to be higher within the hydrodynamic boundary layer for both pure fluid and water-based CNTs. It can be seen that the magnetic field reduces the hydrodynamic boundary layer thickness in both cases. It is important to note, for pure water (when  $\phi = 0$ ), the dimensionless velocities are the same in both cases. They increase with a rise in the CNTs volume fraction of both SW and MWCNTs.

The effects of CNTs volume fraction on the dimensionless velocities are illustrated in Figs. 3.3(a) and 3.3(b) for stretching and shrinking sheets in the presence of a magnetic field. In both cases, these effects are investigated for water-based SWCNTs. It can be seen in Fig. 3.3(a) that no appreciable effect of  $\phi$  or  $\lambda$  could be found on  $f'(\eta)$ . However, the effects of stretching/shrinking parameters on the dimensionless velocity  $g'(\eta)$  could be observed clearly in Fig. 3.3(b). For both stretching and shrinking sheets, the dimensionless velocity  $g'(\eta)$  converges at the same time.

Figures 3.4(a) and 3.4(b) show the effects of CNTs volume fraction, convective and magnetic parameters on the dimensionless temperature of water-based CNTs. It can be seen that the difference between the dimensions, temperatures of SWCNT and MWCNT is almost negligible in both cases. The dimensionless temperature at the surface is lower for a pure fluid (water) and for smaller values of the convective parameter. In the presence of a magnetic field, the surface temperature increases with CNTs volume fraction and convective parameter, as shown in Fig. 3.4(a). Inside the thermal boundary layer, the dimensionless temperature increases with CNTs volume fraction and magnetic parameter.

The variation of skin friction along x-axis with CNTs volume fraction for different parameters is shown in Figs. 3.5 and 3.6 for different base fluids. Since the thermo-physical properties of both CNTs increase with volume fraction, the skin friction also increases in each

case. Figures 3.5(a)-(c) show the effects of magnetic field on skin friction for three different base fluids with SWCNTs and MWCNTs. In each case, the skin friction increases with magnetic field. Due to the higher viscosity of engine oil, the skin friction is found to be higher in case of engine oil.

In Figs. 3.6(a)-3.6(c), the effects of stretching parameter on the skin friction along x-axis are depicted in the presence of a magnetic field. In each case, the skin friction is found to be higher for SWCNTs due to the higher density of SWCNTs. The effect of stretching is to reduce friction in each case for both CNTs. This reduction is found to be higher for a higher volume fraction of CNTs. The effects of same parameters on the skin friction along y-axis are shown in Figs. 3.7 and 3.8 for three different base fluids with both CNTs. The effects of magnetic fields on the skin friction along y-axis are found to be the same as discussed before. The effects of stretching parameter on the skin friction coefficient along the y-direction are presented in Figs. 3.8(a)-3.8(c) and these results are plotted for three different base fluids in the presence of both SWCNT's and MWCNT's. It is seen that the skin friction increases with stretching parameter in each case. The difference between skin friction of both CNTs increases with volume fraction due to increase in density.

The variation of Nusselt numbers with CNTs volume fraction for different values of convective parameter is depicted in Figs. 3.9(a)-3.9(c) for water, ethylene glycol and engine oil with both CNTs. It can be observed that the Nusselt numbers increase with CNTs volume fraction and convective parameter in each case. This is due to the fact the thermal conductivity of each CNT rises with an increase in the CNTs volume fraction. Also, it is important to note the Nusselt numbers increase in Prandtl numbers as we make a transition from water to engine oil.

The increase in Prandtl numbers actually decreases the thermal boundary layer thickness, thus decreasing the thermal resistance and increasing the heat transfer rate.

Different models of thermal conductivity are compared in Figs. 3.10(a)- 3.10(c) for SWCNTs and in Table 3.3 for MWCNT, respectively. It can be verified that the Xue [10] model gives the highest heat transfer rates for both CNTs in comparison with Maxwell [6] and Hamilton & Crosser [7] models. This is due to the fact that Xue [10] model considers rotational elliptical nanotubes with very large axial ratio and compensating the effects of the space distribution on CNTs.

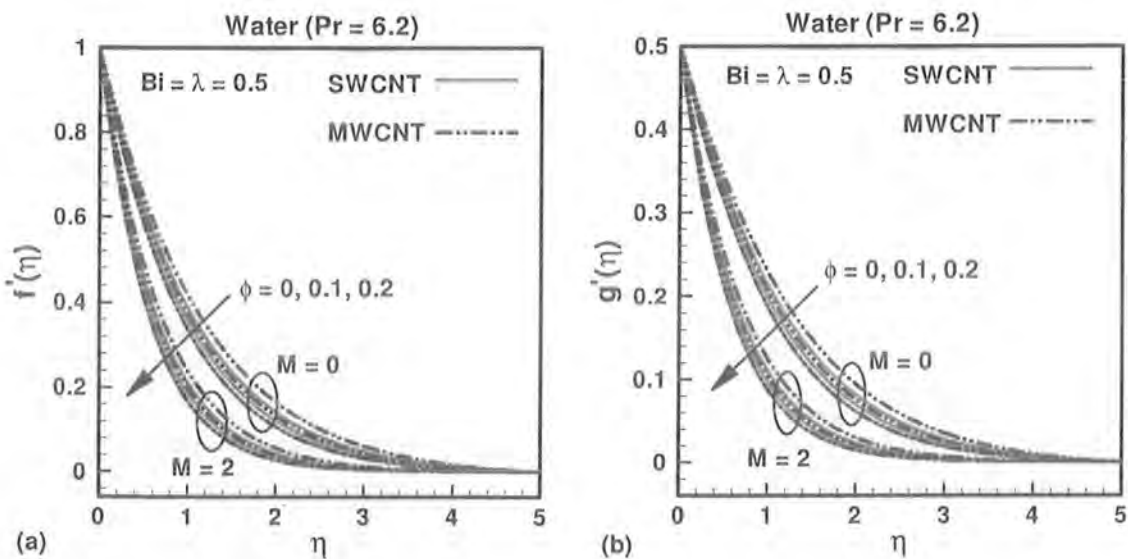


Fig 3.2: Effects of nanoparticle volume fraction and magnetic parameters on dimensionless velocities for CNTs.

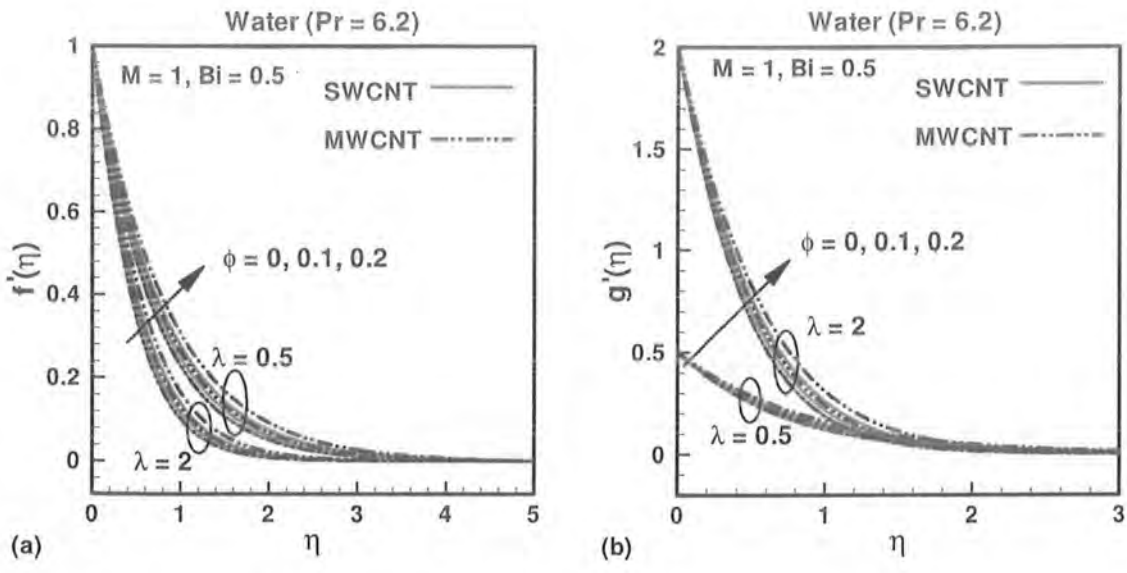


Fig 3.3: Effects of nanoparticle volume fraction and stretching parameters on dimensionless velocities for SWCNT.

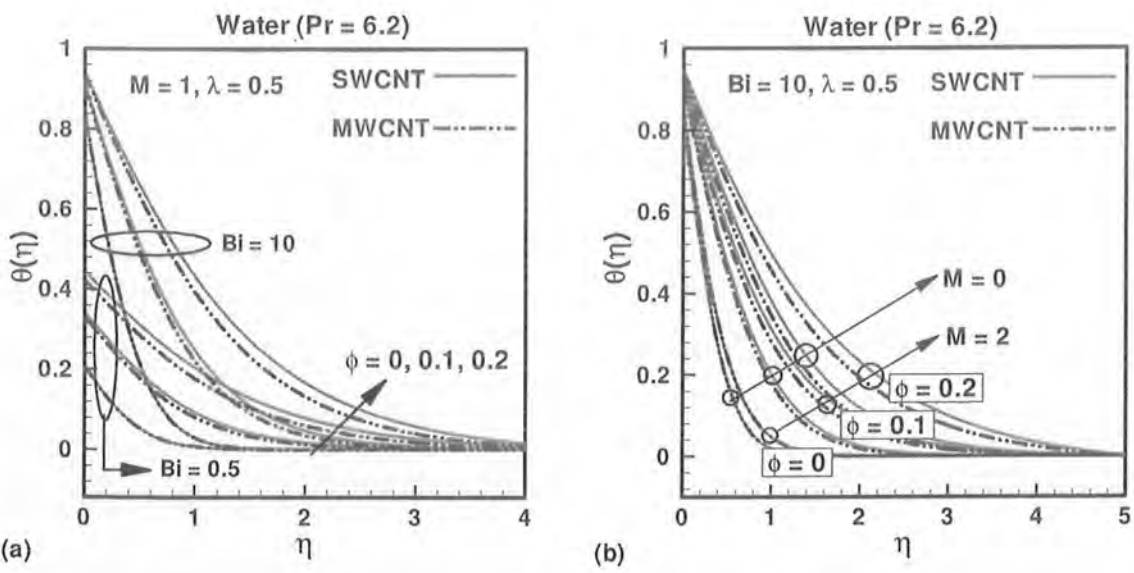


Fig 3.4: Effects of nanoparticle volume fraction, convective and magnetic parameters on dimensionless temperature for CNTs.

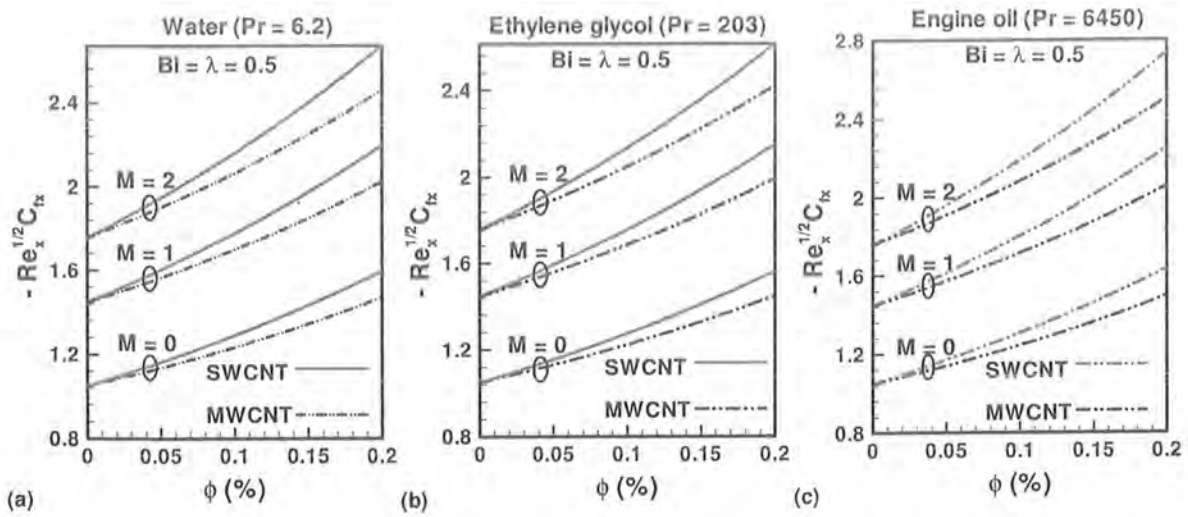


Fig 3.5: Variation of skin friction coefficient along  $x$ -direction with CNTs volume fraction  $\phi$  and magnetic parameter  $M$ .

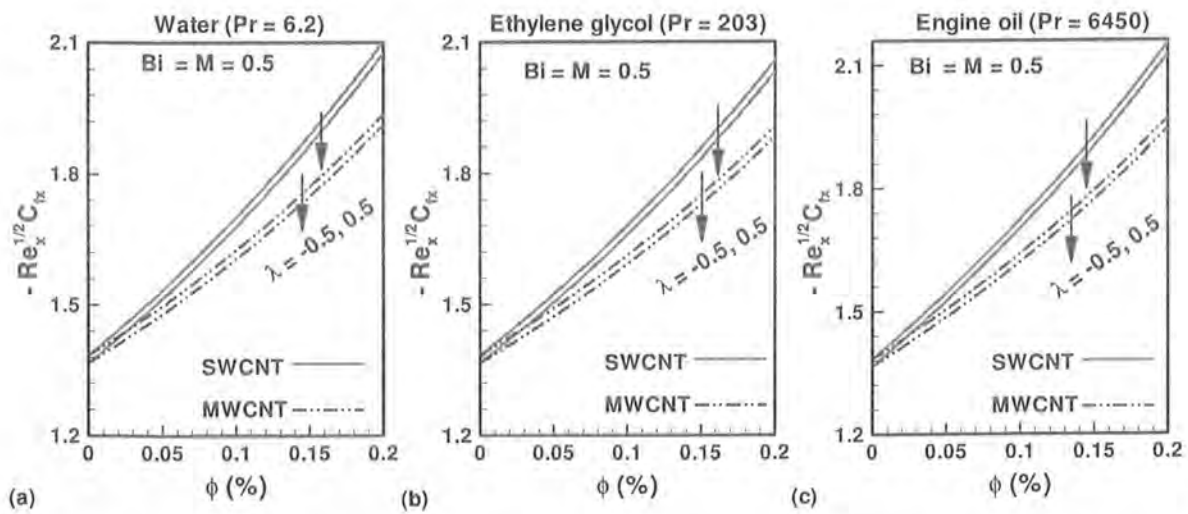


Fig 3.6: Variation of skin friction coefficient along  $x$ -direction with CNTs volume fraction  $\phi$  and stretching parameter  $\lambda$ .

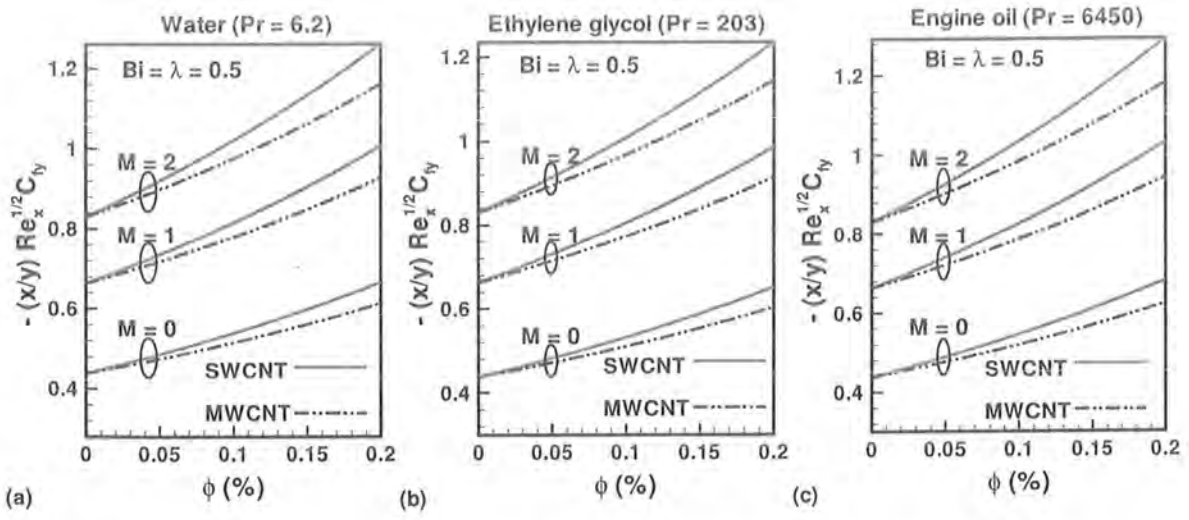


Fig 3.7: Variation of skin friction coefficient along y-direction with CNTs volume fraction  $\phi$  and magnetic parameter  $M$ .

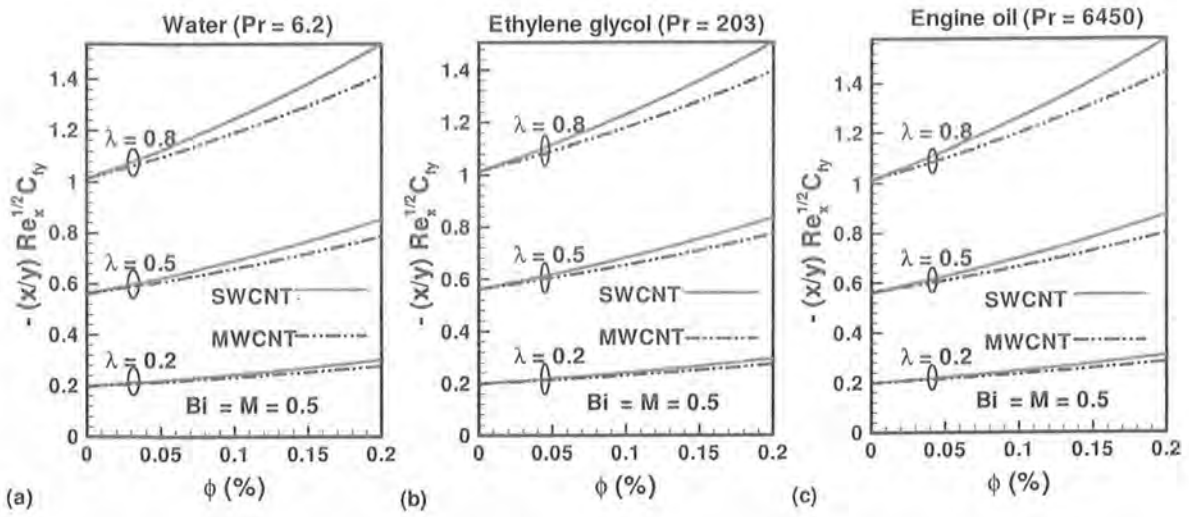


Fig 3.8: Variation of skin friction coefficient along y-direction with CNTs volume fraction  $\phi$  and stretching parameter  $\lambda$ .

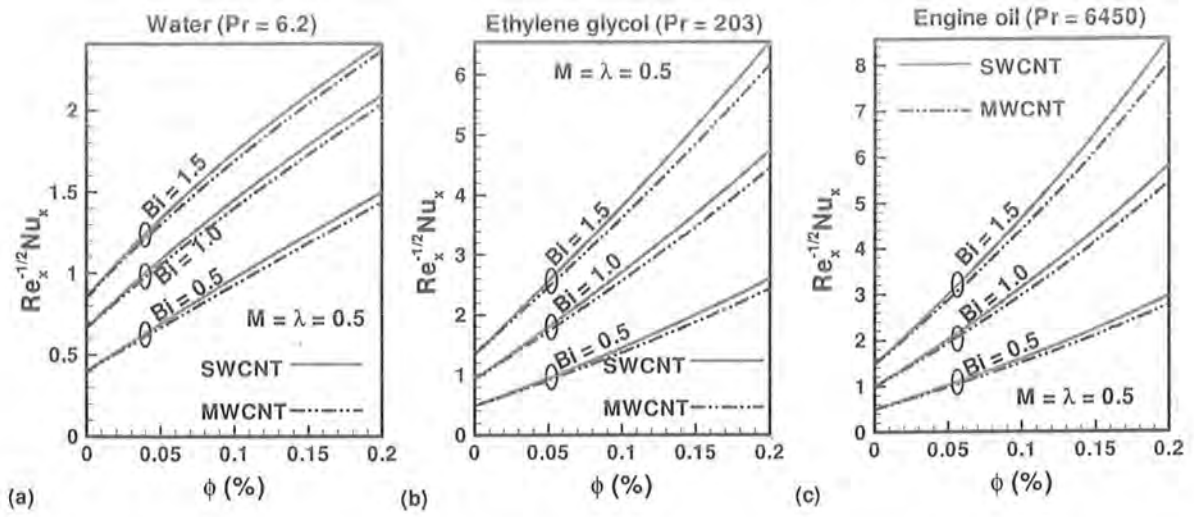


Fig 3.9: Variation of Nusselt number with CNTs volume fraction  $\phi$  and convective parameter  $Bi$ .

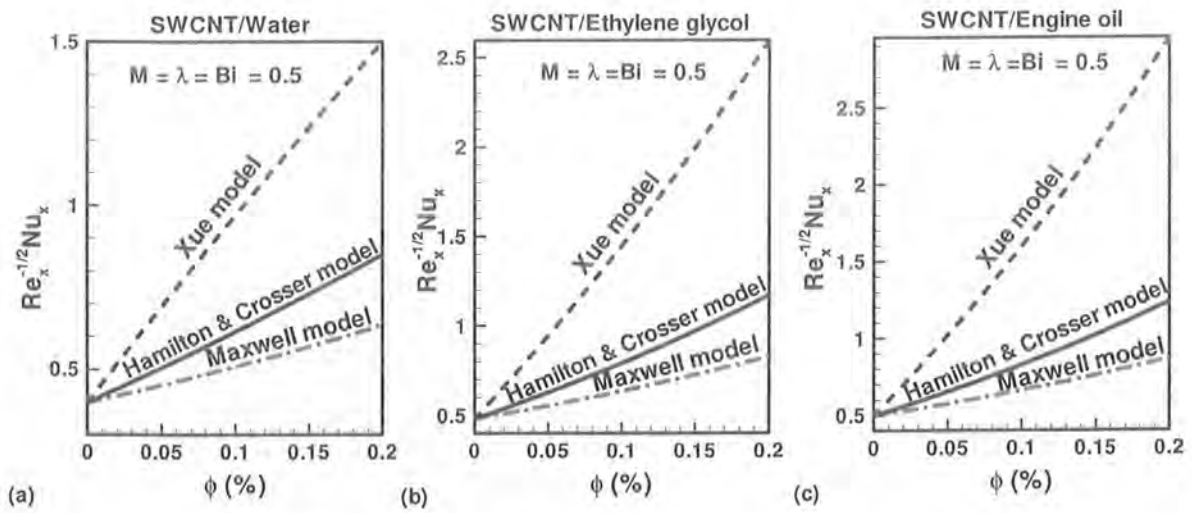


Fig 3.10: Comparison among the theoretical models for single-wall CNT with different base fluids. In the calculation,  $n = 6$  for the Hamilton–Crosser model [7].



**Table 3.1:** Comparison of results for skin friction and Nusselt number for pure fluid with  $Bi \rightarrow \infty$  and  $\lambda = 1$ .

$M$	Present Results		Ahmad and Nazar [18]		Wang [29]
	$-g''(0)$	$-\theta'(0)$	$-g''(0)$	$-\theta'(0)$	$-g''(0)$
0	1.173721	3.306792	1.1748	3.3078	1.173720
10	3.367240	5.830448	3.3667	5.8309	-
100	10.066473	1.680774	10.0663	1.5471	-

**Table 3.2:** Thermophysical properties of base fluids and CNTs [37].

Physical properties	Base fluids			Nanoparticles	
	Water	Ethylene glycol	Engine oil	SWCNT	MWCNT
$\rho$ (kg/m <sup>3</sup> )	997	1115	884	2600	1600
$c_p$ (J/kg-K)	4179	2430	1910	425	796
$k$ (W/m-K)	0.613	0.253	0.144	6600	3000
Pr	3.2	203	6450	-	-

**Table 3.3:** Comparison among three theoretical models for Nusselt Numbers with MWCNTs suspended in three different base fluids, where  $Bi = M = \lambda = 0.5$  and  $n = 6$  for the Xue model.

$\phi \downarrow$	Water			Ethylene glycol			Engine oil		
	Xue	H&C	Maxwell	Xue	H&C	Maxwell	Xue	H&C	Maxwell
0.0	0.65077	0.65077	0.65077	1.90009	1.90009	1.90009	3.44808	3.44808	3.44808
0.02	0.66346	0.66681	0.67574	1.94042	1.94252	1.94894	3.50818	3.50887	3.51115
0.04	0.67640	0.68302	0.69807	1.98247	1.98662	1.99722	3.57156	3.57290	3.57660
0.06	0.68966	0.69950	0.71909	5.02639	5.03257	5.04617	3.63843	3.64042	3.64508
0.08	0.70328	0.71637	0.73949	5.07233	5.08055	5.09648	3.70904	3.71166	3.71702
0.1	0.7173	0.7337	0.75975	5.1204	5.1307	5.14858	3.7836	3.7869	3.79280

### 3.5 Conclusions

In this article, we have presented similarity solutions for the momentum and energy equations governing a 3-D MHD flow and heat transfer of CNTs along a stretching sheet. Results for the reduced friction factor and reduced Nusselt number are presented with convective boundary condition for three different base fluids mixed with SWCNTs and MWCNTs. It is concluded that,

- The hydro-thermal boundary layer thickness increases with CNTs volume fraction.
- The shear stresses in  $x$ - and  $y$ -direction and surface heat transfer increase with CNTs volume fraction.
- Engine oil-based CNTs have higher skin friction and heat transfer rates than water and ethylene glycol-based CNTs.
- Xue [10] model for the thermal conductivity of CNTs shows the highest enhancement in heat transfer rates.

# Three-dimensional flow of water-based nanofluid over an exponentially stretching sheet

## 4.1 Introduction

In the present chapter, the flow of three dimensional water-based nanofluid over an exponentially stretching sheet is analyzed. Compatible exponential type similarity transformations are applied for the first time on basic boundary layer equations for nanofluid. Different type of nanoparticles, such as copper ( $Cu$ ), alumina ( $Al_2O_3$ ) and titanium ( $TiO_2$ ) are considered with water as the base fluid. Structure of the mathematical model is constructed according to above mentioned assumptions and then reduced system of coupled differential equations along with the boundary conditions are solved numerically. Physical behavior of velocities and temperature profiles are examined through graphs and discussed for both  $x$ - and  $y$ -directions. The reduced skin friction coefficient along each direction and reduced Nusselt number with nanoparticle volume fraction  $\phi$  are presented through graphs.

## 4.2 Mathematical formulation

Consider three dimensional (3D) steady boundary layer flow past a stretching sheet in the presence of nanoparticles. It is also considered that the sheet is stretched with different velocities  $U_w$ ,  $V_w$  along the Cartesian coordinate axis,  $x$ - and  $y$ -axis respectively whereas the fluid placed along the  $z$  direction is taken to be at rest (see Fig.1). Moreover, it is considered the constant temperature  $T_w$  at wall and the ambient temperature  $T_\infty$ .

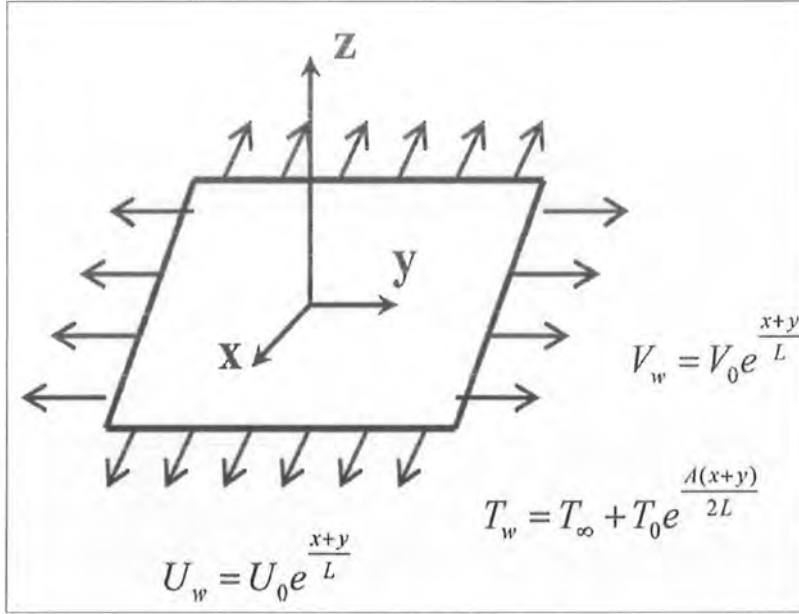


Fig. 4.1: Geometry of the problem.

Under the above assumptions the governing continuity, momentum and energy equations are

$$\frac{\partial u}{\partial x} + \frac{\partial v}{\partial y} + \frac{\partial w}{\partial z} = 0, \quad (4.1)$$

$$\rho_{ef} \left( u \frac{\partial u}{\partial x} + v \frac{\partial u}{\partial y} + w \frac{\partial u}{\partial z} \right) = \mu_{ef} \left( \frac{\partial^2 u}{\partial z^2} \right), \quad (4.2)$$

$$\rho_{ef} \left( u \frac{\partial v}{\partial x} + v \frac{\partial v}{\partial y} + w \frac{\partial v}{\partial z} \right) = \mu_{ef} \left( \frac{\partial^2 v}{\partial z^2} \right), \quad (4.3)$$

$$\left( u \frac{\partial T}{\partial x} + v \frac{\partial T}{\partial y} + w \frac{\partial T}{\partial z} \right) = \alpha_{ef} \left( \frac{\partial^2 T}{\partial z^2} \right). \quad (4.4)$$

The corresponding boundary conditions are stated as

$$\begin{aligned} u = U_w, v = V_w, w = 0, T = T_w, \text{ at } z = 0, \\ u \rightarrow 0, v = 0, T = T_\infty, \text{ as } z \rightarrow \infty. \end{aligned} \quad (4.5)$$

In above expressions  $u$ ,  $v$  and  $w$  are the velocity components along the  $x$ -,  $y$ - and  $z$ -axes, respectively,  $T$  is the temperature,  $\rho_{nf}$  is the nanofluid density and  $\mu_{nf}$  is the thermal diffusivity of nanofluid defined as,

$$\begin{aligned}\mu_{nf} &= \frac{\mu_f}{(1-\phi)^{2.5}}, \quad \alpha_{nf} = \frac{k_{nf}}{(\rho C_p)_{nf}}, \\ \rho_{nf} &= (1-\phi)\rho_f + \phi(\rho)_s, \\ \rho_{nf} &= (1-\phi)(C_p \rho)_f + \phi(\rho C_p)_s, \\ \frac{k_{nf}}{k_f} &= \frac{(k_s + 2k_f) - 2\phi(k_f - k_s)}{(k_s + 2k_f) + \phi(k_f - k_s)},\end{aligned}\tag{4.6}$$

where  $\phi$  is the nanoparticle fraction,  $(\rho C_p)_{nf}$  is the effective heat capacity of a nanoparticle,  $k_{nf}$  is the thermal conductivity of nanofluid,  $k_f$  and  $k_s$  are the thermal conductivities of the base fluid and nanoparticle, respectively,  $\rho_f$  and  $\rho_s$  are the thermal conductivities of the base fluid and nanoparticle, respectively. In the present study it is considered the stretching velocity and temperature at wall are defined as,

$$U_w = U_0 e^{\frac{x+y}{L}}, V_w = V_0 e^{\frac{x+y}{L}}, T_w = T_\infty + T_0 e^{\frac{A(x+y)}{2L}},\tag{4.7}$$

where  $U_0$ ,  $V_0$ , and  $T_0$  are constants,  $L$  is the reference length and  $A$  is the temperature exponent coefficient. Introducing the following similarity transformations,

$$\begin{aligned}u &= U_0 e^{\frac{x+y}{L}} f'(\eta), \quad v = U_0 e^{\frac{x+y}{L}} g'(\eta), \\ w &= \left(\frac{\nu U_0}{2L}\right)^{1/2} e^{\frac{x+y}{L}} [f(\eta) + \eta f'(\eta) + g(\eta) + \eta g'(\eta)], \\ T &= T_\infty + T_0 e^{\frac{A(x+y)}{2L}} \theta(\eta), \quad \eta = \left(\frac{U_0}{2\nu L}\right)^{1/2} e^{\frac{x+y}{L}} z.\end{aligned}\tag{4.8}$$

Making use of Eq. (4.8) in Eqs. (4.1) to (4.6), we have

$$\frac{1}{(1-\phi)^{2.5}[1-\phi+\phi(\rho_s/\rho_f)]} f''' + (f+g)f'' - 2(f'+g')f' = 0, \quad (4.9)$$

$$\frac{1}{(1-\phi)^{2.5}[1-\phi+\phi(\rho_s/\rho_f)]} g''' + (f+g)g'' - 2(f'+g')g' = 0, \quad (4.10)$$

$$\frac{1}{\text{Pr} [1-\phi+\phi(\rho C_p)_s / (\rho C_p)_f]} \frac{(k_{nf} / k_f)}{\text{Pr} [1-\phi+\phi(\rho C_p)_s / (\rho C_p)_f]} \theta'' + (f+g)\theta' - A(f'+g')\theta = 0, \quad (4.11)$$

$$\left. \begin{aligned} f(0) = 0, f'(0) = 1, f'(\infty) = 0, \\ g(0) = 0, g'(0) = \alpha, g'(\infty) = 0, \\ \theta(0) = 1, \theta(\infty) = 0, \end{aligned} \right\} \quad (4.12)$$

where  $\text{Pr} = (\mu C_p)_f / (k_f)$  is the Prandtl number and  $\alpha = V_0 / U_0$  is the stretching ratio.

Expressions for the skin-friction coefficients  $c_{fx}$  and  $c_{fy}$  along  $x$  and  $y$ -directions, respectively

and the local Nusselt number  $Nu_x$  are defined as

$$c_{fx} = \frac{\tau_{wx}}{\rho_f U_0^2 / 2}, \quad c_{fy} = \frac{\tau_{wy}}{\rho_f U_0^2 / 2}, \quad Nu_x = \frac{xq_w}{k_f (T_w - T_\infty)}, \quad (4.13)$$

where  $\tau_{wx}$  and  $\tau_{wy}$  are the surface shear stresses along the  $x$ - and  $y$ -directions,

respectively and  $q_w$  is the heat flux, which are given by

$$\tau_{wx} = \mu_{nf} \left( \frac{\partial u}{\partial z} \right)_{z=0}, \quad \tau_{wy} = \mu_{nf} \left( \frac{\partial v}{\partial z} \right)_{z=0}, \quad q_w = -k_{nf} \left( \frac{\partial T}{\partial z} \right)_{z=0}. \quad (4.14)$$

Reduced form of Eq. (4.13) takes the form

$$\begin{aligned}
c_{fx} &= (\text{Re})^{-1/2} e^{\frac{3(x+y)}{2L}} \frac{f''(0)}{(1-\phi)^{2.5}}, \\
c_{fy} &= (\text{Re})^{-1/2} e^{\frac{3(x+y)}{2L}} \frac{g''(0)}{(1-\phi)^{2.5}}, \\
R_{\nu}^{-1/2} Nu_x &= -\frac{x}{L} (\text{Re})^{1/2} e^{\frac{3x}{2L}} \frac{k_{nf}}{k_f} \theta'(0).
\end{aligned} \tag{4.15}$$

where Reynolds number  $\text{Re}$  is defined as  $\text{Re} = U_0 L / 2\nu$ .

### 4.3 Numerical Method

The systems of nonlinear differential equations (4.9-4.11) along with the boundary condition (4.12) are solved numerically using fourth-order Runge-Kutta-Fehlberg with the shooting technique. The step size  $\Delta\eta = 0.001$  is used to obtain the numerical solution with  $\eta_{\max}$  and the accuracy to the fifth decimal place is taken as the criterion of convergence. To handle the condition at infinity we consider a suitable value of  $\eta \rightarrow \infty$ , say  $\eta_{\infty}$ .

### 4.4 Results and discussions

Present section highlights the influence of emerging parameters such as nanoparticle volume fraction  $\phi$ , stretching parameter  $\alpha$  and temperature exponent coefficient  $A$  for velocities  $f'(\eta)$ ,  $g'(\eta)$  and temperature  $\theta(\eta)$ . Moreover, we are considering three different nanoparticles, namely: copper ( $\text{Cu}$ ), alumina ( $\text{Al}_2\text{O}_3$ ) and titanium ( $\text{TiO}_2$ ) by considering water as the base fluid. Thermo-physical properties of base fluid and particles are mentioned in Table 4.1. It is noticed that the plotted results (see Fig. 4.2-4.3) are only for  $\text{Cu}$ -water when  $\text{Pr} = 6.2$  and  $A = 0.5$  for velocities  $f'(\eta)$  and  $g'(\eta)$  along  $x$  and  $y$ -direction, respectively. Figs. 4.2 and 4.3 are plotted for least values of nanoparticle volume fraction  $\phi$ . It is found that nanoparticle

volume fraction is the decreasing function of velocities  $f'(\eta)$  and  $g'(\eta)$ . Moreover, it is visualized from Figs. 4.2 and 4.3, both velocities  $f'(\eta)$  and  $g'(\eta)$  predict the same decreasing behavior for stretching parameter  $\alpha = 0.5$  and  $\alpha = 1$ . Variation of temperature profile  $\theta(\eta)$  against nanoparticle fraction  $\phi$  is plotted in Fig. 4.4 for  $\alpha = 0.5$  and  $\alpha = 1$ . From Table. 6.1, it is noticed that thermal conductivity of copper ( $Cu$ ) is much higher than the base fluid water. So it may affects in the enhancement of temperature profile  $\theta(\eta)$ . Consequently, from Fig. 4.4 with an increase in nanoparticle volume fraction  $\phi$ , temperature profile  $\theta(\eta)$  also increases for  $Cu - water$ .

Combined effects of  $Cu$ ,  $TiO_2$  and  $Al_2O_3$  for velocities and temperature profile are plotted in Figs. 4.5-4.7. Through Table. 4.1, it is noticed that the density of copper is less than the density of titanium so as the density of titanium is less than the density of alumina. As a result,  $Cu - water$  produces higher resistance in the movement of nanofluid as compared to  $TiO_2 - water$  and  $Al_2O_3 - water$  (see Fig. 4.5 and 4.6). Variation of velocities  $f'(\eta)$  and  $g'(\eta)$  for different nanoparticles  $Cu$ ,  $TiO_2$  and  $Al_2O_3$  are plotted in Fig. 4.5 and 4.6. Fig. 4.7 depicts the variation of temperature profile  $\theta(\eta)$  for different nanoparticles according to the thermo physical properties mentioned in Table. 4.1. As shown in Fig. 4.6, the temperature profile  $\theta(\eta)$  provides same behavior for temperature exponent coefficient  $A = -1$ ,  $A = 0$  and  $A = 1$ .

Table 4.2, presents the excellent comparison with previous literature presented by Magyari and Keller [19], in the absence of nanoparticles i.e ( $\phi = 0$ ) and  $\alpha = 0$ . In Table. 4.3, results are in excellent comparison with Chung Liu et al [20] in the absence of nanoparticles i.e ( $\phi = 0$ ). Fig. 4.8 and 4.9 provide the results of reduced skin friction coefficient along  $\phi$  with



different nanoparticles when  $Pr = 6.2$ ,  $\alpha = 0.5$  and  $\alpha = 1$ . For both values of  $\alpha$ , it is observed that skin friction coefficient for  $Cu$  – water copper is higher than  $TiO_2$  – water and  $Al_2O_3$  – water (see Figs. 4.8 and 4.9). Figs. 4.10-4.13, show the behavior of variation of reduced Nusselt number with nanoparticle volume fraction  $\phi$ , for different nanoparticles. Fig. 4.10 and 4.11, depict the same behavior for  $\alpha = 0.5$  and  $\alpha = 1$  while the rest of the parameters are kept fixed. It is seen from Figs. 4.10 and 4.11, that there is a low heat transfer rate of  $TiO_2$  – water as compared to  $Cu$  – water and  $Al_2O_3$  – water. This is just because of low thermal conductivity of  $TiO_2$  when compared to other nanoparticles (see in Table. 4.1). It is also noticed that for negative values or in the absence of temperature exponent  $A$ , it may affects the heat transfer rate (see Figs. 4.12 and 4.13) for different nanoparticles. Opposite trend of reduced Nusselt number is shown in Fig. 4.12 when it is compared with Fig. 4.11. Moreover, in the absence of temperature exponent heat transfer of alumina ( $Al_2O_3$ ) is higher than both copper ( $Cu$ ) and titanium ( $TiO_2$ ) (see Fig. 4.13).

**Table 4.1:** Thermophysical properties of base fluid and nanoparticles.

Physical properties	Fluid Phase (Water)	$Cu$	$Al_2O_3$	$TiO_2$
$C_p$ (J/kg K)	4179	385	765	686.2
$\rho$ (kg/m <sup>3</sup> )	995.1	8933	3970	4250
$k$ (W/mk)	0.613	400	40	6.9538
$\alpha \times 10^7$ (m <sup>2</sup> /s)	1.47	1166.1	131.7	30.7

**Table 4.2:** Comparison of Numerical Values for local Nusselt number  $Re_x^{-1/2} Nu_x$  in the absence of nanoparticles ( $\phi=0$ ) and  $\alpha = 0$ .

Pr ↓	A ↓	Magyari and Keller [19]	C. Liu et al [20]	Present study
1	-1.5	0.377410	0.37741256	0.377412
	0	-0.549643	-0.54964375	-0.549646
	1	-0.954782	-0.95478270	-0.954786
	3	-1.560294	-1.56029540	-1.560295
5	-1.5	1.353240	1.35324050	1.3532405
	0	-1.521243	-1.52123900	-1.521240
	1	-5.500135	-5.50013157	-5.500135
	3	-6.886555	-6.88655510	-6.886555
10	-1.5	5.200000	5.20002816	5.200028
	0	-5.257429	-5.25742372	-5.257424
	1	-6.660379	-6.66037218	-6.660372
	3	-5.635369	-5.62819631	-5.628196

**Table 4.3:** Comparison of numerical values for local Nusselt number  $Re_x^{-1/2} Nu_x$  in the absence of nanoparticles ( $\phi=0$ ).

		A=-2		A=0		A=2	
$\alpha$ ↓	Pr ↓	Liu et al [20]	Present study	Liu et al [20]	Present study	Liu et al [20]	Present study
0.0	0.7	0.6236183	0.62362	-0.4258380	-0.42584	-1.6416592	-1.64166
	5.0	5.9409444	5.94093	-1.8466056	-1.84661	-5.8978037	-5.89780
0.5	0.7	0.7637845	0.76377	-0.5215410	-0.52154	-5.0106136	-5.01061
	5.0	5.2761412	5.27614	-5.2616208	-5.26162	-5.2233049	-5.22331
1.0	0.7	0.8819431	0.88194	-0.6022235	-0.60222	-5.3216566	-5.32164
	5.0	6.4017642	6.40175	-5.6114948	-5.61150	-6.3407540	-6.34075

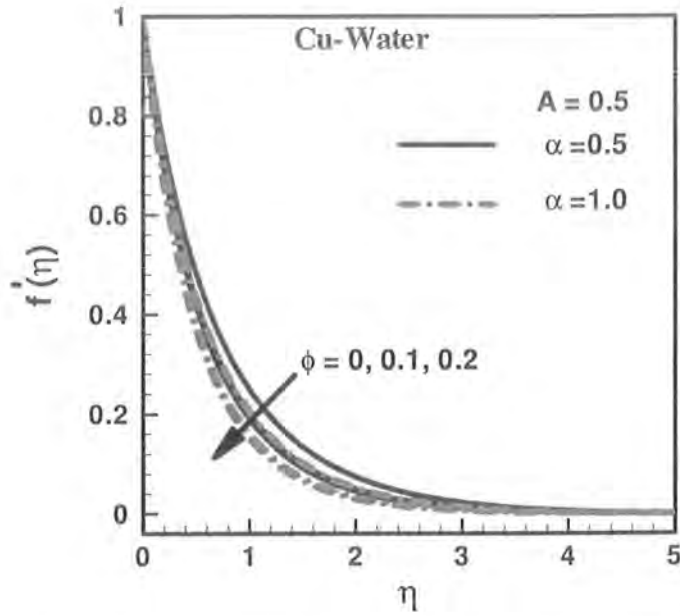


Fig 4.2: Variation of  $f'(\eta)$  for different values of  $\phi$  for *Cu*-water nanofluid when  $Pr=6.5$ .

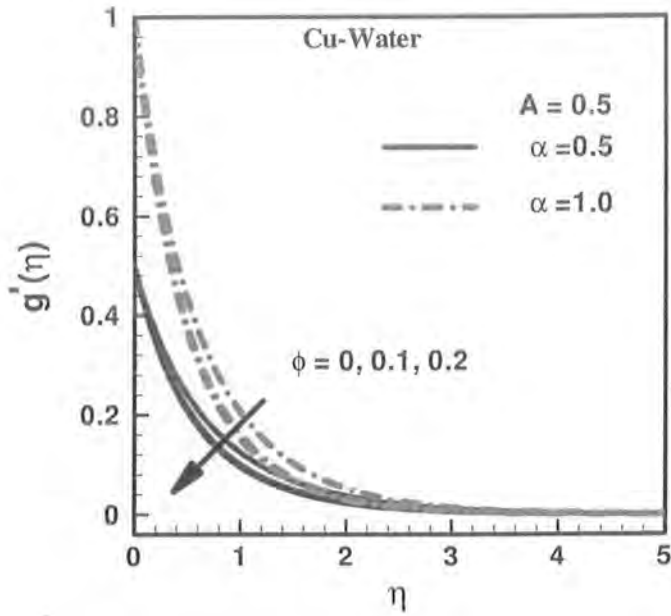


Fig 4.3: Variation of  $g'(\eta)$  for different values of  $\phi$  for *Cu*-water nanofluid when  $Pr=6.5$ .

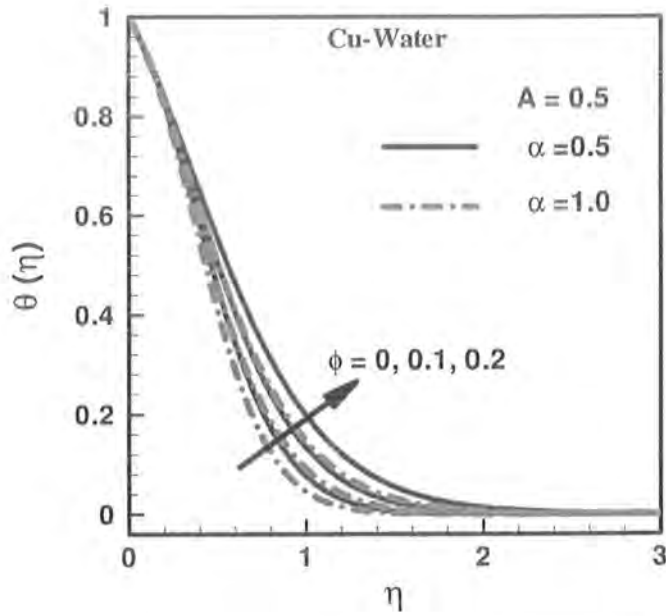


Fig 4.4: Variation of  $\theta(\eta)$  for different values of  $\phi$  for Cu--water nanofluid when  $Pr=6.5$ .

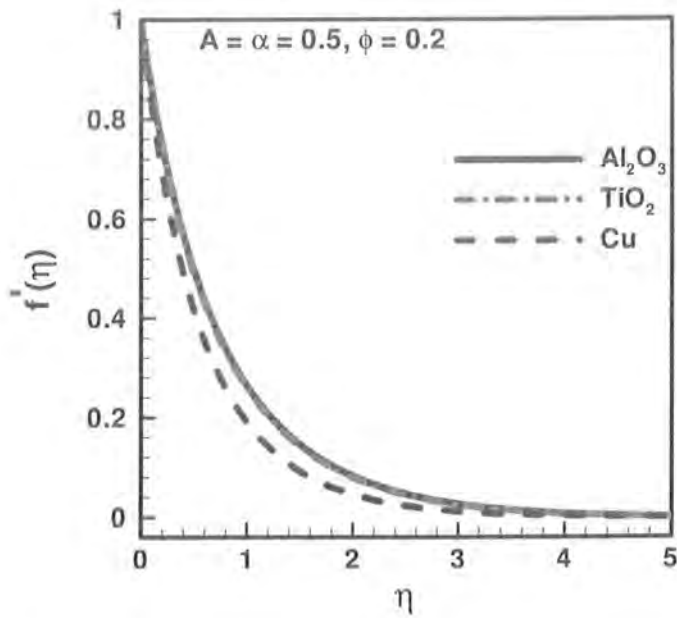


Fig 4.5: Variation of  $f'(\eta)$  for each kind of nanoparticles when  $Pr=6.5$ .

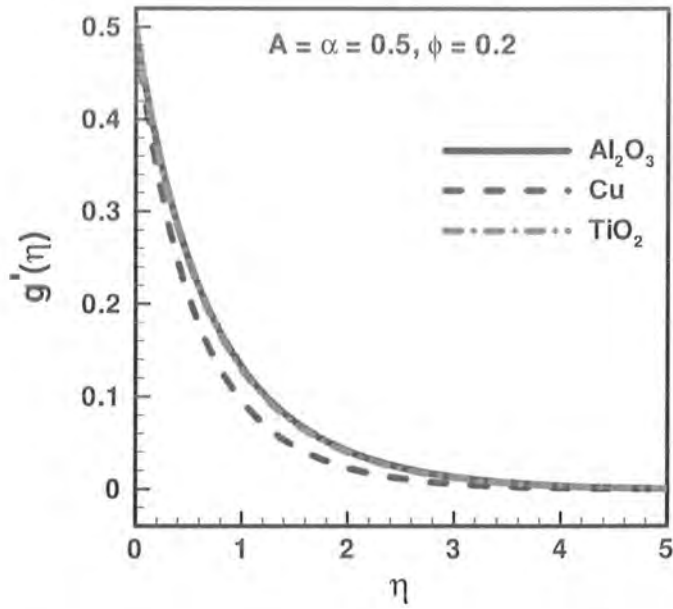


Fig 4.6: Variation of  $g'(\eta)$  for each kind of nanoparticles when  $\text{Pr}=6.5$ .

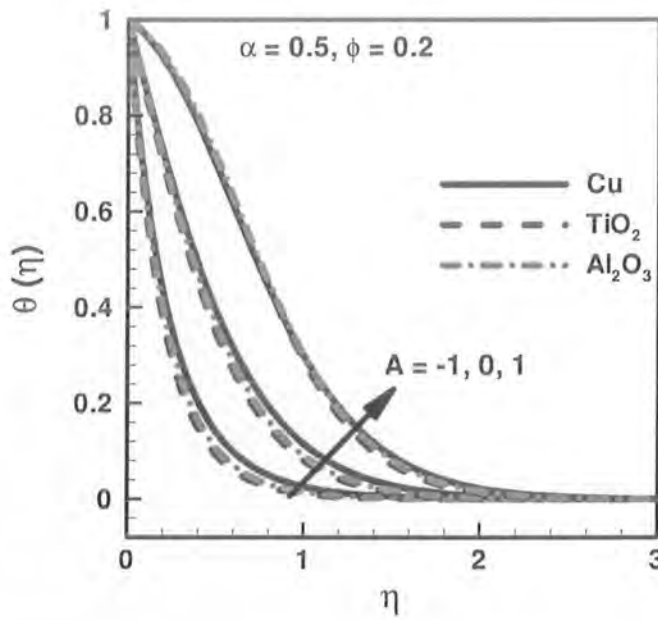


Fig 4.7: Variation of  $\theta(\eta)$  for each kind of nanoparticles when  $\text{Pr}=6.5$ .

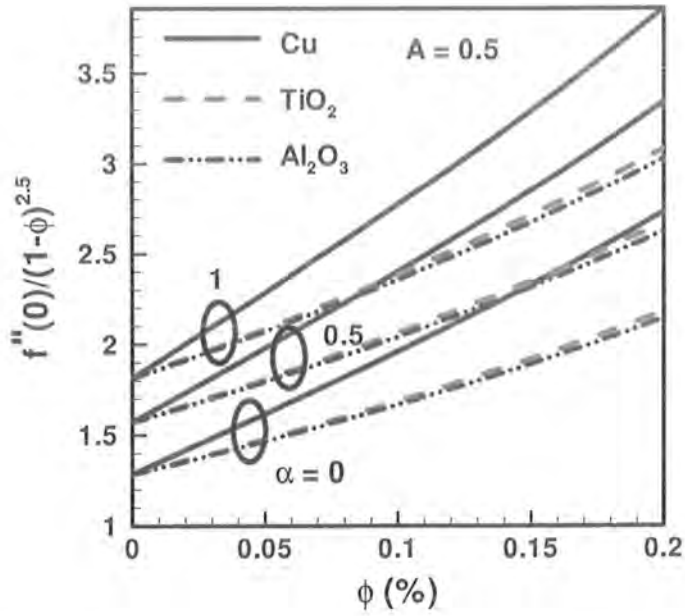


Fig 4.8: Variation of the skin friction coefficient along the  $x$ -direction with  $\phi$  for different nanoparticles when  $\text{Pr}=6.5$ .

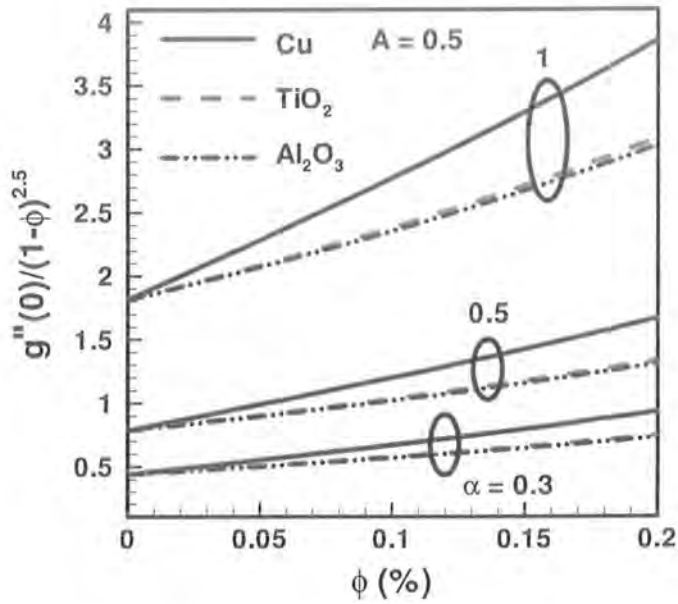


Fig: 4.9: Variation of the skin friction coefficient along the  $y$ -direction with  $\phi$  for different nanoparticles when  $\text{Pr}=6.5$ .

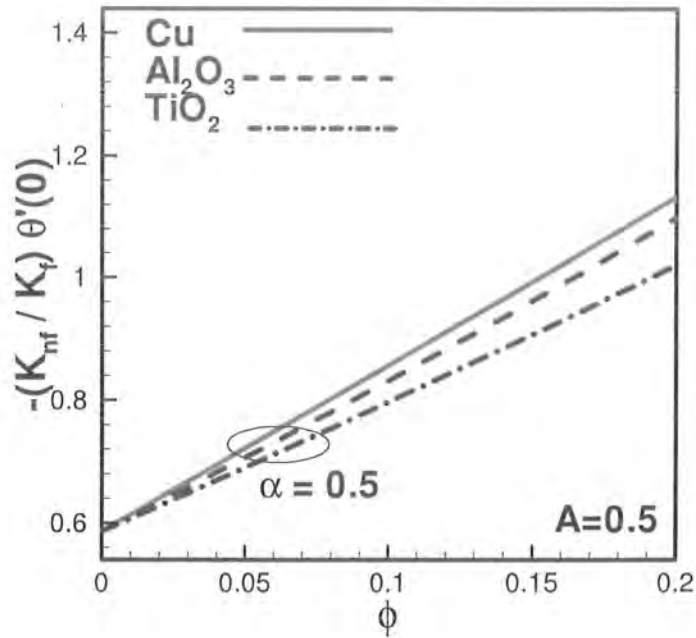


Fig 4.10: Variation of the Nusselt number with  $\phi$  for different nanoparticles when  $Pr=6.2$  and  $\alpha = 0.5$ .

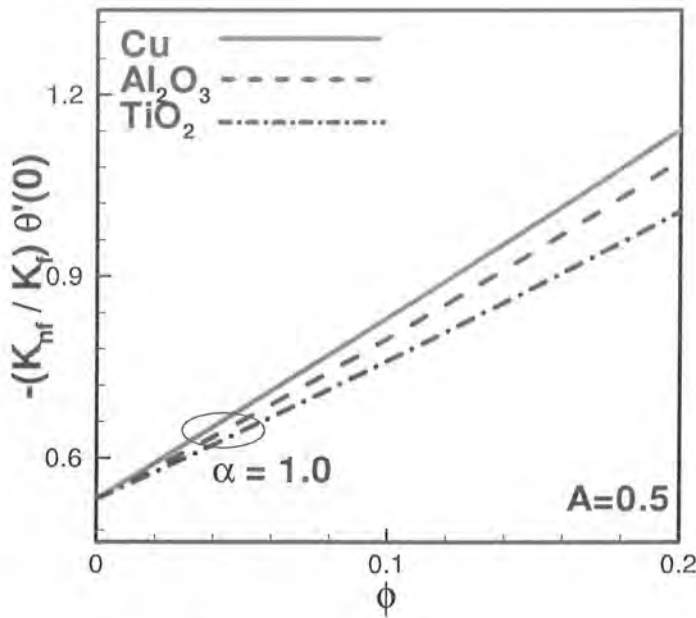


Fig 4.11: Variation of the Nusselt number with  $\phi$  for different nano particles when  $Pr=6.2$  and  $A=0$ .

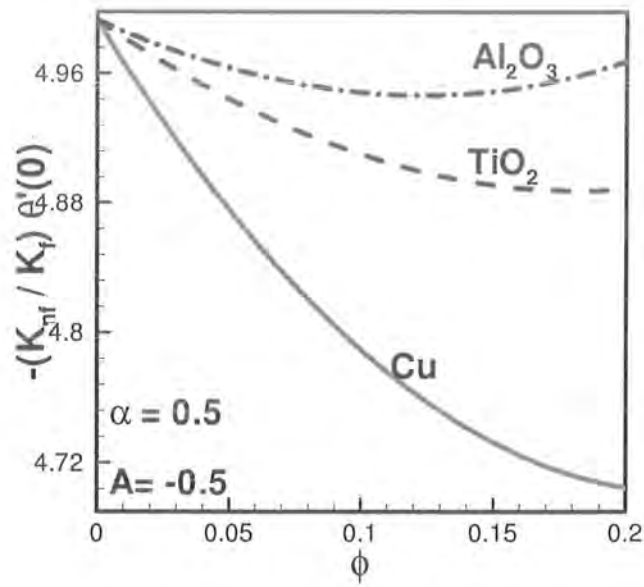


Fig 4.12: Variation of the Nusselt number with  $\phi$  for different nanoparticles when  $\text{Pr}=6.2$  and  $A=-0.5$ .

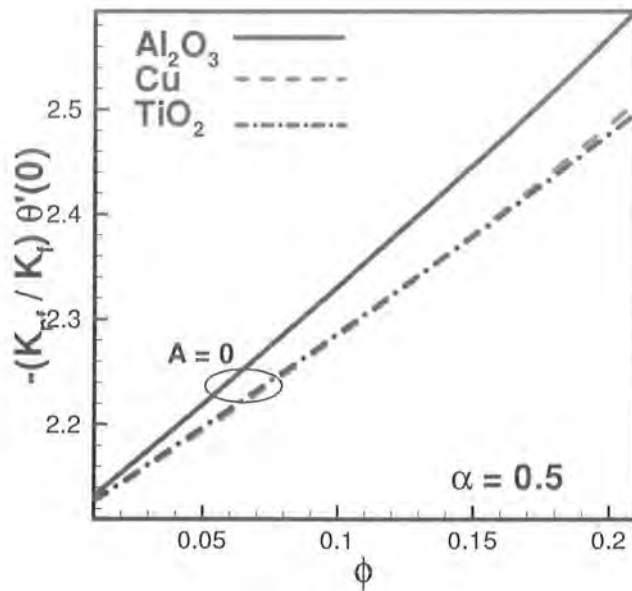


Fig 4.13: Variation of the Nusselt number with  $\phi$  for different nanoparticles when  $\text{Pr}=6.2$  and  $A=0$ .



## 4.5 Key findings

Three dimensional Water-based nanofluid flow over an exponentially stretching sheet has studied numerically. Three kind of metallic particles ( $Cu$ ,  $TiO_2$  and  $Al_2O_3$ ) are saturated with in the base fluid and the behavior of the each mixture is discussed against various values of fluid control parameters. Summary of present work is listed below:

- It is seen that velocities  $f'(\eta)$  and  $g'(\eta)$  decreases with the increasing values of  $\phi$  and the boundary layer thickness also decreases.
- It is also depicted that the temperature profile  $\theta(\eta)$  increases with an increase of nanoparticle volume fraction  $\phi$ .
- Increasing behavior is found for velocities  $f'(\eta)$  and  $g'(\eta)$  for  $Cu$ -water,  $TiO_2$ -water and  $Al_2O_3$ -water.
- It is found that temperature profile  $\theta(\eta)$  is decreasing function in view of  $Cu$ -water,  $TiO_2$ -water and  $Al_2O_3$ -water.
- Same decreasing behavior is found in x- and y-direction for skin friction coefficient with different nanoparticles.
- The heat transfer rate varies with  $A=-0.5$ ,  $A=0$  and  $A=0.5$  for different nanoparticles.

# Convective heat transfer and MHD effects on Casson nanofluid flow over a stretching/shrinking sheet

## 5.1 Introduction

This chapter examines the two dimensional magnetohydrodynamic (MHD) boundary layer flow of a Casson nanofluid over an exponentially permeable shrinking sheet with convective boundary condition using Buongiorno's model. Moreover, we have considered the suction/injection effects on the wall. Mathematical formulation of the problem has been constructed according the above mentioned consideration. By applying the appropriate transformations, system of non-linear partial differential equation along with the boundary conditions are transformed to couple non-linear ordinary differential equations. The resulting systems of non-linear ordinary differential equations are solved numerically using Shooting method. Numerical results for velocity, temperature and nanoparticle volume concentration are presented through graphs for various values of dimensionless parameters. Effects of parameters for heat transfer at wall and nanoparticle volume concentration are also presented through graphs and tables. One of the sections consist of dual solution but in the present chapter our main emphasis is to analyze the results of Casson nanofluid flow and heat transfer so later we discard the unstable part of the dual solution and solutions are only constructed for stable part. At the end, fluid flow behavior is examined through stream lines. Concluding remarks are provided under the observation of whole analysis.

## 5.2 Fundamental equations of Buongiorno's Model

Expressions of conservation laws of mass, momentum, temperature and nanoparticle volume fraction in an incompressible fluid are [31]

$$\operatorname{div} V = 0, \quad (5.1)$$

$$\rho_f \frac{dV}{dt} = -\nabla P + \mu \nabla^2 V, \quad (5.2)$$

$$(\rho c)_f \frac{dT}{dt} = k \nabla^2 T + (\rho c)_p (D_B \nabla C \cdot \nabla T + (D_T / T_\infty) \nabla T \cdot \nabla T), \quad (5.3)$$

$$\frac{dC}{dt} = D_B \nabla^2 C + (D_T / T_\infty) \nabla^2 T, \quad (5.4)$$

Where  $\rho_f$  is the fluid density,  $\rho_p$  the density of the particle,  $c_p$  and  $c_f$  is the heat capacity of the particle and water respectively,  $V$  is the velocity of nanofluid,  $d/dt$  is the material time derivative,  $P$  is the pressure,  $T$  is the temperature of nanofluid,  $C$  is the nanoparticle volume concentration,  $T_\infty$  is the ambient temperature of nanofluid,  $D_B$  the Brownian diffusion coefficient and  $D_T$  is the thermophoretic diffusion coefficient.

## 5.3 Mathematical model

We adjust the geometry of the problem in the Cartesian coordinate system such that  $x$  – axis is taken horizontally and  $y$  – axis is perpendicular to it. The steady situation of two dimensional flow past a shrinking sheet is considered. Moreover, we have considered the Casson nanofluid flow in the presence of magnetohydrodynamic that is normal to the nanofluid and the nanofluid is placed at  $y \geq 0$ , where  $y$  is the coordinate measured normal to the shrinking

surface. Here we are considering the rheological equation of extra stress tensor ( $\tau$ ) for an isotropic and incompressible flow of a Casson fluid can be written as [21]

$$\tau_{ij} = \begin{cases} (\mu_B + p_y / \sqrt{2\pi}) 2e_{ij}, & \pi > \pi_c \\ (\mu_B + p_y / \sqrt{2\pi}) 2e_{ij}, & \pi < \pi_c \end{cases} \quad (5.5)$$

where  $\mu$  is the dynamic viscosity,  $\mu_B$  is plastic dynamic viscosity of the non-Newtonian fluid,  $p_y$  is the yield stress of fluid,  $\pi$  is the product of the component of deformation rate with itself, namely,  $\pi = e_{ij}e_{ij}$ ,  $e_{ij}$  is the  $(i, j)$ -th component of the deformation rate and  $\pi_c$  is critical value of this product based on non-Newtonian model. We assumed that the sheet is shrank exponentially with velocity  $u(x) = U_w \exp(\frac{x}{l})$ , where  $U_w > 0$  is constant and  $x$  is the coordinates along the shrinking surface. Moreover, convective condition is also considering at the wall having temperature  $T_f$  when the fluid is passing over the shrinking surface. The boundary layer equations of (5.1)-(5.4) for two dimensional incompressible Casson nanofluid takes the following form

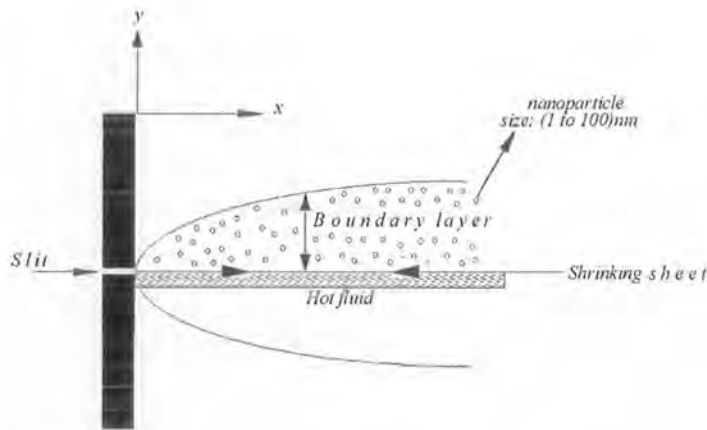


Fig 5.1: Geometry of the problem.

$$\frac{\partial u}{\partial x} + \frac{\partial v}{\partial y} = 0, \quad (5.6)$$

$$u \frac{\partial u}{\partial x} + v \frac{\partial u}{\partial y} = \nu \left( 1 + \frac{1}{\beta} \right) \frac{\partial^2 u}{\partial y^2} - \frac{\sigma B^2}{\rho_f} u, \quad (5.7)$$

$$u \frac{\partial T}{\partial x} + v \frac{\partial T}{\partial y} = \alpha \left( \frac{\partial^2 T}{\partial y^2} \right) + \tau \left\{ D_B \left( \frac{\partial C}{\partial y} \frac{\partial T}{\partial y} \right) + \left( \frac{D_T}{T_\infty} \right) \left( \frac{\partial T}{\partial y} \right)^2 \right\}, \quad (5.8)$$

$$u \frac{\partial C}{\partial x} + v \frac{\partial C}{\partial y} = D_B \left( \frac{\partial^2 C}{\partial y^2} \right) + \left( \frac{D_T}{T_\infty} \right) \left( \frac{\partial^2 T}{\partial y^2} \right), \quad (5.9)$$

where  $u$  and  $v$  denote the respective velocities in the  $x$  – and  $y$  – directions respectively,  $\beta = \mu_B \sqrt{2\pi}$  is the non-Newtonian (Casson) fluid parameter,  $\nu (= \mu_B / \rho_{nf})$  is the kinematic viscosity,  $\alpha$  is the thermal diffusivity,  $D_B$  is the Brownian diffusion coefficient,  $D_T$  is the thermophoretic diffusion coefficient,  $\tau = \frac{(\rho c)_p}{(\rho c)_f}$  is the ratio between the effective heat capacity of the nanoparticle material and heat capacity of the fluid, in which  $\rho_f$  is the density of fluid and  $\rho_p$  is the density of the particles. It is also considered that the magnetic field  $B(x)$  is of the form

$$B = B_0 \exp(x / l), \quad (5.10)$$

where  $B_0$  is the constant magnetic field. The corresponding boundary conditions are

$$\left. \begin{aligned} u_w(x) = U_w \exp(x / l), \quad v_w(x) = V_0 \exp(x / 2l), \\ -k_f \frac{\partial T}{\partial y} = h_f(T_f - T), \quad C = C_w \end{aligned} \right\} \text{at } y = 0, \quad (5.11)$$

$$u \rightarrow 0, v \rightarrow 0, T \rightarrow T_\infty, C = C_\infty \text{ as } y \rightarrow \infty. \quad (5.12)$$

In the above expression,  $u_w(x)$  is the stretching/shrinking velocity of the fluid with  $U_w$  is the stretching/shrinking constant, here it is notice that for  $v_w(x)$  is mass transfer velocity (with  $V_0 > 0$  for mass injection and  $V_0 < 0$  for mass suction),  $k_f$  is the thermal conductivity of the fluid,  $h_f$  is the convective heat transfer coefficient,  $T_f$  is the convective fluid temperature below the shrinking sheet. Introducing the following similarity transformations

$$\begin{aligned} u &= U_0 \exp(x/l) f'(\eta) \text{ and } v = -\sqrt{\nu U_0 / 2l} \exp(x/2l) \{f(\eta) + \eta f'(\eta)\}, \\ \eta &= y \sqrt{\frac{U_0}{2\nu l}} \exp(x/2l), \quad \theta = \frac{T - T_\infty}{T_w - T_\infty}, \quad \phi = \frac{C - C_\infty}{C_w - C_\infty}. \end{aligned} \quad (5.13)$$

Making use of Eq. (5.13), the equation of continuity is identically satisfied and Eqs. (5.7)-(5.9) along with the boundary conditions (5.11) and (5.12) take the following form

$$(1 + 1/\beta) f''' - M^2 f' - 2(f')^2 + ff'' = 0, \quad (5.14)$$

$$\theta'' + \text{Pr}((f\theta' - f'\theta) + Nb\theta'\phi' + Nt(\theta')^2) = 0, \quad (5.15)$$

$$\phi'' + \text{LePr}(f\phi' - f'\phi) + \frac{Nt}{Nb}\theta'' = 0, \quad (5.16)$$

$$f(\eta) = S, f'(\eta) = \lambda, \theta'(\eta) = -Bi(1 - \theta(0)) \text{ and } \phi(\eta) = 1 \text{ at } \eta = 0, \quad (5.17)$$

$$f'(\eta) = 0, \theta(\eta) = 0, \phi(\eta) = 0 \text{ at } \eta \rightarrow \infty. \quad (5.18)$$

Here prime indicates differentiation with respect to  $\eta$ ,  $M^2 = 2\sigma B_0^2 l / \rho U_0$  is the magnetic parameter,  $S$  is the suction/injection parameter,  $\lambda = U_w / U_0$  is the stretching/shrinking parameter (with  $\lambda > 0$  for stretching surface case,  $\lambda < 0$  is for shrinking

surface and  $\lambda = 0$  is for flat surface),  $Pr = \nu / \alpha_D$  is the Prandtl number,  $Nb = (\rho c)_p D_B (C_w - C_\infty) / \nu (\rho c)_f$  is the Brownian motion parameter,  $Nt = (\rho c)_p D_T (T_f - T_\infty) / \nu T_\infty (\rho c)_f$  is the thermophoresis parameter,  $Le = \alpha_D / D_B$  is the Lewis number and  $Bi = (h_f / k_f) \sqrt{2l\nu / U_0}$  is the Biot number.

Expressions for skin friction coefficient  $C_f$ , local Nusselt number  $Nu_x$  and the local Sherwood number  $Sh_x$  are

$$C_{fx} = \frac{\tau_{wx}}{\rho u_w}, \quad Nu_x = \frac{xq_w}{k(T_f - T_\infty)}, \quad Sh_x = \frac{xq_m}{D_B(C_w - C_\infty)}, \quad (5.19)$$

where  $\tau_{wx}$  is the wall shear stresses along  $x$ -direction. Here  $q_w$  and  $q_m$  are the heat flux and the mass flux respectively, defined as:

$$q_w = -k \left( \frac{\partial T}{\partial y} \right)_{y=0}, \quad q_m = -D_B \left( \frac{\partial C}{\partial y} \right)_{y=0}. \quad (5.20)$$

Eq. (5.19) takes the following dimensionless form

$$Re_x^{1/2} C_{fx} = (1 + \frac{1}{\beta}) f''(0), \quad Re_x^{-1/2} Nu_x = -\theta'(0), \quad Re_x^{-1/2} Sh_x = -\phi'(0). \quad (5.21)$$

Here  $Re_x = (xU_0 e^{x/l}) / \nu$  is the local Reynolds number.

## 5.4 Numerical Technique

Numerical solutions to the coupled nonlinear ordinary differential equations (5.14)–(5.16) along with the boundary conditions (5.17) and (5.18) are obtained using the shooting

method. First we convert the boundary value problem (BVP) into the initial value problem (IVP) and assume a suitable finite value for the far field boundary condition, i.e.  $\eta \rightarrow \infty$ , say  $\eta_\infty$ . We then rewrite the system of equations (5.14)–(5.16) in the following form:

$$f''' = \left(1 + \frac{1}{\beta}\right)^{-1} (M^2 f' + 2(f')^2 - ff''), \quad (5.22)$$

$$\theta'' = -\text{Pr} \left( (f\theta' - f'\theta) + Nb\theta'\phi' + Nt(\theta')^2 \right), \quad (5.23)$$

$$\phi'' = -Le \text{Pr} (f\phi' - f'\phi) - \frac{Nt}{Nb} \theta''. \quad (5.24)$$

To convert the above system of coupled higher order nonlinear differential equations into the system of first order differential equations, we introduce:

$$\begin{aligned} x_1 &= f, & x_2 &= x_1' = f', & x_3 &= x_2' = f'', \\ y_1 &= \theta, & y_2 &= y_1' = \theta', \\ z_1 &= \phi, & z_2 &= z_1' = \phi'. \end{aligned} \quad (5.25)$$

Hence, the equations (5.22)–(5.24) take the following form:

$$x_3' = \left(1 + \frac{1}{\beta}\right)^{-1} (M^2 x_2 + 2x_2^2 - x_1 x_3), \quad (5.26)$$

$$y_2' = -\text{Pr} \left( (x_1 y_1 - x_2 y_1) + Nb y_2 z_2 + Nt (y_2)^2 \right), \quad (5.27)$$

$$z_2' = -Le \text{Pr} (x_1 z_2 - x_2 z_1) - \frac{Nt}{Nb} y_2', \quad (5.28)$$

with the boundary conditions are defined as

$$x_1 = S, \quad x_2 = \lambda, \quad y_2 = -Bi(1 - y_1), \quad z_1 = 1 \quad \text{at } \eta = 0, \quad (5.29)$$

$$x_2 = 0, \quad y_1 = 0, \quad z_1 = 0 \quad \text{at } \eta \rightarrow \infty. \quad (5.30)$$



In order to solve (5.26)–(5.28) subject to (5.29)–(5.30) as an IVP, the values for  $x_3(0)$ ,  $y_2(0)$  and  $z_2(0)$ , i.e.  $f''(0)$ ,  $\theta(0)$  and  $\phi'(0)$  for instance, are needed but not given prior to the computation. Thus the initial guess values of  $f''(0)$ ,  $\theta(0)$  and  $\phi'(0)$  are chosen and the Runge-Kutta method is applied to obtain the solution. The step size  $\Delta\eta = 0.001$  is used to obtain the numerical solution with  $\eta_{\max}$ , with accuracy to the fifth decimal place is chosen as the criterion of convergence. The asymptotic boundary conditions given by Eq. (5.18) were replaced by using a value similarity variable  $\eta_{\max} = 12$  as follows:

$$f'(\eta_{\max}) = 0, \theta(\eta_{\max}) = 0 \text{ and } \phi(\eta_{\max}) = 0. \quad (5.31)$$

The choice of  $\eta_{\max} = 12$  ensures that all numerical solutions approached the asymptotic values correctly.

## 5.5 Dual solutions

In this section dual solutions have been constructed for various values of emerging parameters involved in the momentum equations for skin friction coefficient. Fig. 5.2 shows that it is possible to get dual solutions of the boundary layer equations for shrinking parameter  $\lambda < 0$ . These dual solutions in the range of  $\lambda_c < \lambda < 0$  and solution does not exist for  $\lambda < \lambda_c < 0$ , where  $\lambda_c$  is the minimum value of  $\lambda$  for which the solution exists. It is found that decreasing the values of  $|\lambda_c|$  promotes a gradual increase in the skin friction coefficient with respect to increasing values of both the magnetic parameter  $M$  and the non-Newtonian fluid parameter  $\beta$ . This shows that higher values of  $M$  and  $\beta$  decrease the range of the existence of the solution to the proposed boundary value problem. The procedure for describing the stability of dual solutions is extensively available in the literature [22] and [23]. In the above mentioned

literature, it was discussed that in dual nature solution, probably one of the solution is stable while the other is physically not stable. So in the present study we only analyze the stable case with Casson nanofluid and discard the unstable case.

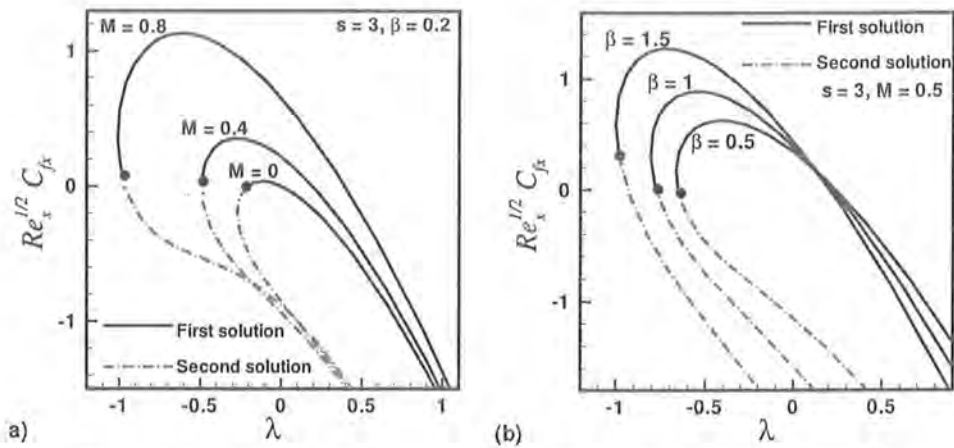


Fig 5.2: Dual solutions for various values of MHD parameter  $M$  and Casson fluid parameter  $\beta$ .

## 5.6 Results and discussions

In the present section we will discuss the velocity profile  $f'(\eta)$ , temperature profile  $\theta(\eta)$  and nanoparticle volume concentration  $\phi(\eta)$  for various physical parameters such as Casson fluid parameter  $\beta$ , Hartmann number  $M$ , suction/injection parameter  $S$ , Biot number  $Bi$ , Prandtl number  $Pr$ , thermophoresis parameter  $Nt$ , Brownian motion parameter  $Nb$  and Lewis number  $Le$ . It is noticed that all the graphical results are depicted for shrinking case  $\lambda = -1$ . It can be found through Table 5.1, for infinitely large values of Casson fluid parameter ( $\beta \rightarrow \infty$ ) our problem reduces to Newtonian fluid. Similarly we can observe that our problem more simplified for constant wall temperature with infinitely large value of Biot number ( $Bi \rightarrow \infty$ ). In addition we can see through Table 5.1, when we discard the nanoparticles and

suction/injection effects; our problem gives the excellent comparison with the results provided by different authors.

From Fig. 5.3, it is observed for higher values of  $M$  it reduce both boundary layer thickness and the magnitude of the velocity. This phenomenon occurs when magnetic field induced current in the conductive fluid, then it creates a resistive-type force on the fluid in the boundary layer which slows down the motion of the fluid. Exactly the same behavior is shown for temperature and nanoparticle volume concentration. So finally, it is concluded that magnetic field is used to control boundary layer separation. Same sort of behavior appears when we compare Fig. 5.4 with Fig. 5.3 for higher values of  $S$ . Fig. 5.5 depicts the effects of non-Newtonian parameter  $\beta$  on the velocity profile  $f'(\eta)$ . Here it is observed that for higher values of non-Newtonian parameter  $\beta$ , it produces resistance in the motion of fluid. That fact is seen in Fig. 5.5, the velocity profile  $f'(\eta)$  and the boundary layer thickness decrease for higher values of  $\beta$ . From Fig. 5.6, we can observe that increasing non-Newtonian parameter will reduce the temperature profile. Moreover, for higher values of non-Newtonian parameter  $\beta$ , the boundary layer thickness decreases (see Fig. 5.4). It is noticed when we increase the non-Newtonian parameter  $\beta$  to infinity, the problem in the given case reduces to Newtonian fluid. Fig. 5.6 shows the behavior of Prandtl number on temperature profile and nanoparticle volume concentration because the Prandtl number is a ratio of kinematic viscosity to thermal diffusivity. Consequently, for higher values of Prandtl number it reduces the thermal diffusivity (see Fig. 5.6). Same behavior can be observed for nanoparticle volume concentration against the Prandtl number when we compare temperature profile with nanoparticle volume concentration.

Effects of Biot number  $Bi$  on temperature and nanoparticle volume concentration are mentioned in (Figs. 5.7 and 5.8). Physically, Biot number is expressed as the convection at the

surface of the body to the conduction within the surface of the body. When thermal gradient applied to the surface then the ratio governs the temperature inside a body varies significantly, while the body heats or cools over a time. Normally, for uniform temperature field inside the surface, we considered  $Bi \ll 1$ . However,  $Bi \gg 1$  depicts that the temperature field inside the surface is not uniform. In Fig. 5.6, we have discussed the effects of Biot number  $Bi$  on temperature profile  $\theta(\eta)$  in three ways. First one is the case when  $Bi < 0.1$ . It is observed from Fig. 5.6 that for smallest values of the Biot number ( $Bi < 0.1$ ), the variation of temperature within the body is slight and can reasonably be approximated as being uniform. While in the second case for  $Bi > 0.1$ , one depicts that the temperature within the body do not perform uniform behavior (see Fig. 5.7). The last case relates when we consider very large value of Biot number corresponds to the case of constant wall temperature (see Fig. 5.7). Same sort of behavior can be seen for nanoparticle volume concentration  $\phi(\eta)$  against the Biot number  $Bi$ , when we compare Fig. 5.8 with the Fig. 5.5. The effect of Brownian motion parameter  $Nb$  on the temperature profile  $\theta(\eta)$  is presented in Fig. 5.4. Here we can observe that with an increase in the motion of Brownian parameter  $Nb$ , the temperature profile  $\theta(\eta)$  increases. These phenomenon present that the enhanced thermal conductivity of a nanofluid is mainly due to Brownian motion which producing micro-mixing, whereas for large value of Brownian parameter  $Nb$ , it reduces the nanoparticle volume concentration  $\phi(\eta)$  (see Fig. 5.9). Similar behavior can be observed when we compare Fig. 5.10 with Fig. 5.9 for temperature profile while nanoparticle volume concentration  $\phi(\eta)$  increases with an increase of thermophoresis parameter  $Nt$ . Finally from Figs. 5.9 and 5.10, it is observed that both Brownian motion and thermophoresis parameter present same sort of behavior for temperature profile while it presents opposite behavior for nanoparticle volume concentration. From Fig. 5.11, it depicts that with an

increase in Lewis number  $Le$ , temperature profile increases while the profile of nanoparticle concentration decreases.

Effects of physical parameters on skin friction coefficient  $(1 + \frac{1}{\beta})f''(0)$ , reduced Nusselt number  $Re_x^{-1/2}Nu$  and reduced Sherwood number  $Re_x^{-1/2}Sh$  are presented in Figs. 5.12-5.14. Through Fig. 5.12, the variation of skin friction along with the physical parameters  $s$  and  $M$  in both Newtonian ( $\beta = \infty$ ) and non-Newtonian ( $\beta \neq \infty$ ) are demonstrated. It is found that in case of Newtonian fluid, less friction occurs at the wall as compare to the non-Newtonian fluid, due to viscosity effects. It is observed from Fig. 5.13, that for higher values of Brownian motion parameter  $Nb$ , it reduces the Nusselt number. In both cases either  $Pr < Le$  or  $Pr > Le$ , same decreasing behavior can be observed for reduced Nusselt number  $Re_x^{-1/2}Nu$  against  $Nt$  for increasing values of Brownian motion parameter  $Nb$ , while the rest of the parameters are fixed. Fig. 5.14 depicts the trend of the reduced Sherwood number against thermophoresis parameter  $Nt$ , while for increasing values of Brownian parameter  $Nb$ , Sherwood number gives same increasing behavior. It can be seen from Fig. 5.14, in both cases either  $Pr < Le$  or  $Pr > Le$ . The Sherwood number presents similar behavior. Finally, we observed from Figs. 5.13 and 5.14 that for higher values of Prandtl number, it produces opposite trend for both heat transfer rate and mass transfer rate. The two dimensional view of variation of the stream lines are presented in Fig. 5.15, for  $S = -0.5$ ,  $S = 0$  and  $S = 0.5$ . Similarly, three dimensional view of the lines for stream function  $\psi(x, \eta)$  along with the dependent variables are presented in the Fig. 5.16. In Tables. 5.2, we have presented the numerical values of the local Nusselt number and Sherwood number for various values of Brownian parameter and thermophoresis parameter while the rest of parameters are fixed.

**Table 5.1:** Variation of local Nusselt number  $Re_x^{-1/2}Nu$  for several values of Prandtl number and magnetic parameter in the absence of nanofluid when  $s = 0$ ,  $\lambda = 1$  and  $Bi \rightarrow \infty$  (Newtonian fluid).

Pr	M	Magyari and Keller [19]	Bidin and Nazar [24]	El-Aziz [25]	Ishak [26]	Present study
1	0	0.9548	0.9547	0.9548	0.9548	0.9548
2	0	-	1.4714	-	1.4715	1.4714
3	0	1.8691	1.8691	1.8691	1.8691	1.8691
5	0	5.5001	-	5.5001	5.5001	5.5001
10	0	6.6604	-	6.6604	6.6604	6.6604
1	1	-	-	-	0.8611	0.8611

**Table 5.2:** Variation of local Nusselt number and Sherwood number with  $Nb$  and  $Nt$  for  $s = 3, \lambda = -1, M = 2, \beta = 3, Bi = 0.3, Pr = 6.2$  and  $Le = 1$ .

$Nt \downarrow$	$Nb = 0.3$		$Nb = 0.4$		$Nb = 0.5$	
	$Re_x^{-1/2}Nu_x$	$Re_x^{-1/2}Sh_x$	$Re_x^{-1/2}Nu_x$	$Re_x^{-1/2}Sh_x$	$Re_x^{-1/2}Nu_x$	$Re_x^{-1/2}Sh_x$
0.0	0.285867	16.001155	0.278889	16.001155	0.268004	16.001155
0.2	0.285633	15.794769	0.278355	15.844328	0.266763	15.873235
0.4	0.285388	15.588241	0.277782	15.687275	0.265386	15.744930
0.6	0.285130	15.381564	0.277166	15.529980	0.263844	15.616200
0.8	0.284860	15.174730	0.276501	15.372425	0.261709	15.228003

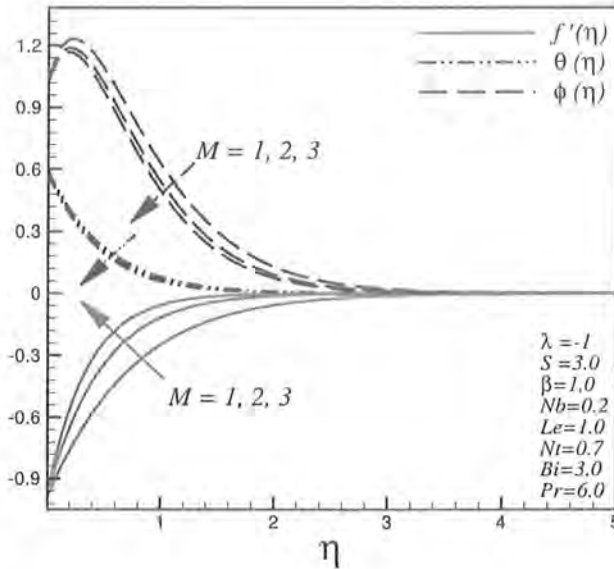


**Fig 5.3:** Effect of MHD parameter  $M$  on velocity, temperature and nanoparticle volume concentration.

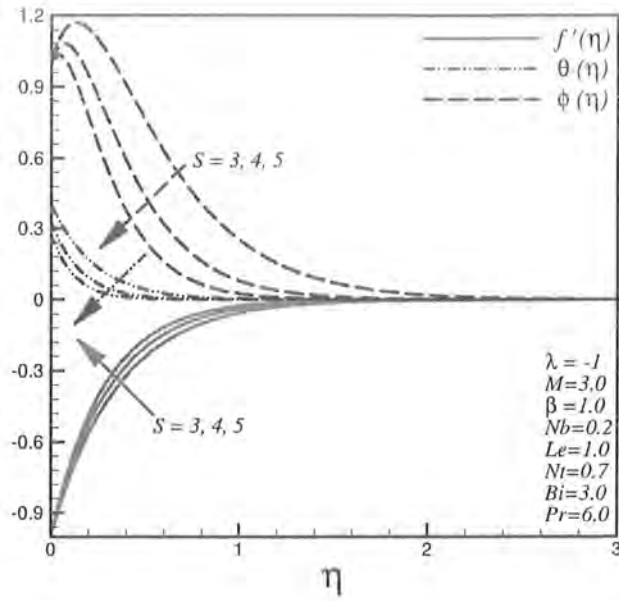


Fig 5.4: Effect of suction/injection parameter  $S$  on velocity, temperature and nanoparticle volume concentration.

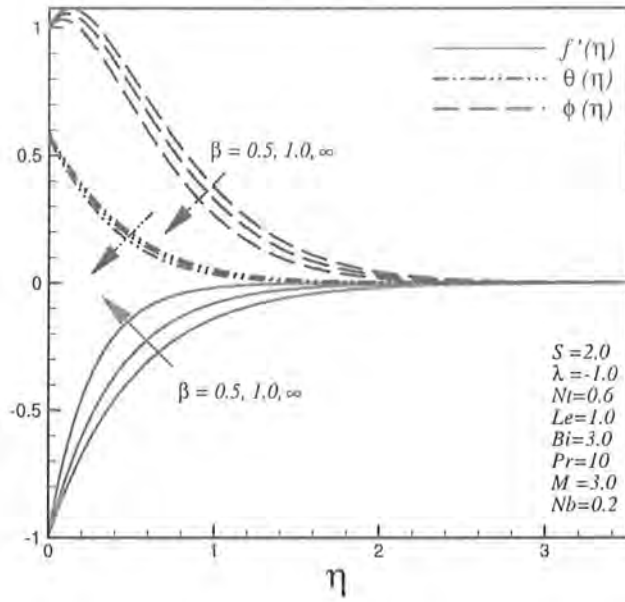


Fig 5.5: Effect of Casson fluid parameter  $\beta$  on velocity, temperature and nanoparticle volume concentration.

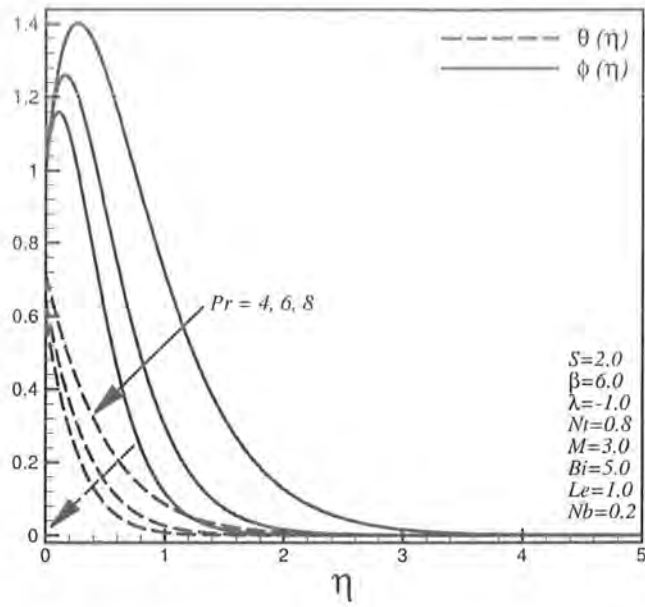


Fig 5.6: Effect of Prandtl number  $Pr$  on temperature and nanoparticle volume concentration.

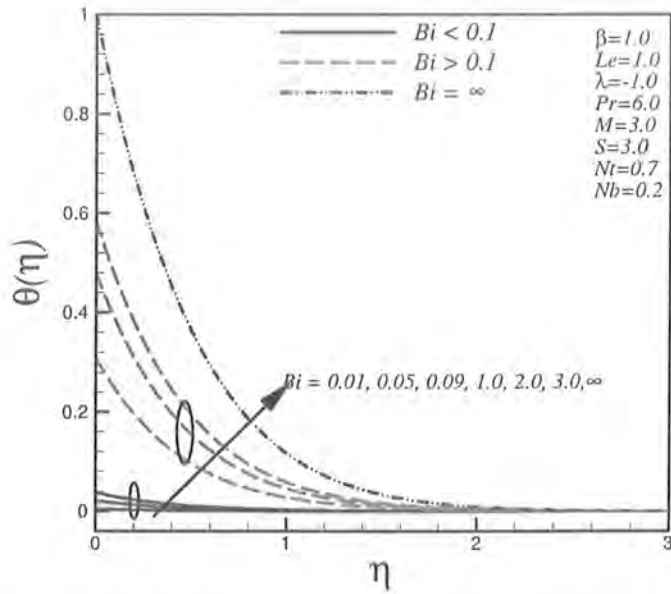


Fig 5.7: Effect of Biot number  $Bi$  on temperature profile.



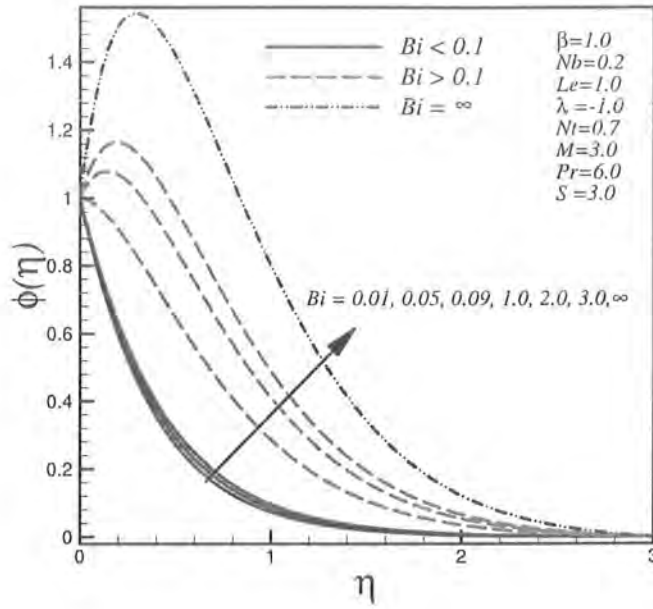


Fig 5.8: Effect of Biot number  $Bi$  on nanoparticle volume concentration.

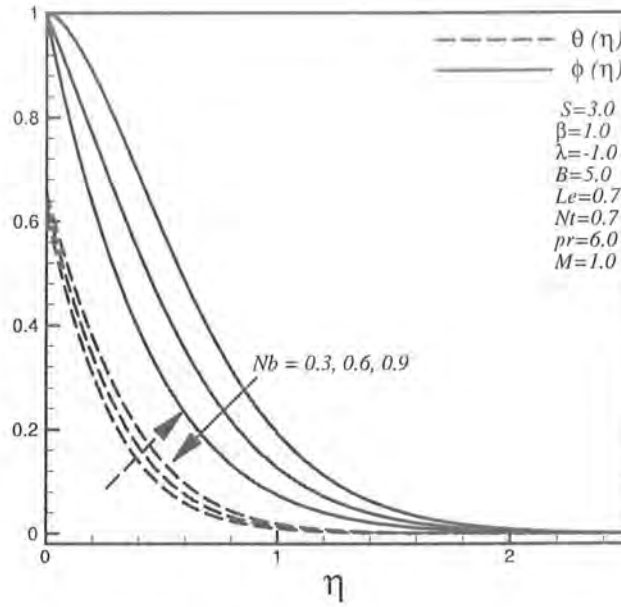


Fig 5.9: Effects of Brownian motion parameter  $Nb$  on temperature and nanoparticle volume concentration.

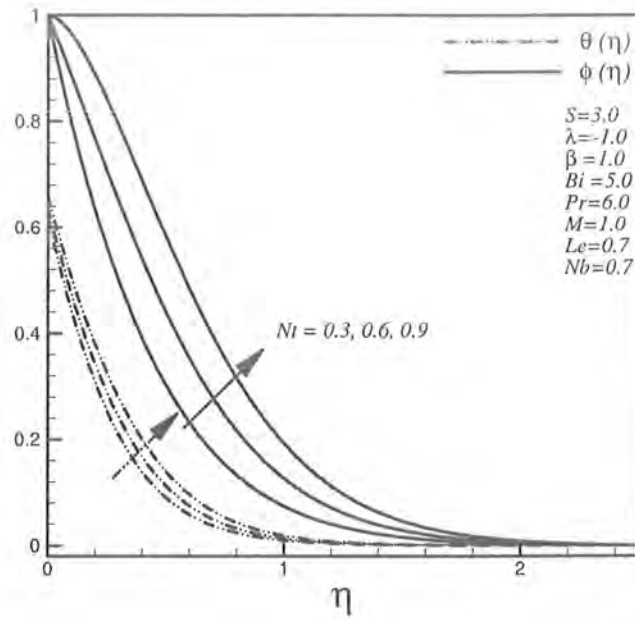


Fig 5.10: Effects of Brownian motion parameter  $Nt$  on temperature and nanoparticle volume concentration.

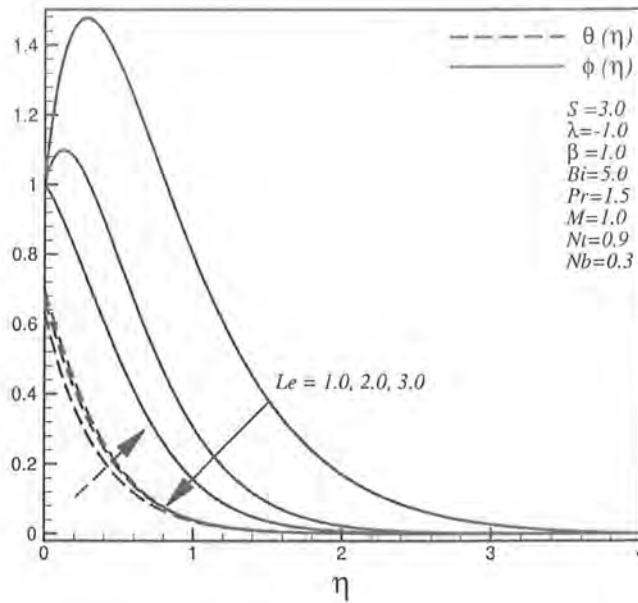


Fig 5.11: Effects of Lewis number  $Le$  on temperature and nanoparticle volume concentration.

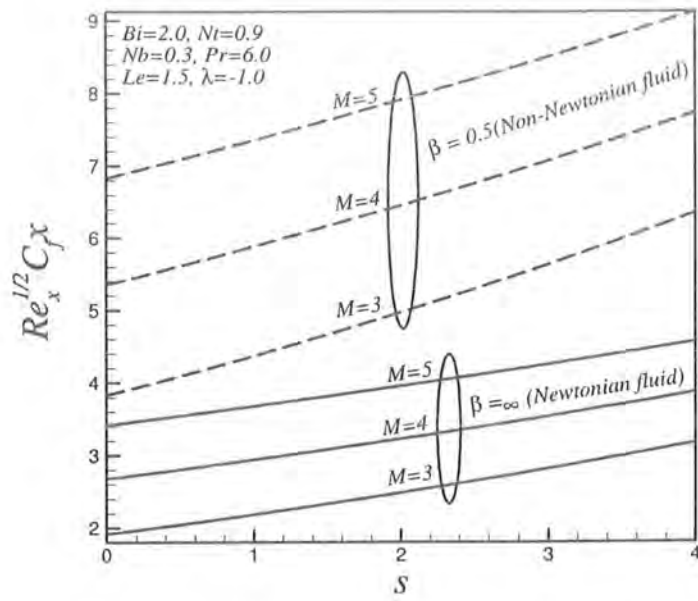


Fig 5.12: Effect of  $s, M$  and  $\beta$  on skin friction coefficient.

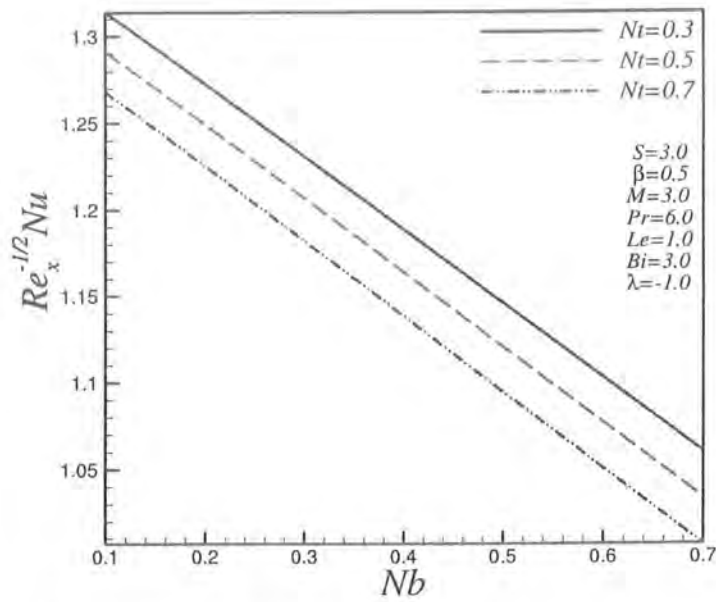


Fig 5.13: Effect of  $Nb$  and  $Nt$  on dimensionless heat transfer rates.

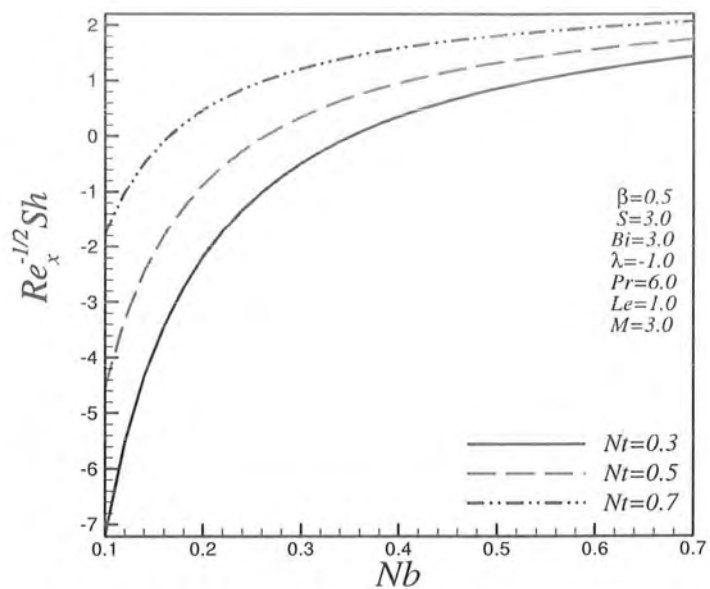


Fig 5.14: Effect of  $Nb$  and  $Nt$  on dimensionless concentration rates.

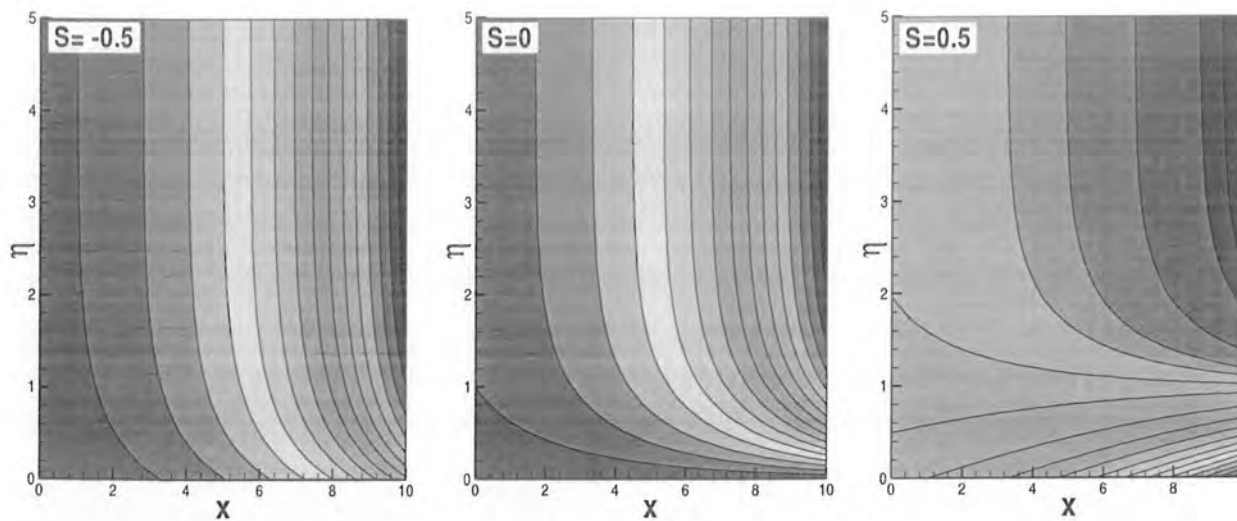
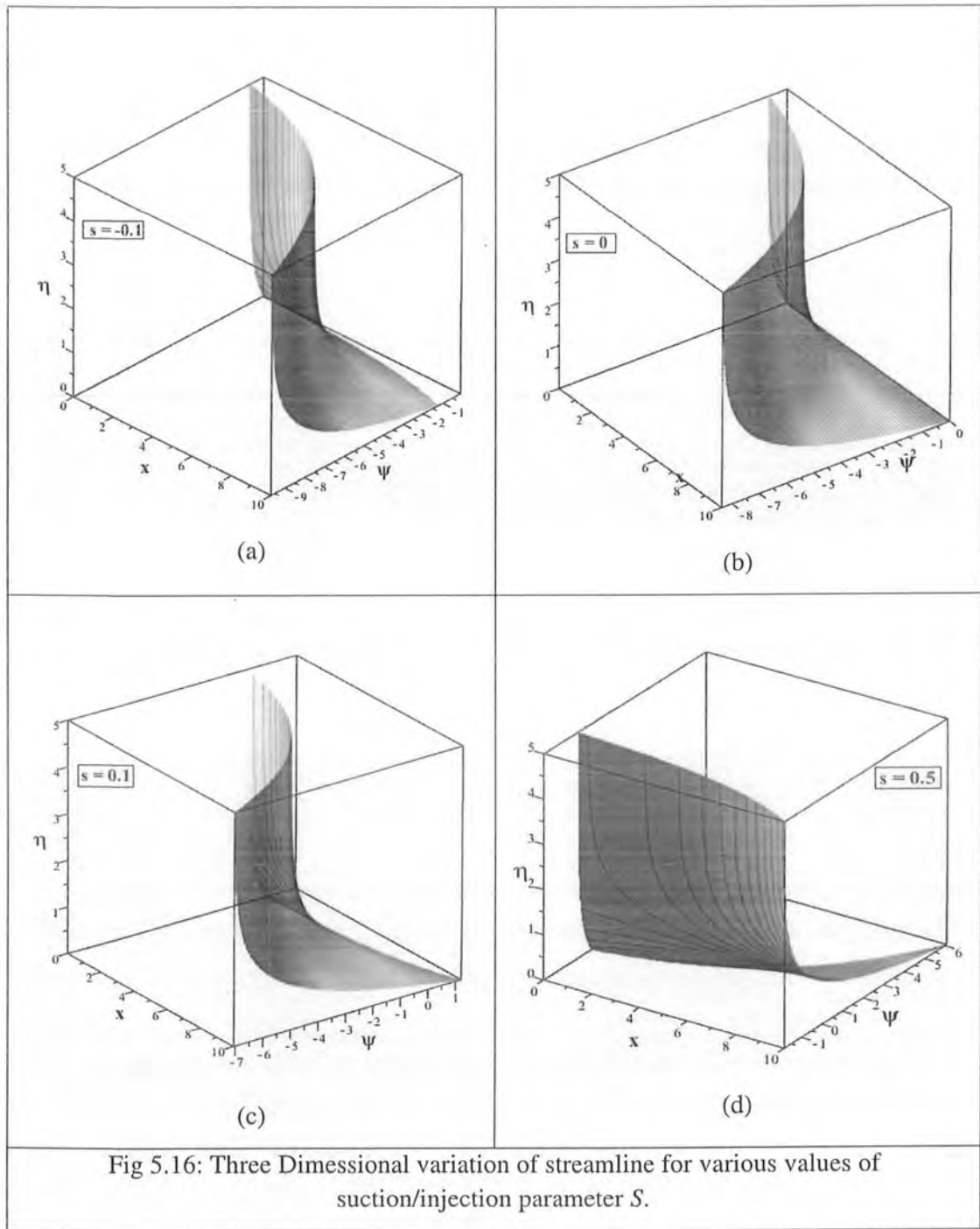


Fig 5.15: Stream line behavior for various values of suction/injection parameter  $S$ .



## 5.7 Conclusion

MHD boundary layer flow of a nanofluid over an exponentially shrinking sheet for Casson model subject to the convective boundary condition is solved numerically. Moreover, effects for various values of existing parameters are discussed for velocity, temperature and concentration. The main results of present analysis can be listed below.

- Trend of velocity is identical for MHD, Casson fluid and shrinking parameters.
- Same behavior of temperature profile is found for both Brownian motion parameter and thermophoresis parameter.
- Opposite behavior of nanoparticle volume concentration is found for both Brownian motion  $Nb$  and thermophoresis parameter  $Nt$ .
- The temperature profile  $\theta(\eta)$  and concentration profile  $\phi(\eta)$  decreases when both  $Pr$  and  $Le$  increases.
- Skin friction for non-Newtonian fluid is comparatively higher than Newtonian fluid.
- The magnitudes of the local Nusselt and Sherwood number show the opposite trend for higher values of Brownian motion parameter.

# MHD three dimensional boundary layer flow of Casson nanofluid past a linearly stretching sheet with convective boundary condition

## 6.1 Introduction

Present chapter deals the study of three dimensional flow of a Casson fluid in the presence of nanoparticle. It is considered that the sheet is stretched in both  $x$  and  $y$  –direction at  $xy$  –plane. Moreover, we have considered the magnetohydrodynamics (MHD) effect within the fluid and convective condition at the lower surface of the sheet. Constructed mathematical model in the form of partial differential equations are transformed into the set of coupled nonlinear ordinary differential equations with the help of similarity transformation which are solved numerically. Behavior of emerging parameters are presented graphically and discussed for velocity, temperature and nanoparticles concentration. Variation of the reduced Nusselt and Sherwood number against physical parameters are presented graphically. It is found that the reduced Nusselt number is a decreasing function and the reduced Sherwood number is an increasing function of Brownian parameter  $Nb$  and thermophoresis parameter  $Nt$ .

## 6.2 Mathematical formulation

Consider three-dimensional ( $3 - D$ ) incompressible Casson nanofluid flow past a stretching sheet. It is considered that the sheet is stretched along the  $xy$  –plane while the fluid is placed along the  $z$ -axis. Moreover, it is also considered that a constant magnetic field is applied normal to the fluid flow and the induced magnetic field is assumed to be negligible. We assumed

that the sheet is stretched with the linear velocities  $u = ax$  and  $v = by$  along the  $xy$  -plane respectively. The boundary layer equations of the three dimensional incompressible Casson nanofluid are stated as,

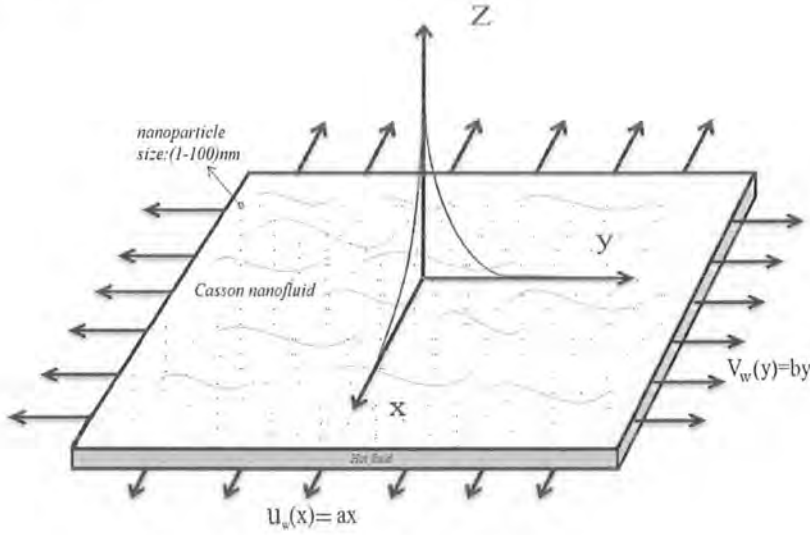


Fig 6.1: Geometry of the problem.

$$\frac{\partial u}{\partial x} + \frac{\partial v}{\partial y} + \frac{\partial w}{\partial z} = 0, \quad (6.1)$$

$$u \frac{\partial u}{\partial x} + v \frac{\partial u}{\partial y} + w \frac{\partial u}{\partial z} = \nu \left( 1 + \frac{1}{\beta} \right) \frac{\partial^2 u}{\partial z^2} - \frac{\sigma B^2}{\rho_f} u, \quad (6.2)$$

$$u \frac{\partial v}{\partial x} + v \frac{\partial v}{\partial y} + w \frac{\partial v}{\partial z} = \nu \left( 1 + \frac{1}{\beta} \right) \frac{\partial^2 v}{\partial z^2} - \frac{\sigma B^2}{\rho_f} v, \quad (6.3)$$

$$\left. \begin{aligned} u \frac{\partial T}{\partial x} + v \frac{\partial T}{\partial y} + w \frac{\partial T}{\partial z} &= \alpha_D \left( \frac{\partial^2 T}{\partial z^2} \right) + \\ \tau D_B \left( \frac{\partial T}{\partial z} \frac{\partial C}{\partial z} \right) + \frac{\tau D_T}{T_\infty} \left( \frac{\partial T}{\partial z} \right)^2, & \end{aligned} \right\} \quad (6.4)$$



$$u \frac{\partial C}{\partial x} + v \frac{\partial C}{\partial y} + w \frac{\partial C}{\partial z} = D_B \left( \frac{\partial^2 C}{\partial z^2} \right) + \left. \begin{array}{l} \\ \frac{D_T}{T_\infty} \left( \frac{\partial^2 T}{\partial z^2} \right), \end{array} \right\} \quad (6.5)$$

The associated boundary conditions related to Eqs. (6.2) and (6.3) are defined as:

$$\left. \begin{array}{l} u = u_w(x) = ax, \\ v = v_w(y) = by, \\ -k_f \left( \frac{\partial T}{\partial z} \right) = h_f (T_f - T), \\ C = C_w(x) \end{array} \right\} \text{at } z = 0, \quad (6.6)$$

$$\left. \begin{array}{l} u \rightarrow 0, v \rightarrow 0, \\ T \rightarrow T_\infty, C \rightarrow C_\infty \end{array} \right\} \text{as } z \rightarrow \infty. \quad (6.7)$$

where  $u, v$  and  $w$  denote the respective velocities in the  $x$ -,  $y$ - and  $z$ - directions respectively,  $\beta$  is the Casson fluid parameter,  $D_B$  is the Brownian diffusion coefficient,  $D_T$  is the thermophoretic diffusion coefficient,  $\tau = (\rho c)_p / (\rho c)_f$  is the ratio between the effective heat capacity of the nanoparticle material and capacity of the fluid with  $\rho$  is the density,  $a$  and  $b$  are positive constant,  $u_w$  and  $v_w$  are stretching velocities in  $x$  and  $y$  directions,  $T_w$  is the temperature, which takes the constant value at the wall and the constant value  $T_\infty$  far away from the wall,  $B_0$  is the magnetic induction,  $k_f$  is the thermal conductivity of the fluid,  $h_f$  is the convective heat transfer coefficient and  $T_f$  is the convective fluid temperature below the moving sheet. Introducing the following similarity transformations

$$\left. \begin{aligned} \eta = z\sqrt{\frac{a}{\nu}}, u = axf'(\eta), v = byg'(\eta), \\ W = -\sqrt{\frac{a}{\nu}}(f(\eta) + cg(\eta)), \\ \theta(\eta) = \frac{T - T_\infty}{T_f - T_\infty}, \quad \phi(\eta) = \frac{C - C_\infty}{C_w - C_\infty} \end{aligned} \right\}, \quad (6.8)$$

where  $c = b/a$  is the ratio of the velocities in  $y$  – and  $x$  – directions, and prime denotes differentiation with respect to  $\eta$ . Making use of Eq. (6.7), equation of continuity is identically satisfied and Eqs. (6.2)-(6.5) along with boundary conditions define in Eqs. (6.6) and (6.7) take the following form

$$\left(1 + \frac{1}{\beta}\right) f'' - (f')^2 + (f + cg) f'' - M^2 f' = 0, \quad (6.9)$$

$$\left(1 + \frac{1}{\beta}\right) g'' - (g')^2 + (f + cg) g'' - M^2 g' = 0, \quad (6.10)$$

$$\theta'' + Pr \left\{ (f + cg) \theta' + Nb \theta' \phi' + Nt (\theta')^2 \right\} = 0, \quad (6.11)$$

$$\phi'' + Le Pr (f + cg) \phi' + \frac{Nt}{Nb} \theta'' = 0, \quad (6.12)$$

$$\left. \begin{aligned} f(0) = 0, f'(0) = 1, g(0) = 0, g'(0) = c, \\ \theta'(0) = -Bi(1 - \theta(0)), \phi(0) = 1 \end{aligned} \right\} \quad (6.13)$$

$$\left. \begin{aligned} f'(\eta) \rightarrow 0, g'(\eta) \rightarrow 0, \\ \theta(\eta) \rightarrow 0, \phi(\eta) \rightarrow 0 \end{aligned} \right\} \text{as } \eta \rightarrow \infty. \quad (6.14)$$

In these expressions,  $M^2 = \sigma B_0^2 / \rho a$  is the magnetic parameter,  $Pr = \nu / \alpha_D$  is the Prandtl number,  $Le = \alpha_D / D_B$  is the Lewis number,  $Nb = (\rho c)_p (D_B) (C_w - C_\infty) / (\rho c)_f \nu$  is the Brownian motion parameter,  $Nt = (\rho c)_p (D_T) (T_w - T_\infty) / (\rho c)_f T_\infty \nu$  is the thermophoresis parameter and  $Bi = (h_f / k_f) \sqrt{\nu / a}$  is the Biot number.

Expressions for skin friction coefficient  $C_f$  on the surface along the  $x$  and  $y$  directions, denoted by  $C_{fx}$  and  $C_{fy}$  respectively, local Nusselt number  $Nu_x$  and local number  $Sh_x$  are defined as,

$$\begin{aligned} C_{fx} &= \frac{\tau_{wx}}{\rho u_w^2}, \quad C_{fy} = \frac{\tau_{wy}}{\rho u_w^2}, \\ Nu_x &= \frac{xq_w}{k(T_f - T_\infty)}, \\ Sh_x &= \frac{xq_m}{D_B(C_w - C_\infty)}, \end{aligned} \tag{6.15}$$

where  $\tau_{wx}$  and  $\tau_{wy}$  are the wall shear stresses along  $x$  and  $y$  – direction, respectively.  $q_w$  and  $q_m$  are the surface heat flux and mass flux respectively. Using the variables (6.8), we obtain

$$\begin{aligned} C_{fx} Re_x^{\frac{1}{2}} &= \left(1 + \frac{1}{\beta}\right) f''(0), \\ \left(\frac{x}{y}\right) C_{fy} Re_x^{\frac{1}{2}} &= c \left(1 + \frac{1}{\beta}\right) g''(0), \\ Re_x^{-\frac{1}{2}} Nu_x &= -\theta'(0), \\ Re_x^{-\frac{1}{2}} Sh_x &= -\phi'(0). \end{aligned} \tag{6.16}$$

Where  $Re_x = u_x(x)x/\nu$  is local Reynolds number based on the stretching velocity  $u_x(x)$ .

### 6.3 Numerical Technique

The system of nonlinear differential equations (6.9-6.12) along with the boundary conditions (6.13) and (6.14) are solved numerically using Runge-Kutta-Fehlberg method after converting the above system of boundary value problem into initial value problem with the help of shooting technique. The step size  $\Delta\eta = 0.001$  is used to obtain the numerical solution with  $\eta_{max}$ , and an accuracy to the fifth decimal place is chosen as the criterion of convergence.

## 6.4 Results and discussions

Figs. 6.2 – 6.12, present the physical behavior of velocity profiles  $f'(\eta)$ ,  $g'(\eta)$ , temperature profile  $\theta(\eta)$  and nanoparticle volume concentration  $\phi(\eta)$  against various parameters such as Casson fluid parameter  $\beta$ , Hartmann number  $M$ , stretching ratio  $c$ , Prandtl number  $Pr$ , Lewis number  $Le$ , Brownian motion parameter  $Nb$ , the Thermophoresis parameter  $Nt$  and Biot number  $Bi$ . Fig. 6.2, demonstrated the effects of non-Newtonian Casson fluid parameter  $\beta$  on velocity profiles  $f'(\eta)$  and  $g'(\eta)$ . It is observed that with the influence of  $\beta$  implies a decrease in the yield stress of the Casson fluid. This effectively facilitates flow of the fluid i.e. accelerates the boundary layer flow close to the stretching surface, as shown in Fig. 6.3. Moreover, it is found that with large values of  $\beta$ , the fluid is closer to the Newtonian fluid. From Fig. 6.3, it is observed that for higher values of  $M$ , it reduces both boundary layer thickness and the magnitude of the velocity profiles  $f'(\eta)$  and  $g'(\eta)$ . Since the magnetic field induces current in the conductive fluid, then it creates a resistive-type force on the fluid within the boundary layer which slows down the motion of the fluid. So finally, it is concluded that magnetic field is used to control boundary layer separation. Fig. 6.4, exhibits the effects of stretching parameter  $c$  on the velocity profiles. Present phenomenon reduces to the two-dimensional flow when  $c = 0$  ( $g = 0$ ), while for  $c = 1$  ( $f = g$ ) the problem reduces to the axisymmetric flow. Fig. 6.4 depicts that for increasing values of the stretching parameter  $c$ , it reduces the velocity  $f'(\eta)$ , while  $g'(\eta)$  varies with respect to various values of the stretching parameter  $c$ . In fact, increasing values of Casson fluid parameter  $\beta$  enhance both the temperature  $\theta(\eta)$  and nanoparticle concentration  $\phi(\eta)$  (see Fig. 6.5). In fact, magnetic field is the best source to enhance the temperature and nanoparticle volume concentration. The effects of magnetic parameter  $M$  on the temperature

profile  $\theta(\eta)$  and nanoparticle volume concentration  $\phi(\eta)$  is mentioned in Fig. 6.6. It is illustrated that due to increase in  $M$ , both the temperature profile  $\theta(\eta)$  and the nanoparticle volume concentration  $\phi(\eta)$  increase. Fig. 6.7, demonstrates that the stretching ratio  $c$  also affects the temperature profile  $\theta(\eta)$  and nanoparticle concentration  $\phi(\eta)$ . The effects of Prandtl number  $Pr$  on  $\theta(\eta)$  and  $\phi(\eta)$  can be seen in Fig. 6.6. Since  $Pr$  is a ratio of viscous diffusion rate to a thermal diffusion rate, so for higher Prandtl number causes the thermal diffusivity to reduce. Consequently, for higher values of  $Pr$ , the temperature profile  $\theta(\eta)$  and the nanoparticle volume concentration  $\phi(\eta)$  illustrate the decreasing behavior. It is also illustrated from Fig. 6.9 that both temperature and nanoparticles volume concentration present the opposite behavior for higher values of  $Le$  when it is compared with the Fig. 6.6. In Figs. 6.10 and 6.11, we have discussed the behavior of both temperature profile  $\theta(\eta)$  and nanoparticles volume fraction  $\phi(\eta)$  for two main parameters of nanoparticles namely: Brownian motion  $Nb$  and thermophoresis parameter  $Nt$ . Hypothetically, enhanced thermal conductivity of a nanofluid is mainly due to Brownian motion  $Nb$  which producing micro-mixing. As expected, temperature is an increasing function of Brownian motion parameter (see Fig. 6.10). However, for large values of the Brownian motion parameter, it reduced the nanoparticle volume concentration. On the other hand, it is observed from Fig. 6.11 that for higher values of thermophoresis parameter  $Nt$ , both the temperature and nanoparticle volume concentration are increasing. Comparatively, it is examined from Figs. 6.10 and 6.11, that there is an enhancement in the temperature profile with respect to large values of both Brownian and thermophoresis parameters, however opposite behavior predicted for nanoparticles volume concentration with the increase of Brownian and thermophoresis parameters. Effects of Biot number  $Bi$  on the temperature is illustrated in Fig. 6.15. Physically, Biot number is expressed as the convection at the surface of the body to the conduction within

the surface of the body. When thermal gradient applied on the surface then the ratio governs the temperature inside a body varies significantly, while the body heats or cools over a time. Normally, for uniform temperature field inside the surface we consider  $Bi \ll 1$ . However,  $Bi \gg 1$  depicts that temperature field inside the surface is not uniform. In Fig. 6.11, we have discussed the effects of Biot number  $Bi$  on temperature profile  $\theta(\eta)$  in three ways. The first one is the case when  $Bi < 1$ . It is observed from Fig. 6.11 that for smallest values of the Biot number ( $Bi < 1$ ), the variation of temperature within the body is slight and can reasonably be approximated as being uniform. While in the second case, for  $Bi > 1$  depicts that the temperature within the body do not performing uniform behavior (see Fig. 6.12). The third and last case relates when we consider the value of Biot number tends to infinity ( $Bi \rightarrow \infty$ ) correspond to the case of constant wall temperature (see Fig. 6.12).

Effects of physical parameters on skin friction coefficients are presented in Figs. 6.13 (a) and 6.13(b). Table 6.1 shows that the excellent comparison has been achieved with the earlier work of Ahmad and Nazar [18] and Nadeem et al [27] for  $(1 + (1/\beta))f''(0)$  and  $(1 + (1/\beta))cg''(0)$ . We prominently observed that in the Figs. 6.13 (a) and (b), Newtonian nanofluid produces the low friction at the wall as compared to non-Newtonian nanofluid. Consequently, it is observed that with an increase of both stretching ratio parameter  $c$  and non-Newtonian fluid parameter  $\beta$  causes retardation in the fluid motion in both  $x$  and  $y$  directions at the surface. Figs. 6.14(a) – 6.14(b) shows that for higher values of  $\beta$ , both local Nusselt and Sherwood numbers decreases with an increase of  $c$ . Table 6.2 present the comparison for local Nusselt number  $Re_x^{-1/2}Nu_x$  and the local Sherwood number  $Re_x^{-1/2}Sh_x$  with results of Khan and Pop [34], in the absence of  $M$  and  $c$  when  $Pr = 10, Le = 1$  and  $\beta \rightarrow \infty$ . From Fig. 6.15, increasing values of Brownian motion parameter  $Nt$  caused the local Nusselt number  $\theta'(0)$  to

reduce with  $Nt$ . From Fig. 6.14, local Sherwood number  $\phi'(0)$  increases with an increase in Brownian motion parameter  $Nb$ . So it is observed from this phenomenon that there is low thermal conductivity for higher Prandtl number. Table 6.3 shows the numerical values of the local Nusselt number  $Re_x^{-1/2}Nu_x$  and the local Sherwood number  $Re_x^{-1/2}Sh_x$  when  $c = M = \beta = Bi = 0.5, Pr = 4$  and  $Le = 1$ .

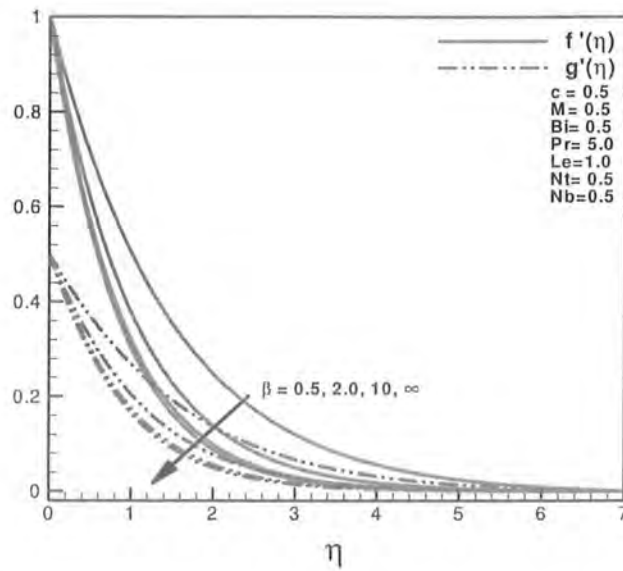


Fig 6.2: Effect of  $\beta$  on velocities  $f'(\eta)$  and  $g'(\eta)$ .

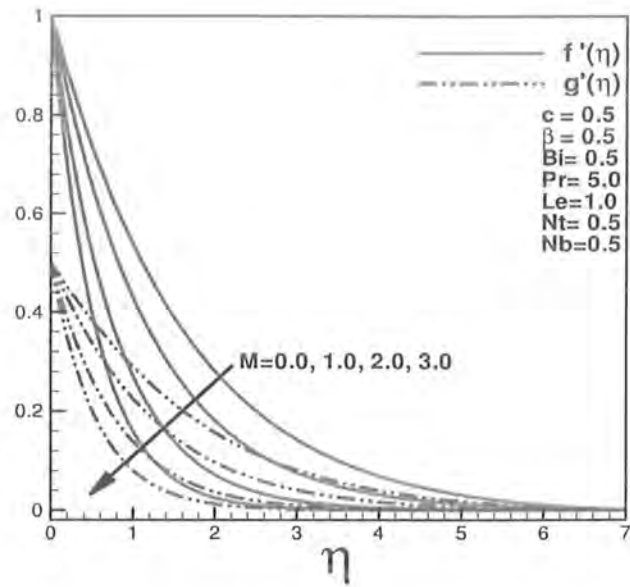


Fig 6.3: Effect of  $M$  on velocities  $f'(\eta)$  and  $g'(\eta)$ .

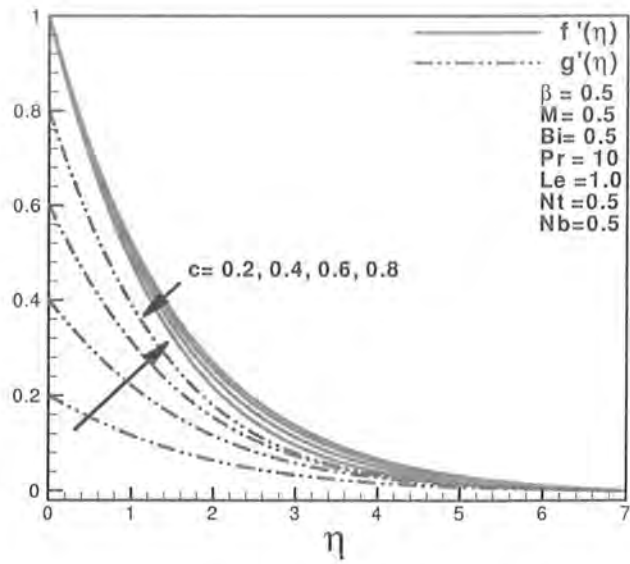


Fig 6.4: Effect of  $c$  on velocities  $f'(\eta)$  and  $g'(\eta)$ .



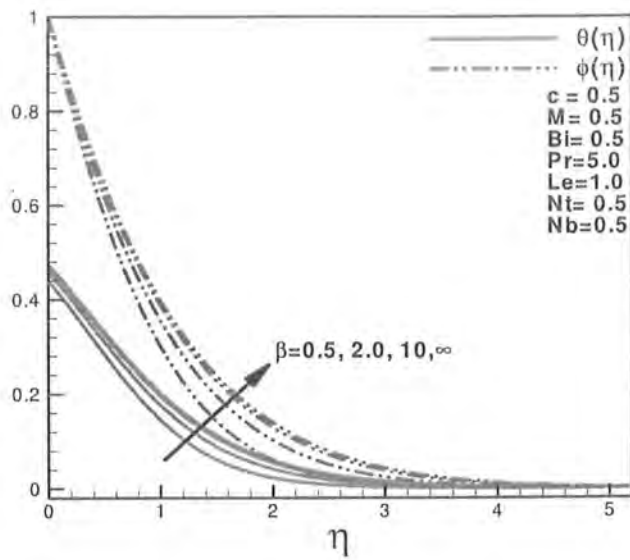


Fig 6.5: Effect of  $\beta$  on temperature  $\theta(\eta)$  and nanoparticle volume concentration  $\phi(\eta)$ .

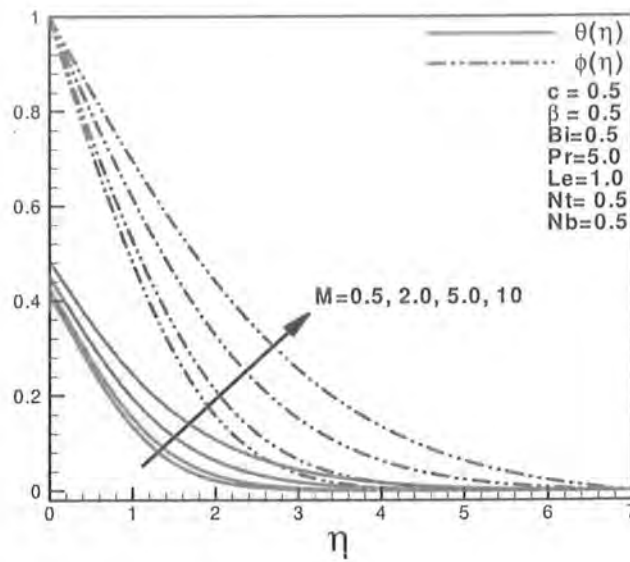


Fig 6.6: Effect of  $M$  on temperature  $\theta(\eta)$  and nanoparticle volume concentration  $\phi(\eta)$ .

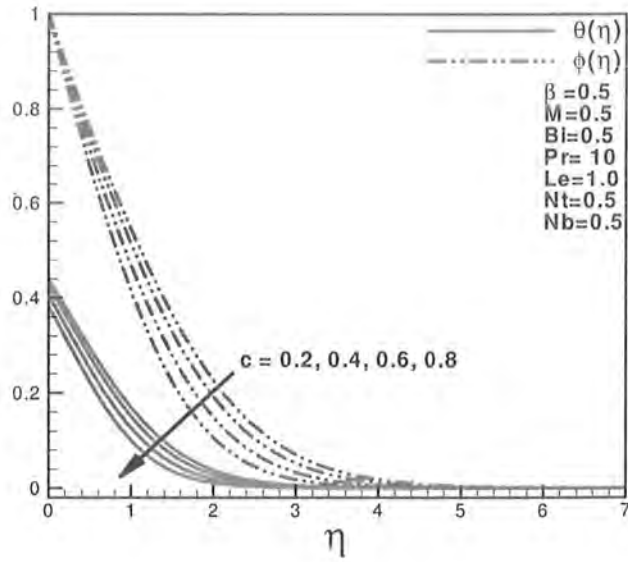


Fig 6.7: Effect of  $c$  on temperature  $\theta(\eta)$  and nanoparticle volume concentration  $\phi(\eta)$ .

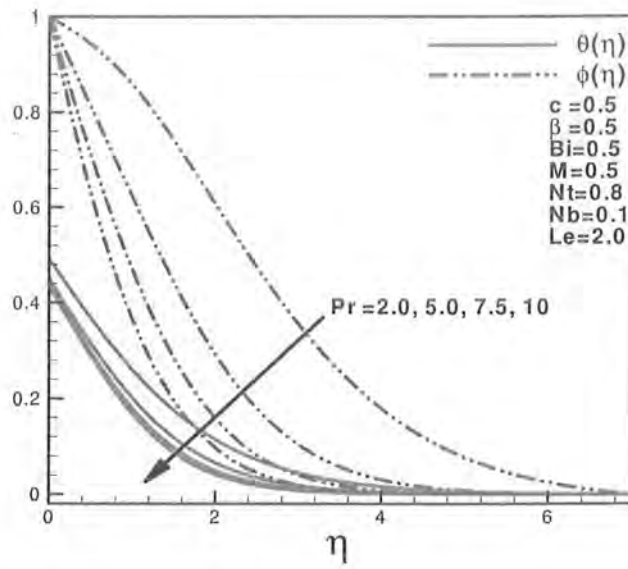


Fig 6.8: Effect of  $Pr$  on temperature  $\theta(\eta)$  and nanoparticle volume concentration  $\phi(\eta)$ .

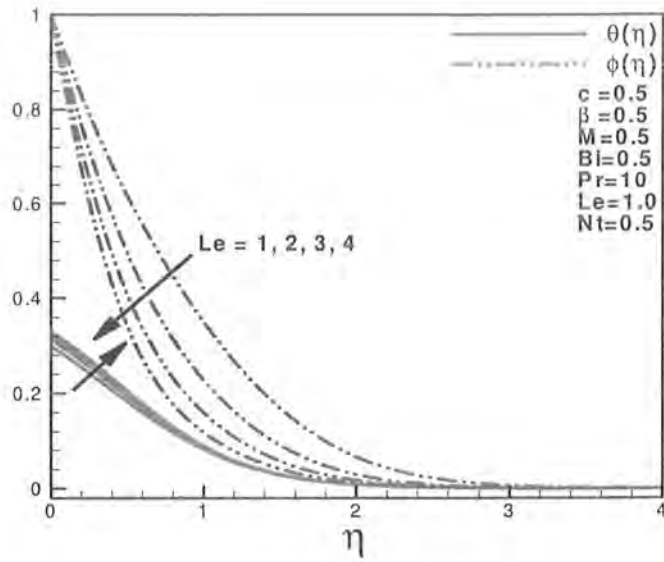


Fig 6.9: Effect of  $Le$  on temperature  $\theta(\eta)$  and nanoparticle volume fraction  $\phi(\eta)$ .

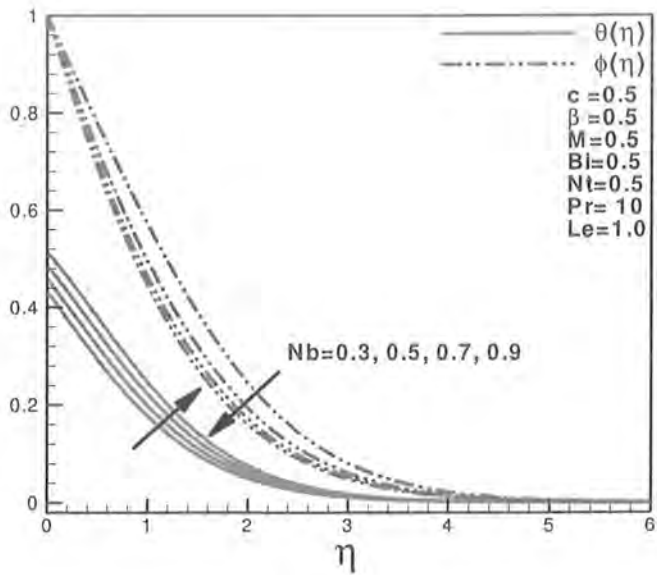


Fig 6.10: Effect of  $Nb$  on temperature  $\theta(\eta)$  and nanoparticle volume concentration  $\phi(\eta)$ .

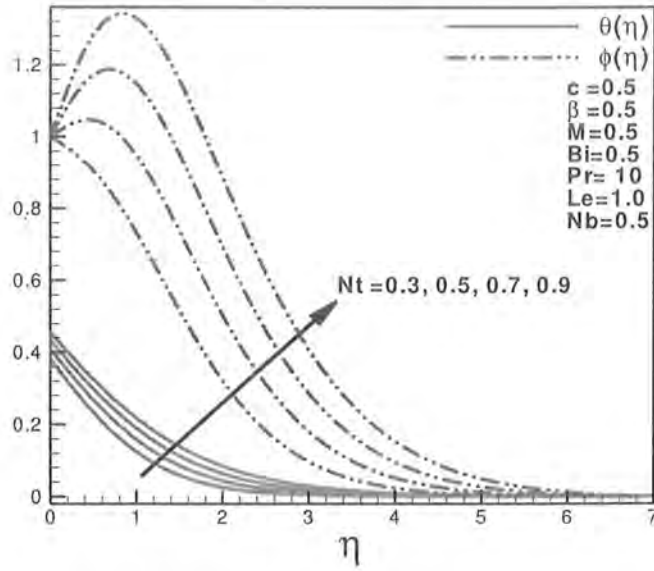


Fig 6.11: Effect of  $Nt$  on temperature  $\theta(\eta)$  and nanoparticle volume concentration  $\phi(\eta)$ .

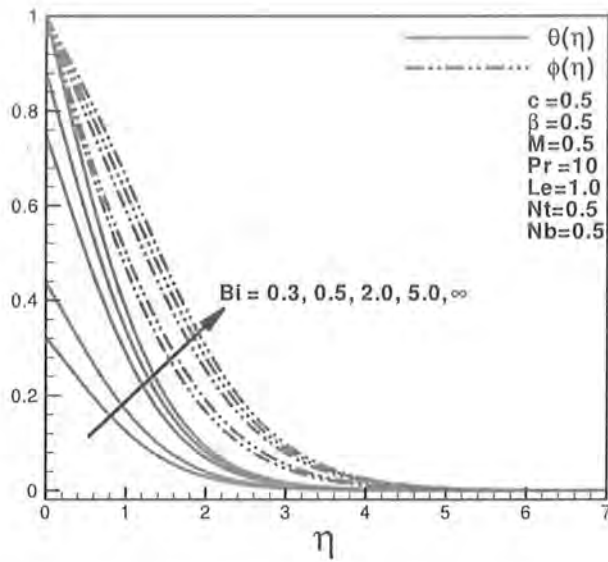


Fig 6.12. Effect of  $Bi$  on temperature  $\theta(\eta)$  and nanoparticle volume concentration  $\phi(\eta)$ .

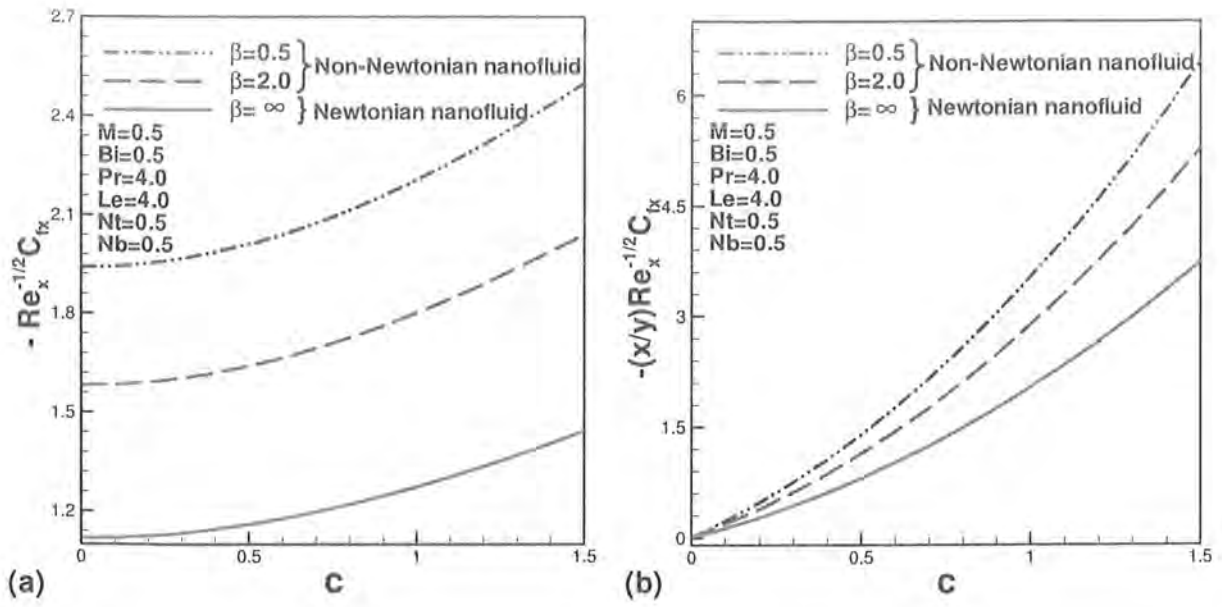


Fig. 6.13: Variation of skin friction coefficient along  $x$  and  $y$  directions with  $\beta$  and  $c$ .

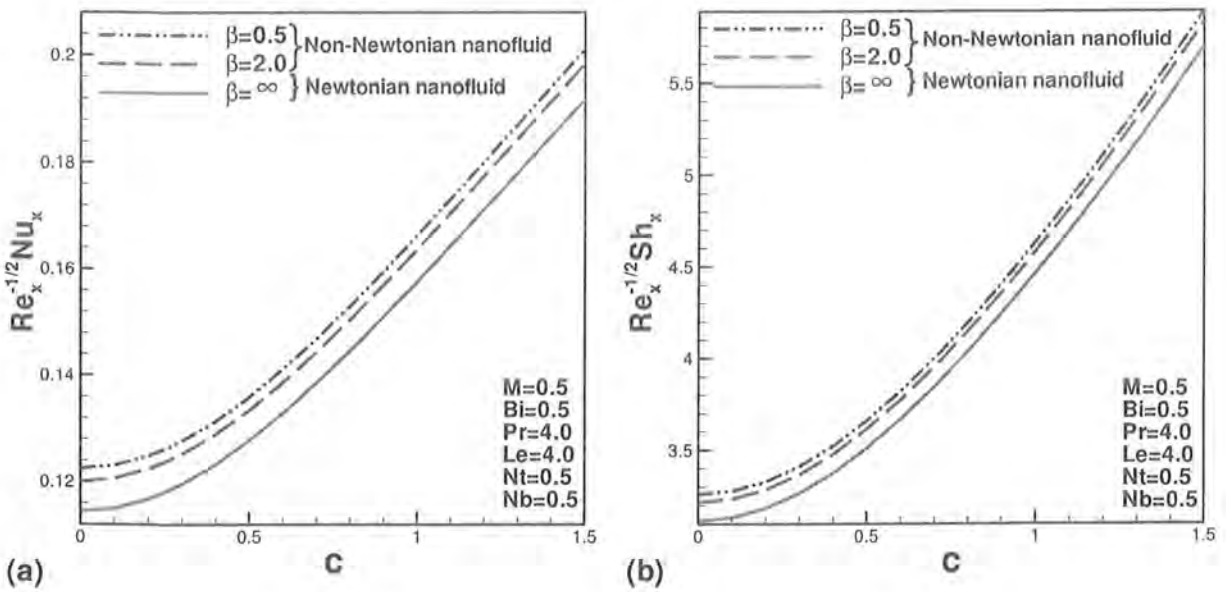


Fig 6.14: Variation of local Nusselt number  $Re_x^{-1/2} Nu_x$  and Sherwood number  $Re_x^{-1/2} Sh_x$  with  $\beta$  and  $c$ .

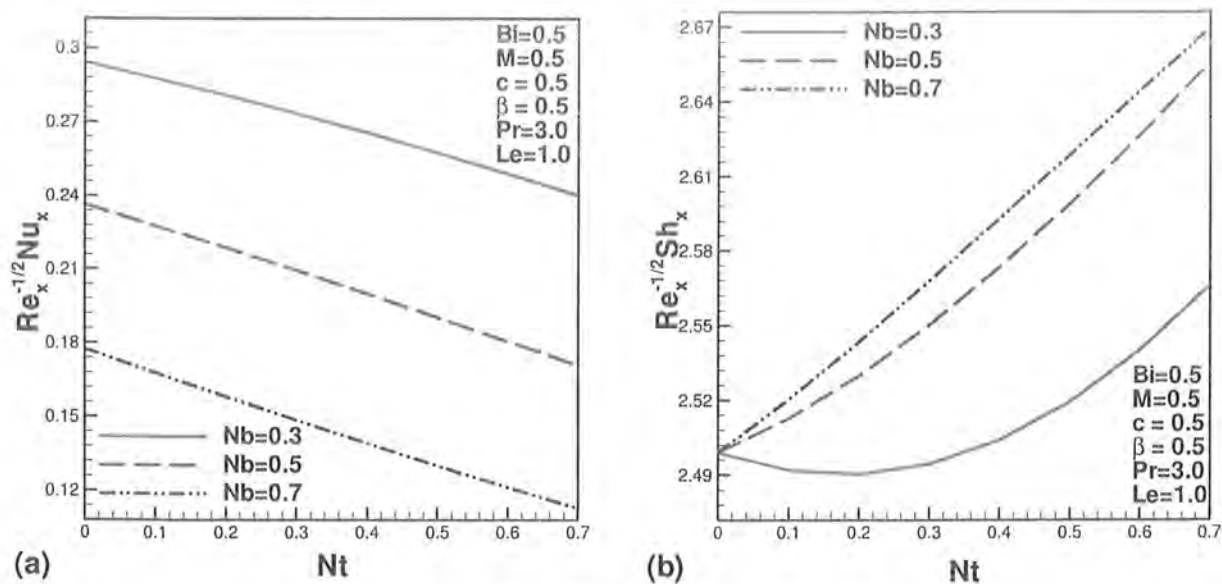


Fig 6.15: Variation of local Nusselt number  $Re_x^{-1/2} Nu_x$  and Sherwood number  $Re_x^{-1/2} Sh_x$  with  $Nb$  and  $Nt$ .

**Table 6. 1:** Comparison of Numerical Values for local Nusselt number and the Sherwood number in the absence of  $M$  and  $c$  when  $Pr = 10$ ,  $Le = 1$ ,  $Nb = 0.1$ ,  $Bi \rightarrow \infty$  and  $\beta \rightarrow \infty$ .

Present results $M = c = 0$			Khan and Pop [34]	
$Nt$	$-\theta'(0)$	$-\phi'(0)$	$-\theta'(0)$	$-\phi'(0)$
0.1	0.9524	5.1294	0.9524	5.1294
0.2	0.6932	5.2732	0.6932	5.2740
0.3	0.5201	5.5286	0.5201	5.5286
0.4	0.4026	5.7952	0.4026	5.7952
0.5	0.3211	6.0351	0.3211	6.0351

**Table 6.2:** Comparison of numerical results with present study for skin friction coefficients in the absence of heat transfer and nanopartilces.

$M^2$	$\beta$	$c = 0$	$c = 0.5$		$c = 1$
		$-C_{fx} Re_x^{\frac{1}{2}}$	$-C_{fx} Re_x^{\frac{1}{2}}$	$-\left(\frac{x}{y}\right) C_{fy} Re_x^{\frac{1}{2}}$	$-\left(\frac{x}{y}\right) C_{fy} Re_x^{\frac{1}{2}}$
0	$\infty$	1.0042 (Ref [18])	1.0932 (Ref [18])	0.4653 (Ref [18])	1.1748 (Ref [18])
	5	1.0954 (Ref [27])	1.1974 (Ref [27])	0.5096 (Ref [27])	1.2857 (Ref [27])
	1	1.4142 (Ref [27])	1.5459 (Ref [27])	0.6579 (Ref [27])	1.6599 (Ref [27])
10	$\infty$	3.3165 (Ref [18])	3.3420 (Ref [18])	1.6459 (Ref [18])	3.3667 (Ref [18])
	5	3.6331 (Ref [27])	3.6610 (Ref [27])	1.8030 (Ref [27])	3.6886 (Ref [27])
	1	4.6904 (Ref [27])	4.7263 (Ref [27])	5.3276 (Ref [27])	4.7620 (Ref [27])
100	$\infty$	10.049 (Ref [18])	10.058 (Ref [18])	5.0208 (Ref [18])	10.066 (Ref [18])
	5	11.0091 (Ref [27])	11.0182 (Ref [27])	5.5000 (Ref [27])	11.0272 (Ref [27])

**Table 6.3:** Numerical Values of present study for local Nusselt number and Sherwood number when  $c = M = \beta = Bi = 0.5, Pr = 4$  and  $Le = 1$ .

$Nt \downarrow$	$Nb = 0.3$		$Nb = 0.5$		$Nb = 0.7$	
	$-\theta'(0)$	$-\phi'(0)$	$-\theta'(0)$	$-\phi'(0)$	$-\theta'(0)$	$-\phi'(0)$
0.3	0.293872	1.585361	0.223435	1.671176	0.152409	1.702893
0.5	0.277199	1.584743	0.201045	1.714678	0.130133	1.754949
0.7	0.258084	1.617605	0.177710	1.774545	0.109759	1.810687
0.9	0.236659	1.684341	0.154751	1.844936	0.092151	1.865292

## 6.5 Final remarks

Three dimensional MHD boundary layer flow for Casson fluid model over a stretching sheet along with the convected condition and radiation effects are investigated numerically. Moreover, effects for various values of emerging parameters are discussed for velocities  $f'(\eta)$ ,  $g'(\eta)$ , temperature  $\theta(\eta)$  and nanoparticle volume concentration  $\phi(\eta)$ . The main results of present analysis are listed below.

- Hartmann number  $M$ , Casson fluid parameter  $\beta$  and stretching parameter  $c$  reduce for the velocity profiles in both  $x$  and  $y$  directions.
- Hartmann number  $M$  and Casson fluid parameter  $\beta$  contribute to the increasing behavior while stretching parameter  $c$  shows the decreasing behavior for both temperature  $\theta(\eta)$  and nanoparticle volume concentration  $\phi(\eta)$ .
- Opposite trend is found when the results of temperature profile  $\theta(\eta)$  for  $Nb$  and  $Nt$  are compared.
- Effects of both  $Nb$  and  $Nt$  on nanoparticle volume concentration  $\phi(\eta)$  show the quite opposite behavior.
- Effects of  $Le$  on both temperature  $\theta(\eta)$  and nanoparticle concentration  $\phi(\eta)$  shows the opposite behavior.
- Convective parameter  $Bi$  shows the same increasing behavior for both temperature  $\theta(\eta)$  and nanoparticle volume concentration  $\phi(\eta)$ .
- It is found that Newtonian nanofluid provides lower skin friction and heat transfer rates as compared to non-Newtonian nanofluid with the increase of stretching ratio parameter.



# Numerical study of MHD boundary layer flow of a Maxwell fluid past a stretching sheet in the presence of nanoparticles

## 7.1 Introduction

In the present article, two dimensional boundary-layer flow and heat transfer of Maxwell fluid past a stretching sheet is studied numerically. The effects of magnetohydrodynamic (MHD) and elasticity on the flow are considered. Moreover, effects of nanoparticles are also investigated. Similarity transformations are defined to convert the governing nonlinear partial differential equation to ordinary differential equations. The reduced boundary layer equations of Maxwell nanofluid model are solved numerically. The effects of emerging parameters, namely, magnetic parameter  $M$ , elastic parameter  $K$ , Prandtl parameter  $Pr$ , Brownian motion  $Nb$ , thermophoresis parameter  $Nt$  and Lewis number  $Le$  on temperature and concentration profile are discussed. Interesting results are shown graphically. The skin friction coefficient, dimensionless heat transfer rate and concentration rate are also plotted against the flow control parameters.

## 7.2 Problem Formulation

Consider two-dimensional steady incompressible fluid past a stretching sheet. In addition, The fluid is saturated with nanoparticles and imposed with MHD effects while the sheet is stretching with the plane  $y = 0$ . The flow is assumed to be confined to  $y > 0$ . Here we assumed that the sheet is stretched with the linear velocity  $u(x) = ax$ , where  $a > 0$  is a constant and  $x$  – axis is measured along the stretching surface. A uniform constant magnetic

field is applied normal to the stretching surface. The effects of the induced magnetic field are negligible. The boundary layer equations of the Maxwell fluid in the presence of nanoparticles are [28],

$$\frac{\partial u}{\partial x} + \frac{\partial v}{\partial y} = 0, \quad (7.1)$$

$$u \frac{\partial u}{\partial x} + v \frac{\partial u}{\partial y} = \nu \left( \frac{\partial^2 u}{\partial y^2} \right) + k_0 \left( v^2 \frac{\partial^2 u}{\partial y^2} + 2uv \frac{\partial^2 u}{\partial x \partial y} \right) - \frac{\sigma B_0^2}{\rho_f} \left( u + k_0 v \frac{\partial u}{\partial y} \right), \quad (7.2)$$

$$u \frac{\partial T}{\partial x} + v \frac{\partial T}{\partial y} = \alpha \left( \frac{\partial^2 T}{\partial y^2} \right) + \tau \left\{ D_B \left( \frac{\partial C}{\partial y} \frac{\partial T}{\partial y} \right) + \left( \frac{D_T}{T_\infty} \right) \left[ \left( \frac{\partial T}{\partial y} \right)^2 \right] \right\}, \quad (7.3)$$

$$u \frac{\partial C}{\partial x} + v \frac{\partial C}{\partial y} = D_B \left( \frac{\partial^2 C}{\partial y^2} \right) + \left( \frac{D_T}{T_\infty} \right) \left( \frac{\partial^2 T}{\partial y^2} \right), \quad (7.4)$$

where  $u$  and  $v$  denote the respective velocities in the  $x$  – and  $y$  – directions respectively,  $\rho_f$  is the density of the base fluid,  $\nu$  is the kinematic viscosity of the fluid,  $\sigma$  is the electrical conductivity,  $B_0$  is the magnetic induction,  $k_0$  is the relaxation time of the upper convection Maxwell (UCM) fluid,  $\alpha$  is the thermal diffusivity,  $T$  is the fluid temperature,  $C$  the nanoparticle volume concentration,  $T_w$  and  $C_w$  are the temperature of fluid and nanoparticle fraction at wall respectively,  $D_B$  is the Brownian diffusion coefficient,  $D_T$  is the thermophoretic diffusion coefficient,  $\tau = (\rho c)_p / (\rho c)_f$  is the ratio between the effective heat capacity of the nanoparticle material and heat capacity of the fluid,  $C$  is the volumetric volume expansion coefficient and  $\rho_p$  is the density of the particles, when  $y$  tends to infinity then the ambient

values of  $T$  and  $C$  are denoted by  $T_\infty$  and  $C_\infty$ . The associated boundary conditions for Eqs.

(7.2)-(7.4), are

$$\begin{aligned} u = u_w(x) = ax, \quad v = 0, \quad T = T_w, \quad C = C_w \quad \text{at } y = 0, \\ u = 0, \quad v = 0, \quad T = T_\infty, \quad C = C_\infty \quad \text{as } y \rightarrow \infty. \end{aligned} \quad (7.5)$$

Introducing the following similarity transformations

$$\begin{aligned} \psi = (a\nu)^{1/2} x f(\eta), \quad \theta(\eta) = \frac{T - T_\infty}{T_w - T_\infty}, \\ \phi(\eta) = \frac{C - C_\infty}{C_w - C_\infty}, \quad \eta = \sqrt{\frac{a}{\nu}} y, \end{aligned} \quad (7.6)$$

where the stream function  $\psi$  is defined as  $u = \frac{\partial\psi}{\partial y}$  and  $v = -\frac{\partial\psi}{\partial x}$ . Making use of Eq. (7.6),

the equation of continuity is identically satisfied and Eqs. (7.2) - (7.4) along with (7.5) take the following forms

$$f''' - (M^2)f' - (f')^2 + (1 + M^2K)ff'' - K(f^2f''' - 2ff'f'') = 0, \quad (7.7)$$

$$\theta'' + \text{Pr}[f\theta' + Nb(\theta'\phi') + Nt(\theta')^2] = 0, \quad (7.8)$$

$$\phi'' + Le \text{Pr}(f\phi') + \frac{Nt}{Nb}\theta'' = 0, \quad (7.9)$$

$$\begin{aligned} f(0) = 0, \quad f'(0) = 1, \quad f'(\infty) = 0, \\ \theta(0) = 1, \quad \theta(\infty) = 0, \\ \phi(0) = 1, \quad \phi(\infty) = 0. \end{aligned} \quad (7.10)$$

In these expressions,  $M^2 = \sigma B_0^2 / \rho a$  is the Hartmann number,  $K = ak_0 (\geq 0)$  is the elastic parameter,  $\text{Pr} = \nu / \alpha$  is the Prandtl number,  $Nb = (\rho c)_P D_B (C_w - C_\infty) / \nu (\rho c)_f$  is the Brownian motion,  $Nt = (\rho c)_P D_T (T_w - T_\infty) / \nu T_\infty (\rho c)_f$  is the thermophoresis parameter,

$Le = \alpha / D_B$  the Lewis number. Expressions for the local skin friction coefficient  $C_f$ , local Nusselt number  $Nu$  and the local Sherwood number  $Sh$  are

$$C_f = \frac{\tau_w}{\rho u_w^2(x)}, \quad Nu = \frac{xq_w}{\alpha(T_w - T_\infty)}, \quad Sh = \frac{xq_m}{D_B(C_w - C_\infty)}, \quad (7.11)$$

where  $\tau_w$  is the wall shear stress,  $q_w$  and  $q_m$  are the heat flux and mass flux, respectively.

$$\tau_w = \mu(1 + K) \left( \frac{\partial u}{\partial y} \right)_{y=0}, \quad q_w = -\alpha \left( \frac{\partial T}{\partial y} \right)_{y=0}, \quad q_m = -D_B \left( \frac{\partial C}{\partial y} \right)_{y=0}. \quad (7.12)$$

Dimensionless form of Eq. (7.12) takes the following form

$$Re_x^{1/2} C_f = (1 + K) f''(0), \quad Re_x^{-1/2} Nu = -\theta'(0), \quad Re_x^{-1/2} Sh = -\phi'(0). \quad (7.14)$$

In the above equation,  $Re_x = u_w(x)x / \nu$  is local Reynolds number based on the shrinking velocity  $u_w(x)$ .

### 7.3 Results and discussions

The nonlinear coupled ordinary differential equations (7.7)-(7.9) subject to the boundary conditions (7.10) have been solved numerically by using a Runge-Kutta-Fehlberg method with shooting technique. Figs. 7.1-7.6 illustrate the behavior of emerging parameters such as magnetic parameters  $M$ , elastic parameters  $K$ , Prandtl parameter  $Pr$ , Brownian parameter  $Nb$ , thermophoresis parameter  $Nt$  and Lewis number  $Le$  for velocity profile  $f'(\eta)$ , temperature profile  $\theta(\eta)$  and nanoparticle volume concentration  $\phi(\eta)$ . Fig. 7.1 presents the velocity, temperature and nanoparticle volume concentration obtained for various values of magnetic parameter  $M$ , while the values of the rest of the parameters are taken to be fixed. It is seen from

Fig. 7.1, both temperature profile and nanoparticle volume concentration show the increasing behavior for increasing values of  $M$ . However, velocity profile  $f'(\eta)$  shows the decreasing behavior for increasing values of  $M$  (see Fig. 7.1). On the other hand, boundary layer thickness reduced for higher values of  $M$ . Physically,  $M$  is normal to the fluid so for higher values of  $M$  it raises the temperature and nanoparticle fraction, and resists the fluid flow. From Fig. 7.2, it is observed that velocity profile  $f'(\eta)$  increases with an increase of elastic parameter  $K$ . On the other hand, temperature profile  $\theta(\eta)$  and nanoparticle volume concentration reduces for higher values of  $K$  (see Fig. 7.2). It is observed from Fig. 7.2, opposite trend is found for both velocity profile  $f'(\eta)$  and temperature profile  $\theta(\eta)$  for higher values of elastic parameter  $K$ . Hence the boundary layer thickness decreases for same values of  $K$ . Physically, it is observed that an increase in the elastic parameter will increase the resistance of fluid motion. Table 7.2 illustrates the excellent agreement of [34] in the absence of both magneto-hydrodynamic and non-Newtonian effects. As expected, it is found from Fig. 7.3 that both the temperature profile and nanoparticle volume concentration profiles demonstrate, decreasing behavior with the influence of  $Pr$ . Consequently, boundary layer thickness decreases drastically with an increase in  $Pr$ . It is illustrated from Fig. 7.4, that both temperature and nanoparticle volume concentration exhibit the similar behavior when these are compared with Fig. 7.3 for higher values of  $Le$ . Effects of Brownian motion and thermophoresis parameter on temperature profile  $\theta(\eta)$  and nanoparticle volume concentration  $\phi(\eta)$  are shown in Figs. 7.5 and 7.6. It is observed from Figs. 7.4 and 7.5 that for higher values of both  $Nb$  and  $Nt$ , it raises the temperature profile. However, Fig. 7.4 shows opposite behavior for nanoparticle volume fraction when it is compared with the Fig. 7.5 for increasing values of both  $Nb$  and  $Nt$ . Consequently, boundary layer thickness reduces for increasing values of both  $Nb$  and  $Nt$  (see Fig. 7.4 and 7.5). In the absence of both nanoparticles

and non-Newtonian effects, there is an excellent agreement with [29]. That is validated in Table 7.1. The effects of magnetic parameter, elastic parameter, Prandtl number, Brownian parameter, thermophoresis parameter and Lewis number on the skin friction  $(1 + K)f''(0)$ , Nusselt number  $\theta'(0)$  and Sherwood number  $\phi'(0)$  are presented in Figs. 7.7-7.15. It is seen from Fig. 7.7 that higher values of  $K$  reduces the skin friction. Variation of both Nusselt and Sherwood numbers with the variation of both magnetic parameter  $M$  and Prandtl number  $Pr$  are shown in Fig. 7.6. It is found that increasing values of both magnetic parameter  $M$  and Prandtl number  $Pr$ , opposite behavior is found for Nusselt and Sherwood numbers. It is noticed that for increasing values of  $K$ , both Nusselt and Sherwood number show the increasing behavior with  $M$  (see Figs. 7.9 and 7.10). Fig. 7.11, depicts the effect of Brownian parameter  $Nb$  on Nusselt number  $\theta'(0)$  for various values of  $Pr$  and  $Le$ . It is observed through Fig. 7.11, that higher values of  $Nb$  reduce the Nusselt number for both the cases when  $Pr < Le$  or  $Pr > Le$ . On the other hand, it increases the Sherwood number  $\phi'(0)$  with higher values of Brownian motion  $Nb$  for various values of both Prandtl number and Lewis number (see Figs. 7.12). Finally, it is point out that there is low thermal conductivity for higher Prandtl number. Consequently, it reduces the conduction while the heat transfer rate increases at the surface of sheet.

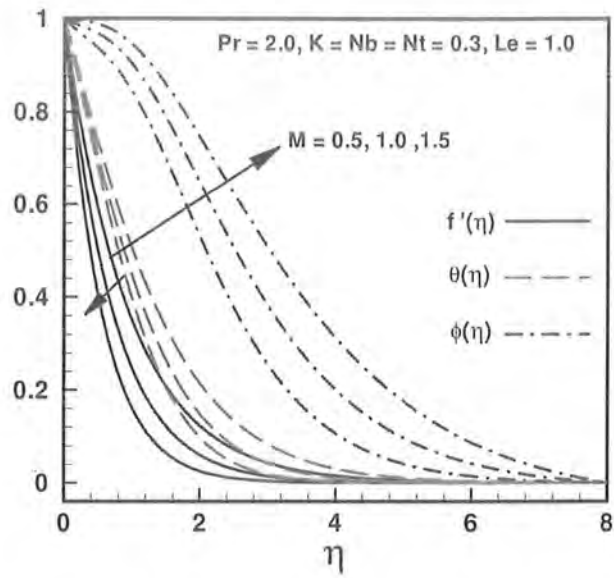


Fig 7.1: Variation of velocity, temperature and nanoparticle volume concentration for various values of  $M$ .

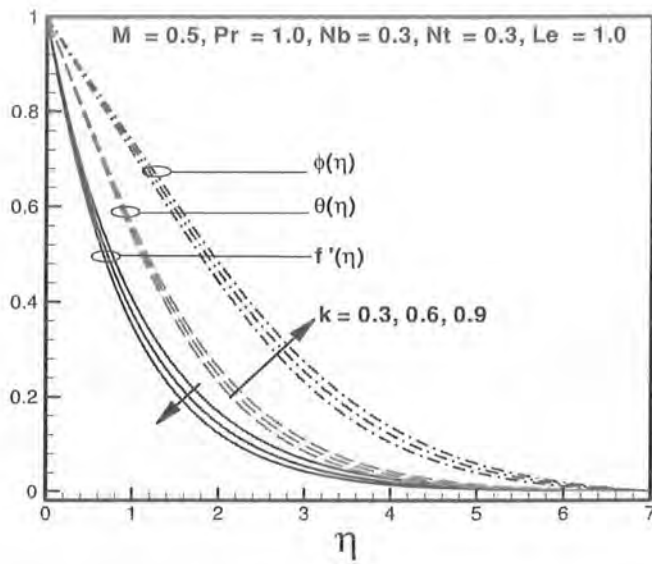


Fig 7.2: Variation of velocity, temperature and nanoparticle volume concentration for various values of  $K$ .

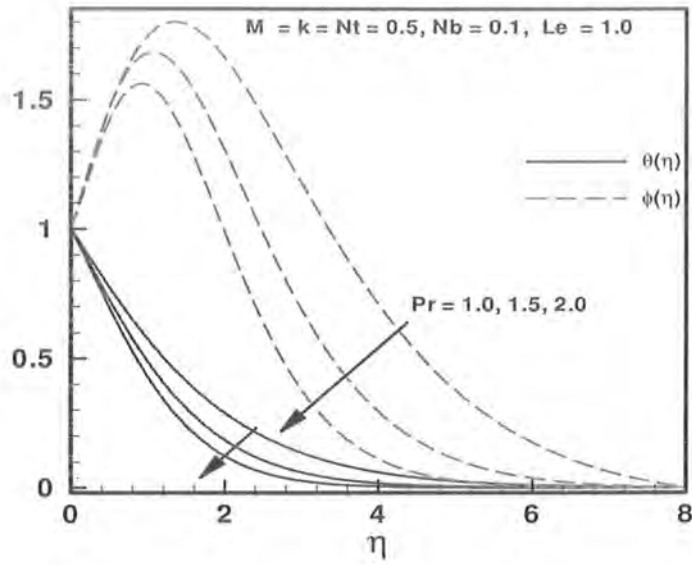


Fig 7.3: Variation of temperature and nanoparticle volume concentration for various values of  $Pr$ .

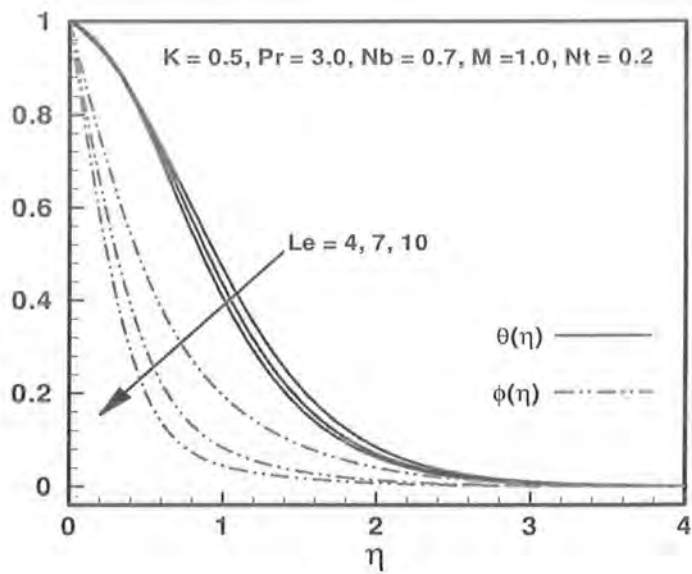


Fig 7.4: Variation of temperature and nanoparticle volume concentration for various values of  $Le$ .



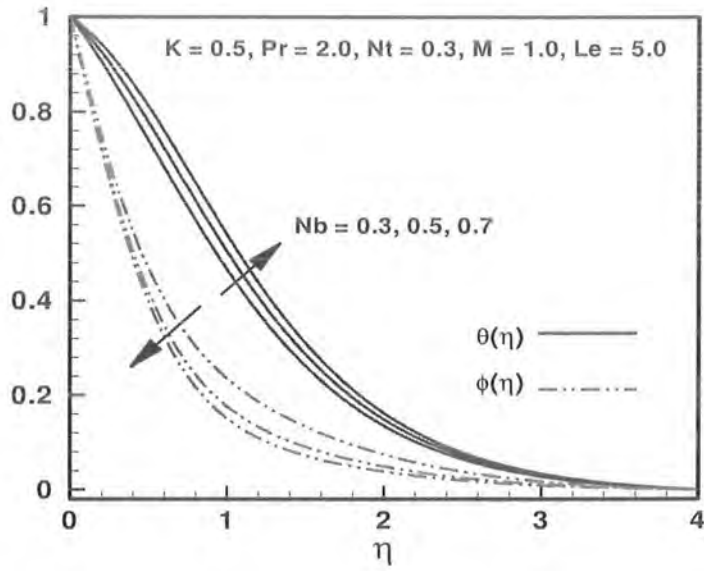


Fig 7.5: Variation of temperature and nanoparticle volume concentration for various values of  $Nb$ .

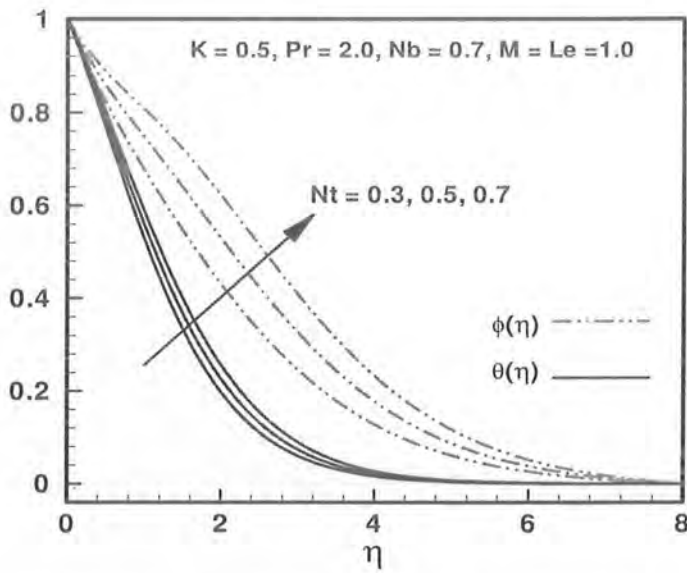


Fig. 7.6: Variation of temperature and nanoparticle volume concentration for various values of  $Nt$ .

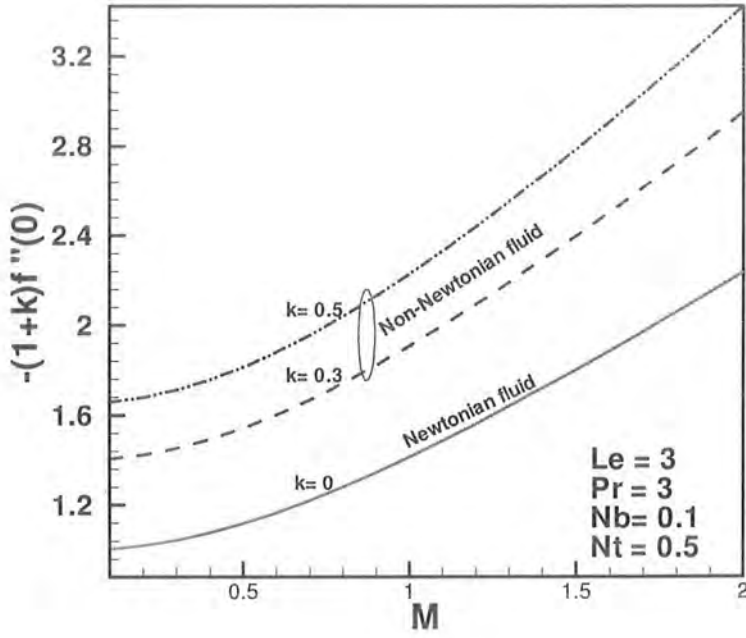


Fig. 7.7: Effects of  $M$  and  $k$  on skin friction coefficient.

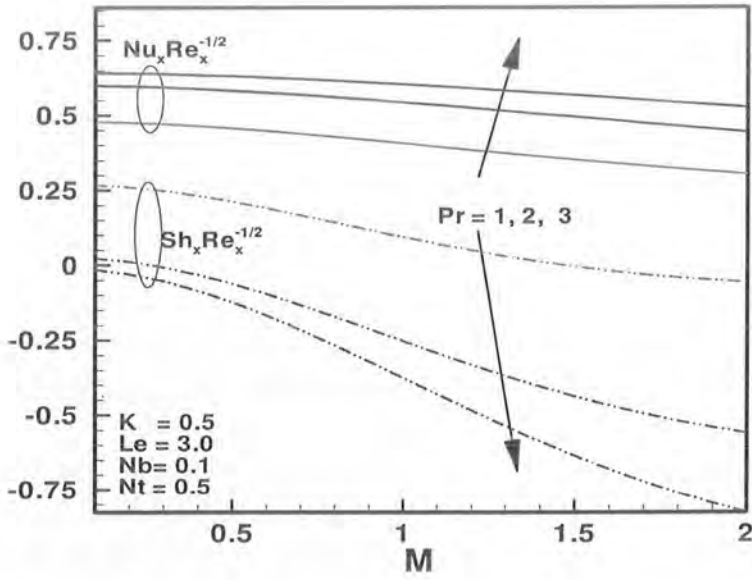


Fig. 7.8: Effects of  $M$  and  $Pr$  on reduced Nusselt and Sherwood number.

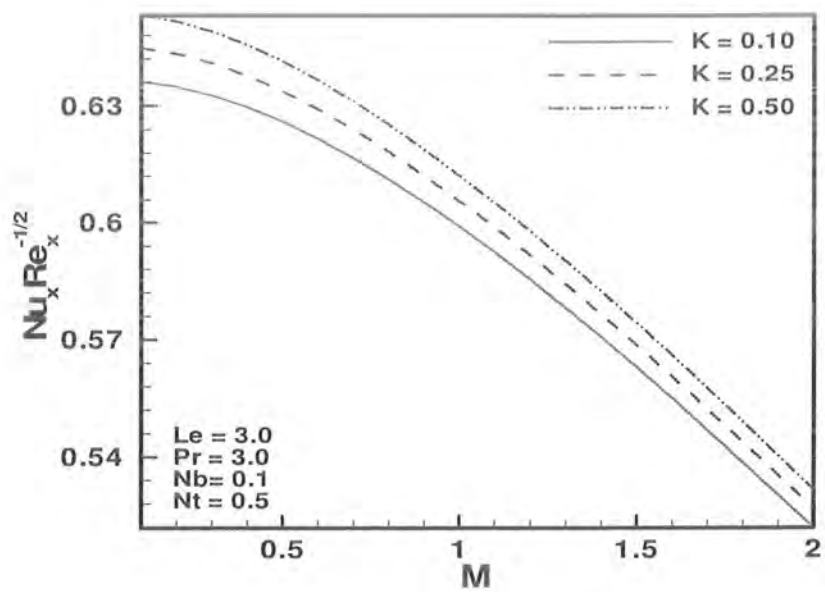


Fig. 7.9: Effects of  $M$  and  $K$  on reduced Nusselt number.

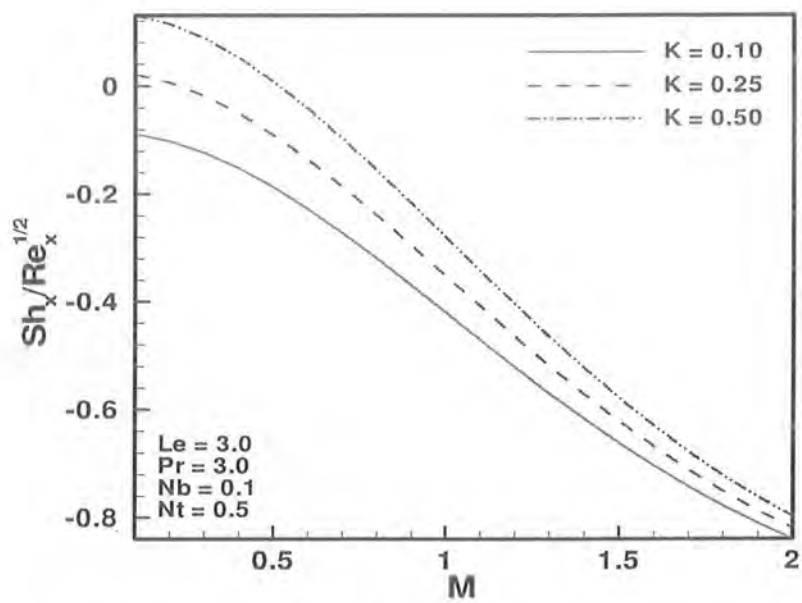


Fig. 7.10: Effects of  $M$  and  $K$  on reduced Sherwood number.

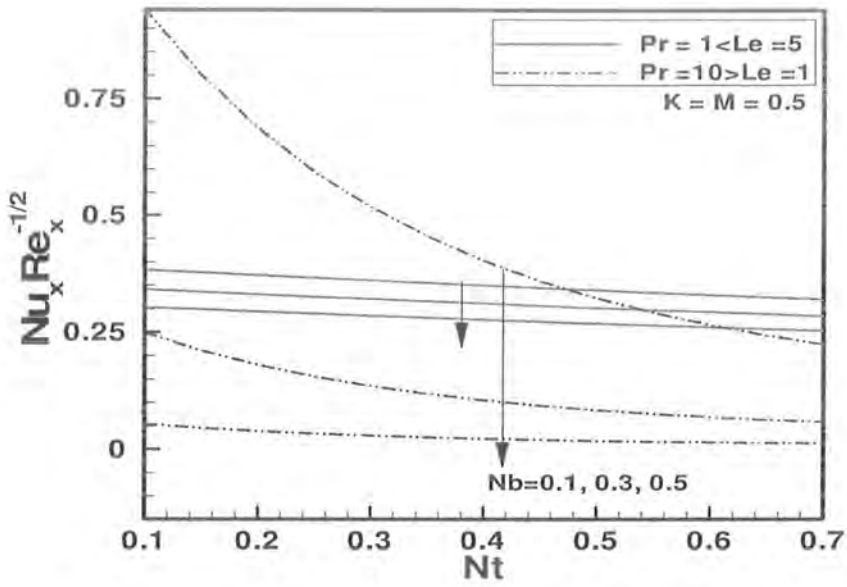


Fig. 7.11: Effects of  $Nb$  and  $Nt$  on reduced Nusselt number.

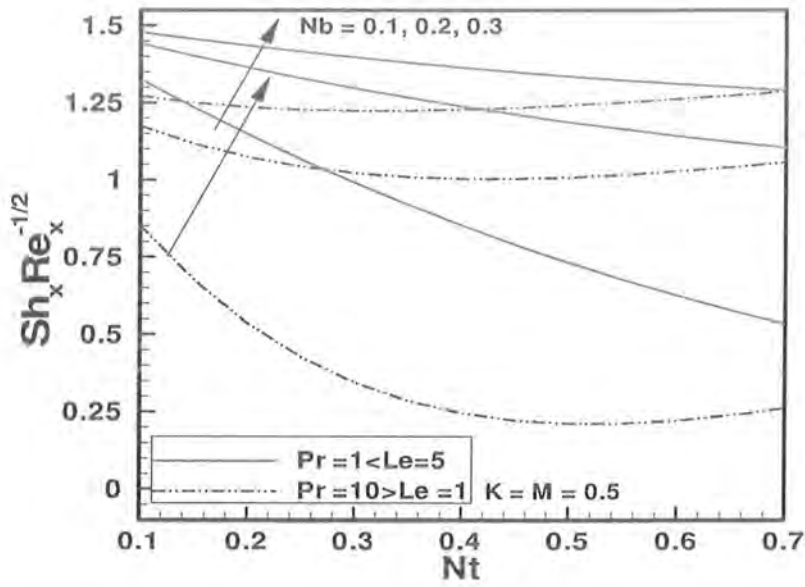


Fig. 7.12: Effects of  $Nb$  and  $Nt$  on reduced Sherwood number.

**Table 7.1:** Comparison of numerical values for reduced Nusselt number  $Re_x^{-1/2}Nu_x$  in the absence of nanoparticle volume concentration and  $M = K = 0$ .

Pr	Present results for $-\theta'(0)$	Wang [15]
0.7	0.4582	0.4539
5.0	0.9114	0.9114
5.0	1.8954	1.8954
20	6.3539	6.3539
70	6.4622	6.4622

**Table 7.2:** Comparison of numerical values for reduced Nusselt number  $Re_x^{-1/2}Nu_x$  and the reduced Sherwood number  $Re_x^{-1/2}Sh$  in the absence of MHD and elastic parameter when  $Pr = 10$ ,  $Le = 1$  and  $Nb = 0.1$ .

Present results $K=M=0$			Khan and Pop [34]	
$Nt$	$-\theta'(0)$	$-\phi'(0)$	$-\theta'(0)$	$-\phi'(0)$
0.1	0.9524	5.1294	0.9524	5.1294
0.2	0.6932	5.2732	0.6932	5.2740
0.3	0.5201	5.5286	0.5201	5.5286
0.4	0.4026	5.7952	0.4026	5.7952
0.5	0.3211	6.0351	0.3211	6.0351

**Table 7.3:** Numerical Values for reduced Nusselt number  $Re_x^{-1/2}Nu_x$  and the reduced Sherwood number  $Re_x^{-1/2}Sh$  in the absence of MHD and elastic parameter when  $M=K=0.5$ ,  $Pr = 10$ ,  $Le = 1$ .

$Nb \downarrow$	$Nt$		$Nt$		$Nt$	
	$-\theta'(0)$	$-\phi'(0)$	$-\theta'(0)$	$-\phi'(0)$	$-\theta'(0)$	$-\phi'(0)$
0.3	0.1352377	5.6037108	0.02907331	5.4936149	0.0055097	5.4275213
0.5	0.0831079	5.7467530	0.01787829	5.5683772	0.0033966	5.4756505
0.7	0.0570193	5.8405019	0.01226842	5.6166732	0.0023337	5.5071765

## 7.4 Closing remarks

In this study we have presented the effect of MHD boundary layer flow of Maxwell nanofluid over stretching sheet. The effects of elastic parameter, Brownian motion and thermophoresis parameters are also discussed. Numerical solutions for velocity, temperature and nanoparticle fraction are developed and discussed. The main results of present analysis can be listed below.

- Influences of  $M$  and  $K$  on temperature profile and nanoparticle fraction are opposite.
- Both temperature and nanoparticle volume concentration give same behavior for  $Pr$  and  $Le$ .
- Influences of  $Nb$  and  $Nt$  on temperature profile are similar.
- Influences of  $Nb$  and  $Nt$  on nanoparticle volume are opposite.
- The magnitude of the reduced Nusselt numbers decreases for higher values of  $Nb$ . The magnitude of the reduced Sherwood numbers increases for higher values of  $Nb$ .

# Numerical Solution of Jeffrey Nanofluid Flow over a Stretching Sheet

## 8.1 Introduction

In the presentation chapter, the steady flow of a Jeffrey fluid model in the presence of nanoparticles is studied. Similarity transformation is used to convert the governing partial differential equations to a set of coupled nonlinear ordinary differential equations which are solved numerically. Behavior of emerging parameters are presented graphically and discussed for velocity, temperature and nanoparticles volume concentration. Variation of the reduced Nusselt and Sherwood number against physical parameters are presented graphically. In conclusion section, it is found that the reduced Nusselt number is a decreasing function while the reduced Sherwood number is increasing function of Brownian parameter  $Nb$  and thermophoresis parameter  $Nt$ .

## 8.2 Problem Formulation

Consider two-dimensional steady incompressible fluid past a stretching sheet. In addition, nanoparticles are saturated within the fluid while the sheet is stretching with the plane  $y = 0$ . The flow is assumed to be confined to  $y > 0$ . In the present case, we assumed that the sheet is stretched with the linear velocity  $u_w(x) = ax$ , where  $a > 0$  is a constant and  $x$ -axis is measured along the stretching surface. The boundary layer equations of Jeffrey fluid saturated with nanoparticles are,

$$\frac{\partial u}{\partial x} + \frac{\partial v}{\partial y} = 0, \quad (8.1)$$

$$u \frac{\partial u}{\partial x} + v \frac{\partial u}{\partial y} = \frac{\nu}{1 + \lambda} \left[ \frac{\partial^2 u}{\partial y^2} + \lambda_1 \left( u \frac{\partial^3 u}{\partial x \partial y^2} - \frac{\partial u}{\partial x} \frac{\partial^2 u}{\partial y^2} + \frac{\partial u}{\partial y} \frac{\partial^2 u}{\partial x \partial y} + v \frac{\partial^3 u}{\partial y^3} \right) \right], \quad (8.2)$$

$$u \frac{\partial T}{\partial x} + v \frac{\partial T}{\partial y} = \alpha \left( \frac{\partial^2 T}{\partial y^2} \right) + \tau \left\{ D_B \left( \frac{\partial C}{\partial y} \frac{\partial T}{\partial y} \right) + \frac{D_T}{T_\infty} \left( \frac{\partial T}{\partial y} \right)^2 \right\}, \quad (8.3)$$

$$u \frac{\partial C}{\partial x} + v \frac{\partial C}{\partial y} = D_B \left( \frac{\partial^2 C}{\partial y^2} \right) + \frac{D_T}{T_\infty} \left( \frac{\partial^2 T}{\partial y^2} \right), \quad (8.4)$$

where  $u$  and  $v$  denote the respective velocities in the  $x$ -and  $y$ -directions respectively,  $\tau = \frac{(\rho_p)_p}{(\rho_f)}$  is the ratio between the effective heat capacity of the nanoparticles material and heat capacity of the fluid,  $\rho_f$  is the density of the base fluid,  $\nu$  is the kinematic viscosity of the fluid,  $\sigma$  is the electrical conductivity,  $\rho$  being the density of the fluid,  $\lambda$  and  $\lambda_1$  are ratio of relaxation to retardation times and retardation time respectively,  $\alpha$  is the thermal diffusivity,  $T$  the fluid temperature,  $C$  the nanoparticles volume concentration,  $T_w$  and  $C_w$  are the temperature of fluid and nanoparticles volume concentration at wall respectively,  $D_B$  is the Brownian diffusion coefficient,  $D_T$  is the thermophoretic diffusion coefficient,  $\beta$  is the volumetric volume expansion coefficient,  $\rho_p$  is the density of the particles. When  $y$  tends to infinity then the ambient values of  $T$  and  $C$  are denoted by  $T_\infty$  and  $C_\infty$ . The associated boundary conditions of Eqs. (8.2)-(8.4) are

$$\begin{aligned} u = u_w(x) = ax, \quad v = 0, \quad T = T_w, \quad C = C_w \quad \text{at } y = 0, \\ u = 0, \quad v = 0, \quad u_y = 0, \quad T = T_\infty, \quad C = C_\infty \quad \text{as } y \rightarrow \infty. \end{aligned} \quad (8.5)$$



Introducing the following similarity transformations

$$\begin{aligned} \psi &= (a\nu)^{1/2} x f(\eta), & \theta(\eta) &= \frac{T - T_\infty}{T_w - T_\infty} \\ \phi(\eta) &= \frac{C - C_\infty}{C_w - C_\infty}, & \eta &= \sqrt{\frac{a}{\nu}} y, \end{aligned} \quad (8.6)$$

where the stream function  $\psi$  is defined as  $u = \frac{\partial \psi}{\partial y}$  and  $v = -\frac{\partial \psi}{\partial x}$ . Making use of Eq.(8.6), the equation of continuity is identically satisfied and Eqs. (8.2) to (8.4) along with (8.5) take the following form

$$f''' + \beta(f''^2 - ff''''') + (1 + \lambda)(ff'' - f'^2) = 0, \quad (8.7)$$

$$\theta'' + \text{Pr} \{ f\theta' + Nb(\theta'\phi') + Nt(\theta')^2 \} = 0, \quad (8.8)$$

$$\phi'' + Le \text{Pr}(f\phi') + \frac{Nt}{Nb} \theta'' = 0, \quad (8.9)$$

$$f(0) = 0, \quad f'(0) = 1, \quad f'(\infty) = 0, \quad f''(\infty) = 0 \quad (8.10)$$

$$\theta(0) = 1, \quad \theta(\infty) = 0, \quad (8.11)$$

$$\phi(0) = 1, \quad \phi(\infty) = 0. \quad (8.12)$$

In these expressions  $\beta = \lambda_1 c$  is Deborah number,  $\text{Pr} = \nu / \alpha$  is the Prandtl number,  $Nb = (\rho c)_p D_B (C_w - C_\infty) / \nu (\rho c)_f$  represents the Brownian motion parameter,  $Nt = (\rho c)_p D_T (T_w - T_\infty) / \nu T_\infty (\rho c)_f$  is the thermophoresis parameter,  $Le = \alpha / D_B$  is the Lewis number. Expressions for the local Nusselt number  $Nu$  and the local Sherwood number  $Sh$  are defined as,

$$Nu_x = \frac{xq_w}{\alpha(T_w - T_\infty)}, \quad Sh_x = \frac{xq_m}{D_B(C_w - C_\infty)}, \quad (8.13)$$

where  $q_w$  and  $q_m$  are the heat flux and mass flux, respectively.

$$q_w = -\alpha \left( \frac{\partial T}{\partial y} \right)_{y=0}, \quad q_m = -D_B \left( \frac{\partial C}{\partial y} \right)_{y=0}. \quad (8.14)$$

Dimensionless form of Eq. (8.13) takes the form

$$Re_x^{-1/2} Nu_x = -\theta'(0), \quad Re_x^{-1/2} Sh_x = -\phi'(0), \quad (8.15)$$

where  $Re_x = u_w(x)x/\nu$  is the local Reynolds number based on the stretching velocity  $u_w(x)$ .

### 8.3 Results and discussions

The above system of ordinary differential equations (8.7)-(8.9) along with the boundary conditions (8.10)-(8.12) are solved numerically. In the present section our main emphasis is to discuss the emerging parameters such as Deborah number  $\beta$ , ratio of relaxation to retardation times parameter  $\lambda$ , Prandtl parameter  $Pr$ , Brownian parameter  $Nb$ , thermophoresis parameter  $Nt$  and Lewis number  $Le$  for velocity profile  $f'(\eta)$ , temperature profile  $\theta(\eta)$  and nanoparticles volume concentration  $\phi(\eta)$ . Fig. 8.1(a) depicts the effects of  $\beta$  on velocity, temperature and nanoparticles volume concentration. It is seen from Fig. 8.1(a) that for higher values of Deborah number  $\beta$ , the velocity profile increases, while the boundary layer thickness decreases gradually. On the other hand, with an increase of  $\beta$ , both temperature and nanoparticles volume concentration profiles reduce. From Fig. 8.1(b), the effects of  $\lambda$  on velocity, temperature and for nanoparticles volume concentration are quite when they are compared with Fig. 8.1(a). It is postulated that an increase in elastic parameter will increase the

resistance of fluid motion. So in the absence of non-Newtonian effects, the present model reduces to the Newtonian model for nanofluid, which presents excellent agreement with results of Khan and Pop [34]. In Figs. 8.2(a) and 8.2(b), we have discussed the behavior of both temperature profile  $\theta(\eta)$  and nanoparticles volume concentration  $\phi(\eta)$  for two main parameters of nanoparticles such as Brownian motion  $Nb$  and thermophoresis parameter  $Nt$ . Hypothetically, enhanced thermal conductivity of a nanofluid is mainly due to Brownian motion which producing micro-mixing. As expected, temperature is an increasing function of Brownian parameter (see Fig. 8.2(a)). Whereas, large values of Brownian motion parameter reduces the nanoparticles volume concentration. On the other hand, it is observed from Fig. 8.2(b) that for higher values of Thermophoresis parameter  $Nt$ , both temperature and nanoparticles volume concentration are increasing. Comparatively, it is examined from Fig. 8.2(a) and 8.2(b), there is an enhancement in temperature with respect to large values of both Brownian and thermophoresis parameter while, opposite behavior can be observed for nanoparticles volume concentration with the increase of Brownian and thermophoresis parameters (see Figs. 8.2(a) and 8.2(b)). The effects of Prandtl number  $Pr$  on  $\theta(\eta)$  and  $\phi(\eta)$  can be seen in Fig. 8.3(a), Since  $Pr$  is a ratio of viscous diffusion rate to the thermal diffusion rate, thus higher Prandtl number reduces the thermal diffusivity. Consequently, same sort of results appear for  $Pr$  in Fig. 8.3(a) for higher values of  $Pr$  it decreases both temperature and nanoparticles volume concentration. It is also illustrated from Fig. 8.3(b) that both temperature and nanoparticles volume concentration show the opposite behavior for higher values of  $Le$ .

Table 8.1 and 8.2, present that excellent comparison between the present results with the results of Khan and Pop [34] for local Nusselt number  $\theta'(0)$  and Sherwood number  $\phi'(0)$ . From Tables. 8.1 and 8.2, it is found that in the absence of non-Newtonian effects for present model

reduces to the Newtonian model with nanoparticle effects. Table 8.3 present the numerical values of both Brownian motion and thermophoresis parameters in the presence of non-Newtonian parameters ( $\beta = \lambda = 0.5$ ), when  $Pr = 10$  and  $Le = 1$ . Effects of physical parameters on non-dimensional Nusselt number  $\theta'(0)$  and Sherwood number  $\phi'(0)$  are also presented through Figs. 8.4-8.7. From Figs. 8.4 and 8.5, for increasing values of Brownian motion parameter it reduces the Nusselt number  $\theta'(0)$  for different values of  $Pr$  and  $Le$ . In both cases either we take higher values of  $Pr$  (see Fig. 8.4(a) and 4.6(b)) or higher values of  $Le$  (see Fig. 8.5(a) and 8.5(b)) same sort of behavior can be seen on reduced Nusselt number  $\theta'(0)$  for higher values of Brownian motion parameter  $Nb$ . From Figs. 8.6 and 8.7, Sherwood number  $\phi'(0)$  increases or decreases with an increase in Brownian motion parameter  $Nb$ , Prandtl number  $Pr$  and Lewis number  $Le$ . Finally it is observed from these phenomena that there is a low thermal conductivity for higher Prandtl number and concentration profile varies with respect to higher or lower values of Prandtl number.

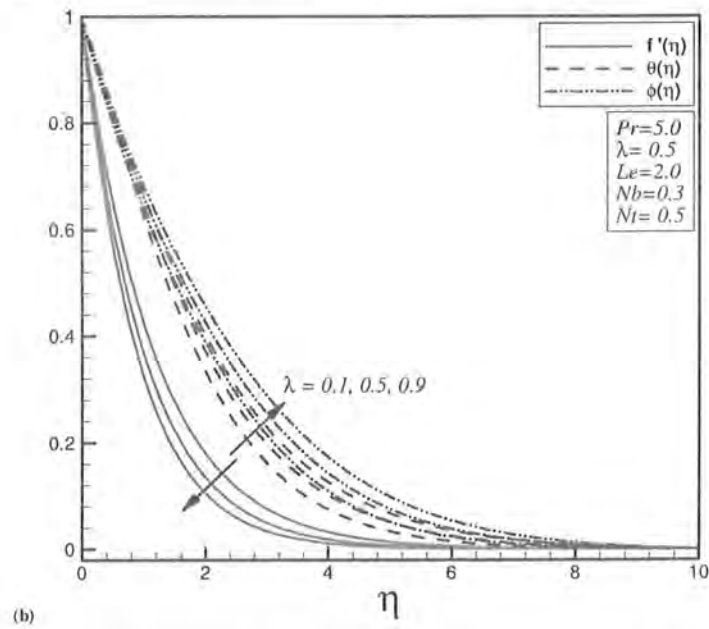
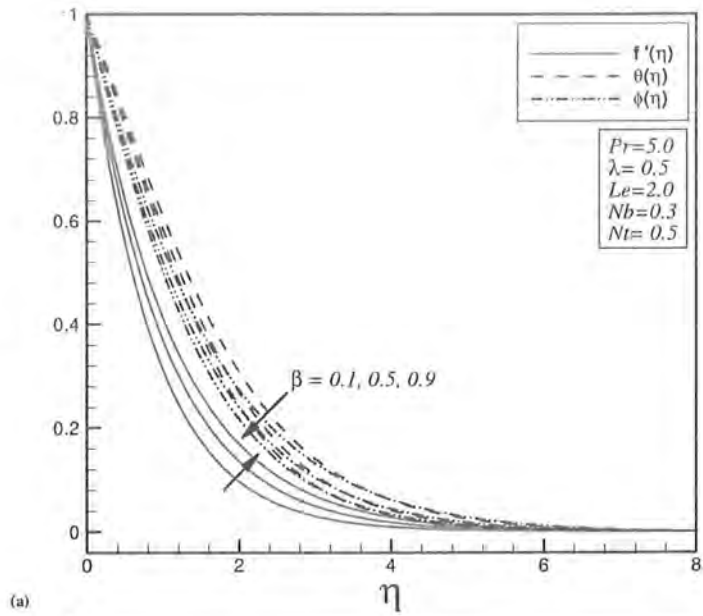


Fig 8.1: Variation of velocity profile  $f'(\eta)$ , temperature profile  $\theta(\eta)$  and nanoparticle volume concentration  $\phi(\eta)$  for (a)  $\beta$  (b)  $\lambda$ .

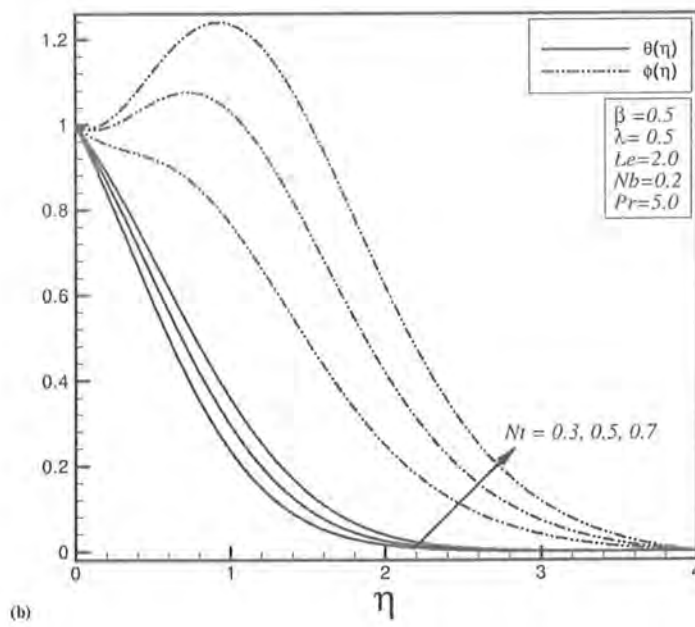
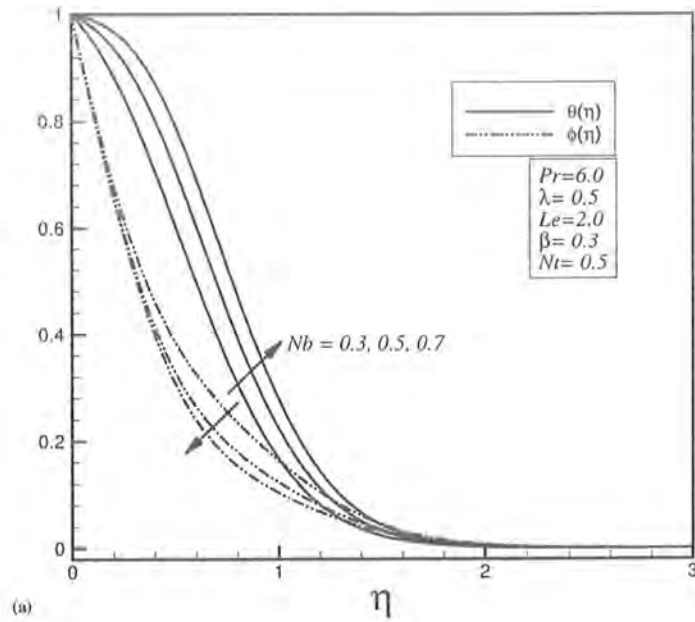


Fig 8.2: Variation of temperature profile  $\theta(\eta)$  and nanoparticle volume concentration  $\phi(\eta)$  for (a)  $Nb$  (b)  $Nt$ .

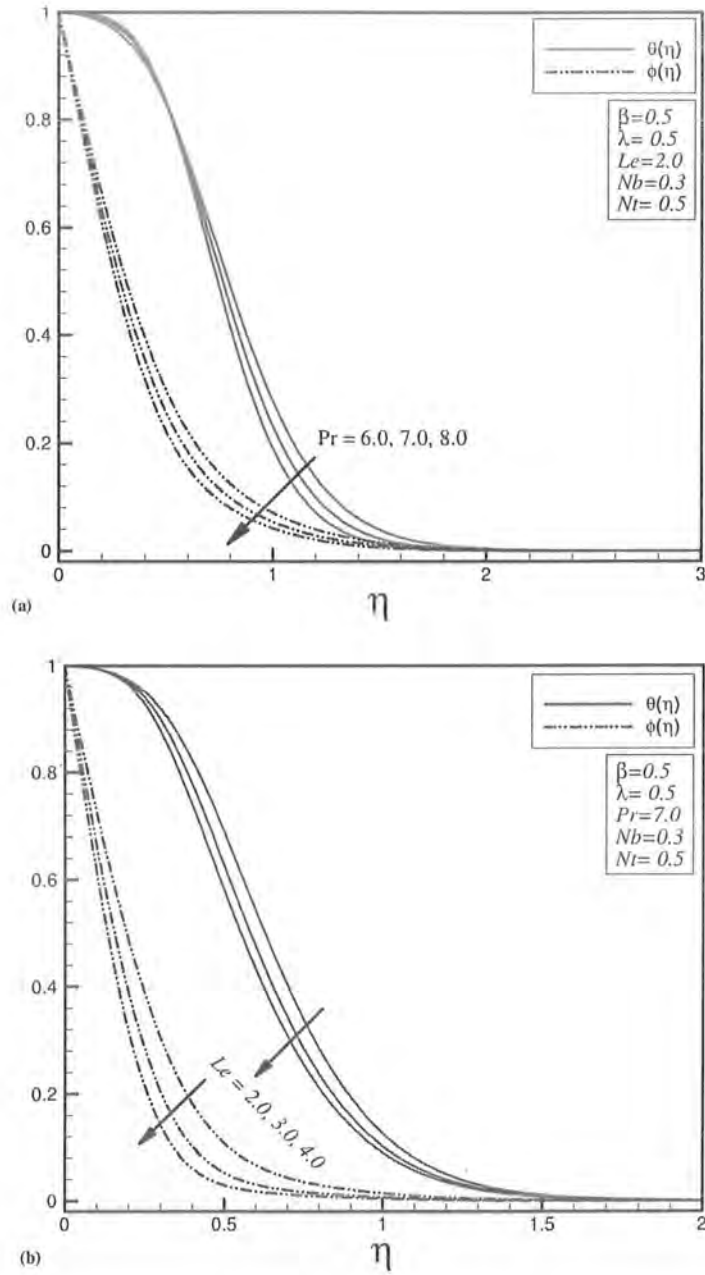
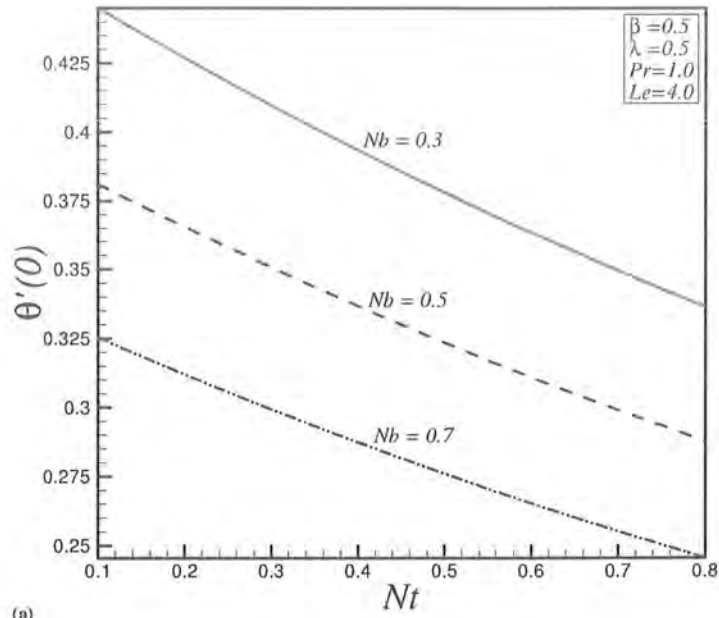
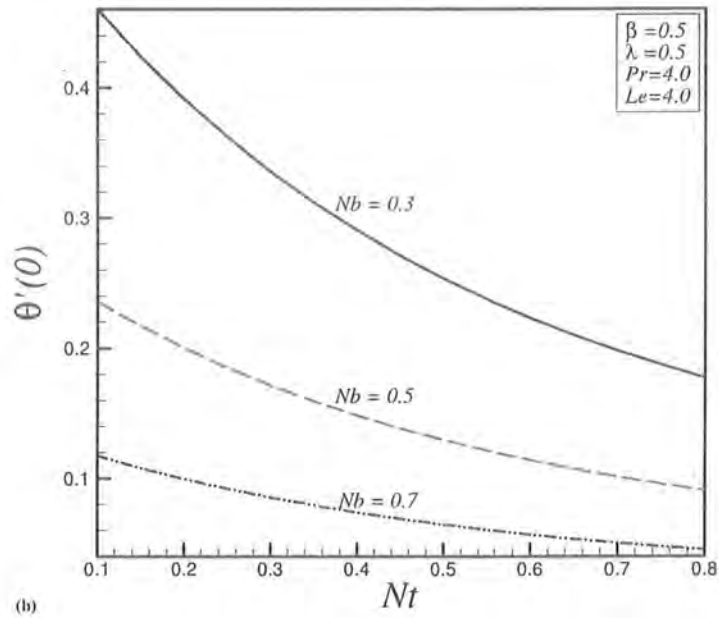


Fig 8.3: Variation of temperature profile  $\theta(\eta)$  and nanoparticle volume concentration  $\phi(\eta)$  (a) Pr (b)  $Le$ .



(a)



(b)

Fig 8.4: Effects of  $Nb$  and  $Nt$  on reduced Nusselt number (a) When  $Pr=1$  (b) When  $Pr=4$ .



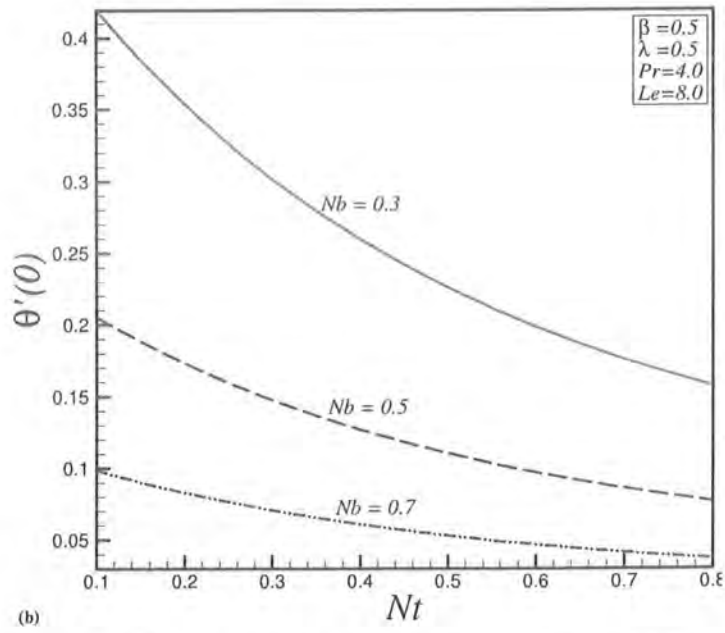
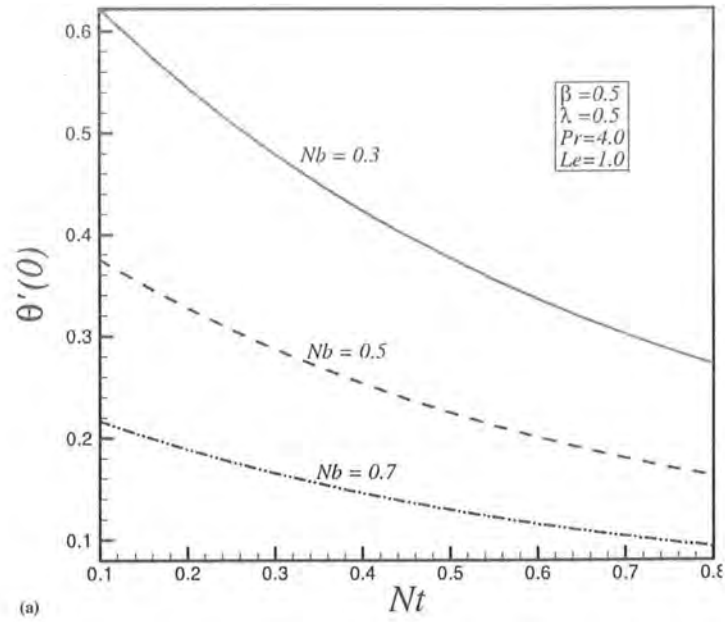


Fig 8.5: Effects of  $Nb$  and  $Nt$  on reduced Nusselt number (a) When  $Le=1$  (b) When  $Le=8$ .

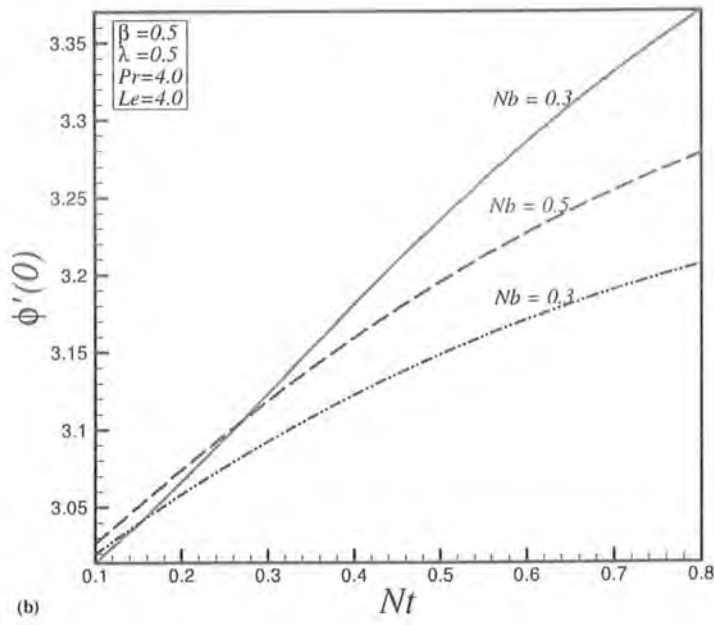
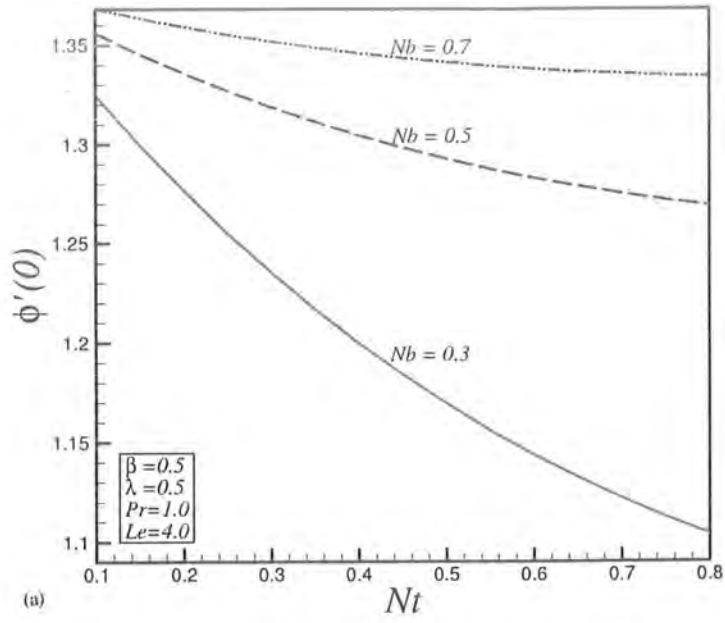
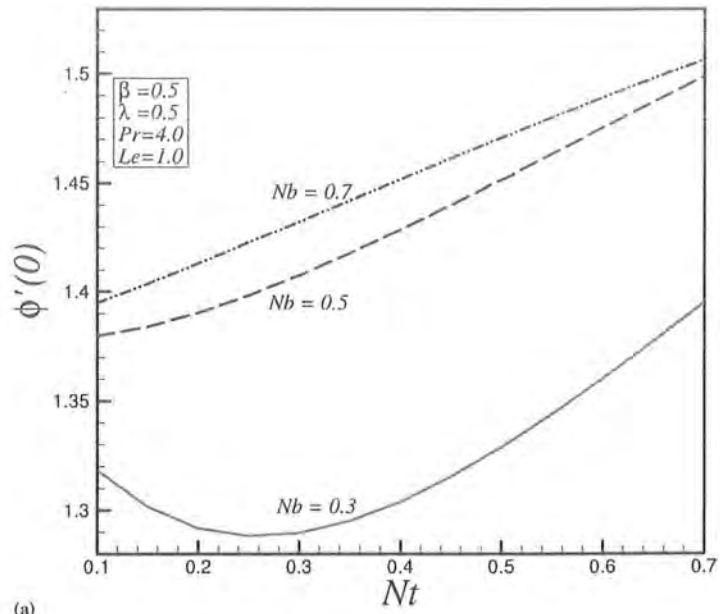
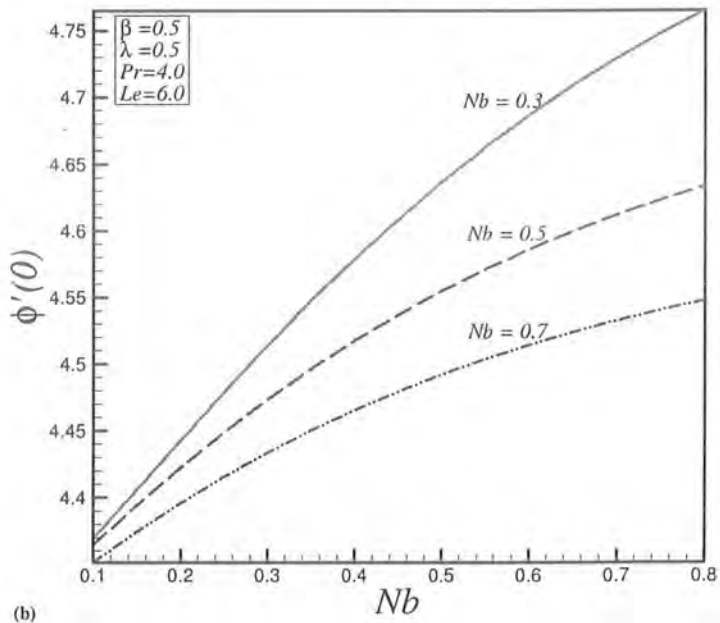


Fig 8.6: Effects of  $Nb$  and  $Nt$  on reduced Sherwood number (a) When  $Pr=1$  (b) When  $Pr=4$ .



(a)



(b)

Fig 8.7: Effects of  $Nb$  and  $Nt$  on reduced Sherwood number (a) When  $Le=1$  (b) When  $Le=8$ .

**Table 8.1:** Comparison of Numerical Values for local Nusselt number  $Re_x^{-1/2} Nu_x$  in the absence of non-Newtonian effects i.e ( $\beta = \lambda = 0$ ) when  $Pr = 10$  and  $Le = 1$ .

$Nt \downarrow$	$Nb = 0.1$		$Nb = 0.3$		$Nb = 0.5$	
	Khan and Pop [34]	Present study	Khan and Pop [34]	Present study	Khan and Pop [34]	Present study
	$-\theta'(0) \downarrow$	$-\theta'(0) \downarrow$	$-\theta'(0) \downarrow$	$-\theta'(0) \downarrow$	$-\theta'(0) \downarrow$	$-\theta'(0) \downarrow$
0.1	0.9524	0.95247	0.2522	0.25223	0.0543	0.05433
0.3	0.5201	0.52013	0.1355	0.13554	0.0291	0.02918
0.5	0.3211	0.32110	0.0833	0.08336	0.0179	0.01794

**Table 8.2:** Comparison of numerical values for local Sherwood number  $Re_x^{-1/2} Sh$  in the absence of non-Newtonian effects i.e ( $\beta = \lambda = 0$ ) when  $Pr = 10$  and  $Le = 1$ .

$Nt \downarrow$	$Nb = 0.1$		$Nb = 0.3$		$Nb = 0.5$	
	Khan and Pop [34]	Present study	Khan and Pop [34]	Present study	Khan and Pop [34]	Present study
	$-\phi'(0) \downarrow$	$-\phi'(0) \downarrow$	$-\phi'(0) \downarrow$	$-\phi'(0) \downarrow$	$-\phi'(0) \downarrow$	$-\phi'(0) \downarrow$
0.1	5.1294	5.12946	5.4100	5.41002	5.3836	5.3836
0.3	5.5286	5.52861	5.6088	5.60881	5.4984	5.4984
0.5	6.0351	6.03515	5.7519	5.75199	5.5731	5.5731

**Table 8.3:** Numerical values for reduced Nusselt number  $Re_x^{-1/2} Nu_x$  and the reduced Sherwood number  $Re_x^{-1/2} Sh$  in the presence of the effects of non-Newtonian fluid when  $\lambda = 0.5$ ,  $\beta = 0.5$ ,  $Pr = 10$  and  $Le = 1$ .

$Nb \downarrow$	$Nt = 0.1$		$Nt = 0.3$		$Nt = 0.5$	
	$-\theta'(0) \downarrow$	$-\phi'(0) \downarrow$	$-\theta'(0) \downarrow$	$-\phi'(0) \downarrow$	$-\theta'(0) \downarrow$	$-\phi'(0) \downarrow$
0.1	-1.710019	-0.763686	-1.302975	5.308676	-0.990168	5.798262
0.3	-1.144226	-0.311453	-0.845832	-0.042291	-0.628085	-0.003197
0.5	-0.708856	-0.499848	-0.509359	-0.439533	-0.370789	-0.458568
0.7	-0.402155	-0.562068	-0.2821123	-0.563054	-0.202194	-0.591438

## 8.4 Concluding points

In the present study we have presented the effect of nanoparticles for Jeffrey fluid over a stretching sheet. The effects of elastic parameter, Brownian motion and thermophoresis parameters are also discussed. Numerical solutions for velocity, temperature and nanoparticle volume concentration are developed and discussed. The main results of present analysis can be listed below.

- Effects of  $\beta$  and  $\lambda$  are opposite for velocity and temperature profiles.
- Both  $Pr$  and  $Le$  give same behavior for temperature.
- Effects of  $Nb$  and  $Nt$  for temperature profile are similar.
- Effects of  $Nb$  and  $Nt$  for nanoparticle volume concentration are opposite.
- The magnitude of the reduced Nusselt numbers decreases for higher values of  $Nb$ .
- The magnitude and direction of the local Sherwood numbers varies with an increase or a decrease of both  $Pr$  and  $Le$ .

# Numerical study of boundary layer flow and heat transfer of Oldroyd-B nanofluid towards a stretching sheet

## 9.1 Introduction

In the present article we considered two-dimensional steady incompressible Oldroyd-B fluid past a stretching sheet saturated with nanoparticles. Using the similarity transformation, reduce the system of nonlinear partial differential equations will reduce into the system of nonlinear ordinary differential equations. The coupled governing nonlinear equations are then solved numerically. Numerical results are presented graphically to see the physical behaviors of the involved fluid parameters namely Deborah numbers  $\beta_1$  and  $\beta_2$ , Prandtl number  $Pr$ , Brownian motion  $Nb$ , thermophoresis parameter  $Nt$  and Lewis number  $Le$  on velocity, temperature and nanoparticle volume concentration profile are discussed. Interesting results are shown graphically. The Nusselt and Sherwood numbers are also computed numerically and plotted against the flow control parameters. To see the validity of the present results, we have made the comparison of present results with the existing literatures through tables.

## 9.2 Problem Formulation

Consider two-dimensional steady incompressible Oldroyd-B fluid past a stretching sheet. In addition, nanoparticles are saturated within the fluid, while sheet is stretching along the plane  $y = 0$ . The flow is assumed to be confined to  $y > 0$ . Here we assumed that the sheet is stretched with the linear velocity  $u(x) = ax$ , where  $a > 0$  is constant and  $x$ -axis is measured along the

stretching surface. The boundary layer equations of Oldroyd-B fluid model along with the thermal energy and nanoparticles equations for nanofluids are,

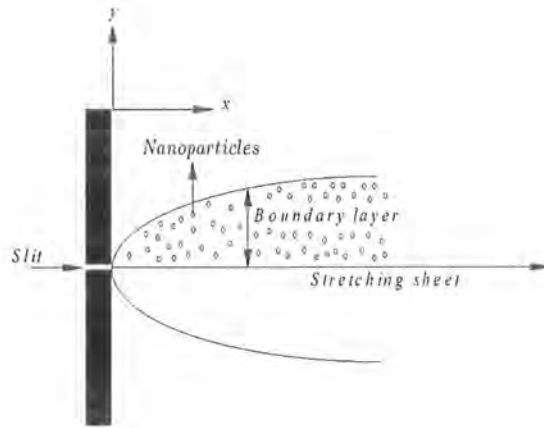


Fig 9.1: Geometry of the problem.

$$u \frac{\partial u}{\partial x} + v \frac{\partial v}{\partial y} = 0, \quad (9.1)$$

$$u \frac{\partial u}{\partial x} + v \frac{\partial u}{\partial y} + \lambda_1 \left( v^2 \frac{\partial^2 u}{\partial y^2} + 2uv \frac{\partial^2 u}{\partial x \partial y} \right) = v \left\{ \frac{\partial^2 u}{\partial y^2} + \lambda_2 \left( v \frac{\partial^3 u}{\partial y^3} - \frac{\partial u}{\partial y} \frac{\partial^2 v}{\partial y^2} \right) \right\}, \quad (9.2)$$

$$u \frac{\partial T}{\partial x} + v \frac{\partial T}{\partial y} = \alpha \left( \frac{\partial^2 T}{\partial y^2} \right) + \tau \left\{ D_B \left( \frac{\partial C}{\partial y} \frac{\partial T}{\partial y} \right) + \frac{D_T}{T_\infty} \left( \frac{\partial T}{\partial y} \right)^2 \right\}, \quad (9.3)$$

$$u \frac{\partial C}{\partial x} + v \frac{\partial C}{\partial y} = D_B \left( \frac{\partial^2 C}{\partial y^2} \right) + \frac{D_T}{T_\infty} \left( \frac{\partial^2 T}{\partial y^2} \right), \quad (9.4)$$

where  $u$  and  $v$  denote the respective velocities in the  $x$ - and  $y$ -directions respectively,  $\rho_f$  is the density of the base fluid,  $\nu$  is the kinematic viscosity of the fluid,  $\sigma$  is the electrical conductivity,  $\lambda_1$  and  $\lambda_2$  are the relaxation and retardation times,  $\alpha$  is the thermal diffusivity,  $T$

is the fluid temperature,  $C$  is the nanoparticle volume concentration,  $T_w$  and  $C_w$  are the temperature of fluid and nanoparticle volume concentration at the wall respectively,  $D_B$  is the Brownian diffusion coefficient,  $D_T$  is the thermophoresis diffusion coefficient,  $\tau = (\rho c)_p / (\rho c)_f$  is the ratio between the effective heat capacity of the nanoparticle material and heat capacity of the fluid,  $\beta$  is the volumetric volume expansion coefficient and  $\rho_p$  is the density of the particles. When  $y$  tends to infinity then the ambient values of  $T$  and  $C$  are denoted by  $T_\infty$  and  $C_\infty$ . The associated boundary conditions of Eqs. 9.2–9.4 are

$$\begin{aligned} u = u_w(x) = ax, \quad v = 0, \quad T = T_w, \quad C = C_w \quad \text{at } y = 0, \\ u = 0, \quad v = 0, \quad T = T_\infty, \quad C = C_\infty \quad \text{as } y \rightarrow \infty. \end{aligned} \quad (9.5)$$

Introducing the following similarity transformations

$$\psi = (av)^{1/2} x f(\eta), \quad \theta(\eta) = \frac{T - T_\infty}{T_w - T_\infty}, \quad \phi(\eta) = \frac{C - C_\infty}{C_w - C_\infty}, \quad \eta = \sqrt{\frac{a}{\nu}} y, \quad (9.6)$$

where the stream function  $\psi$  is defined as  $u = \frac{\partial \psi}{\partial y}$  and  $v = -\frac{\partial \psi}{\partial x}$ . Making use of Eq. (9.6), equation of continuity is identically satisfied and Eqs. (9.2)-(9.4) along with (9.5) take the following form:

$$f''' - (f')^2 + ff'' + \beta_1 (f^2 f''' - 2ff'f'') + \beta_2 (f''^2 - ff''') = 0, \quad (9.7)$$

$$\theta'' + \text{Pr} (f\theta' + \text{Nb}(\theta'\phi') + \text{Nt}(\theta')^2) = 0, \quad (9.8)$$

$$\phi'' + \text{Le Pr} (f\phi') + \frac{\text{Nt}}{\text{Nb}} \theta'' = 0, \quad (9.9)$$

$$f(0) = 0, \quad f'(0) = 1, \quad f'(\infty) = 0, \quad f''(\infty) = 0, \quad (9.10)$$



$$\theta(0) = 1, \theta(\infty) = 0, \quad (9.11)$$

$$\phi(0) = 1, \phi(\infty) = 0. \quad (9.12)$$

Here prime indicates differentiation with respect to  $\eta$ ,  $\beta_1 = a\lambda_1$  and  $\beta_2 = a\lambda_2$  are the Deborah numbers in terms of relaxation and retardation times, respectively,  $Pr = \nu / \alpha$  is the Prandtl number,  $Le = \alpha / D_B$  is the Lewis number,  $Nb = (\rho c)_p D_B (C_w - C_\infty) / \nu (\rho c)_f$  is the Brownian motion and  $Nt = (\rho c)_p D_T (T_w - T_\infty) / \nu T_\infty (\rho c)_f$  is the thermophoresis parameter. Expressions for the local Nusselt number  $Nu$  and the local Sherwood number  $Sh$  are

$$Nu = \frac{xq_w}{\alpha(T_w - T_\infty)}, \quad Sh = \frac{xq_m}{D_B(C_w - C_\infty)}, \quad (9.13)$$

where  $q_w$  and  $q_m$  are the heat flux and mass flux, respectively.

$$q_w = -\alpha \left( \frac{\partial T}{\partial y} \right)_{y=0}, \quad q_m = -D_B \left( \frac{\partial C}{\partial y} \right)_{y=0}. \quad (9.14)$$

Dimensionless form of Eq. (9.13), takes the following form

$$Re_x^{-1/2} Nu = -\theta'(0), \quad Re_x^{-1/2} Sh = -\phi(0). \quad (9.15)$$

where  $Re_x = u_w(x)x / \nu$  is the local Reynolds number based on the stretching velocity  $u_w(x)$ .

### 9.3 Results and discussions

The nonlinear coupled ordinary differential equations (9.7)-(9.9) subject to the boundary conditions (9.10)-(9.12) have been solved numerically by using Runge-Kutta-Fehlberg method with shooting technique. Figs. (9.2)-(9.7) illustrate the behavior of emerging parameters such as relaxation time constant  $\beta_1$ , retardation time constant  $\beta_2$ , Prandtl parameter  $Pr$ , Brownian

parameter  $Nb$ , thermophoresis parameter  $Nt$  and Lewis number  $Le$  for velocity profile  $f'(\eta)$ , temperature profile  $\theta(\eta)$  and nanoparticle fraction  $\phi(\eta)$ . Fig. 9.2, depicts the variation of  $\beta_1$  on  $f'(\eta)$ ,  $\theta(\eta)$  and  $\phi(\eta)$ . Since  $\beta_1$  is a function of relaxation time  $\lambda_1$  and due to viscoelastic properties of fluid it always resists the motion of the fluid. As a result, velocity profile  $f'(\eta)$  and the boundary layer thickness are decreasing functions of  $\beta_1$ . On the other hand, both temperature profile  $\theta(\eta)$  and nanoparticle volume concentration  $\phi(\eta)$  increase with an increase of Deborah number  $\beta_1$  (see Fig. 9.2). Physical behavior of Fig. 9.2 is due to an increase in retardation time of any material enhances the flow. Consequently, with an increase of  $\beta_2$ , velocity profile increases and both temperature and nanoparticle volume concentration decrease (see Fig. 9.2). Thus, it is concluded that  $\beta_1$  and  $\beta_2$  has opposite results on  $f'(\eta)$ ,  $\theta(\eta)$  and  $\phi(\eta)$  due to relaxation and retardation times, respectively (see Fig. 9.2 and 9.3).

Physically it is observed that an increase in elastic parameter will increase the resistance of fluid motion. Table 9.1, illustrates the excellent agreement with results of Khan and Pop [34] in the absence of non-Newtonian parameters  $\beta_1$  and  $\beta_2$ . As expected, it is found from Fig. 9.4, that both temperature profile and nanoparticle volume concentration demonstrate the decreasing behavior with the increase of  $Pr$ . It is illustrated from Fig. 9.5, both temperature and nanoparticle fraction show the same behavior when they are compared with Fig. 9.4, for higher values of  $Le$ . Consequently, boundary layer thickness decreases indefinitely with an increase in  $Pr$ . Effects of Brownian motion and thermophoresis parameter on temperature profile  $\theta(\eta)$  and nanoparticle volume concentration  $\phi(\eta)$  are shown in Figs. 9.6 and 9.9. It is observed from Figs. 9.6 and 9.7, that for higher values of both  $Nb$  and  $Nt$ , the temperature profile arises. On the other hand, Fig. 9.6 shows opposite behavior for nanoparticle volume concentration when it is

compared with Fig. 9.7, for increasing values of both  $Nb$  and  $Nt$ . In fact, in the absence of both nanoparticles and non-Newtonian effects, there is an excellent agreement with Wang [15] that can be seen in Table 9.9. The effects of elastic parameter, Prandtl parameter, Brownian parameter, thermophoresis parameter and Lewis number on the Nusselt number  $\theta'(0)$  and Sherwood number  $\phi'(0)$  are presented in Figs. 9.8-9.11. It is seen from Figs. 9.8 and 9.9 that the variation of Nusselt number  $\theta'(0)$  with  $Nt$  reduces in both cases when  $Pr$  is less or greater than  $Le$  for  $Nb=0.3, 0.5$  and  $0.7$  while the rest of the parameters are fixed. On the other hand, it increases the Sherwood number  $\phi'(0)$  for higher values of Brownian motion  $Nb$  for various values of both Prandtl number and Lewis number (see Fig. 9.10 and 9.11). Finally, it is depicted that there is low thermal conductivity for higher Prandtl number. Consequently, it reduces the conduction and the heat transfer rate increases at the surface of the sheet.

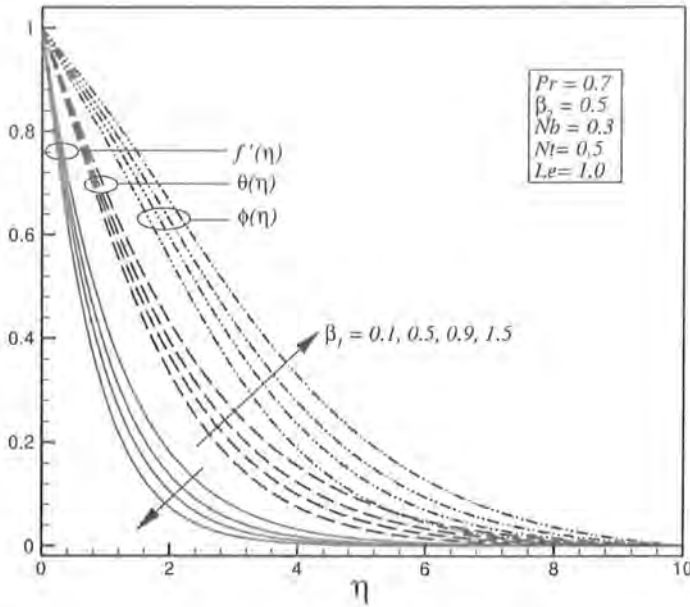


Fig 9.2: Variation of velocity, temperature and nanoparticle volume concentration with  $\beta_1$ .

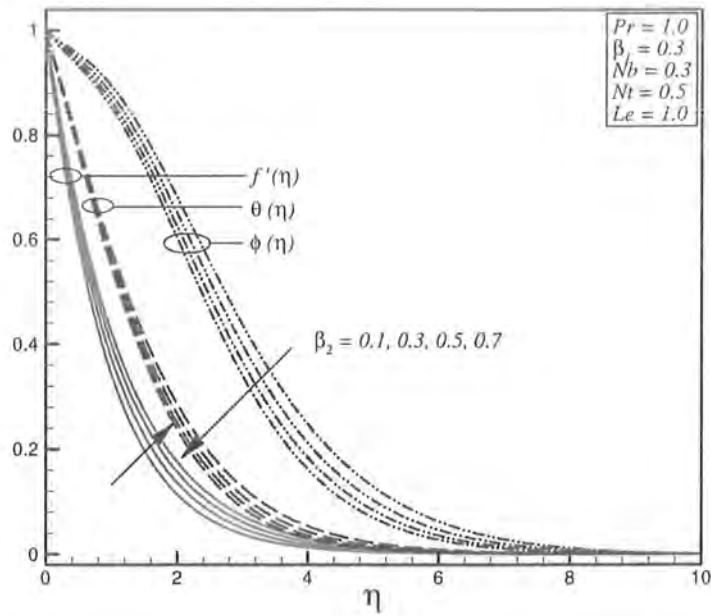


Fig 9.3: Variation of velocity, temperature and nanoparticle volume concentration with  $\beta_2$ .

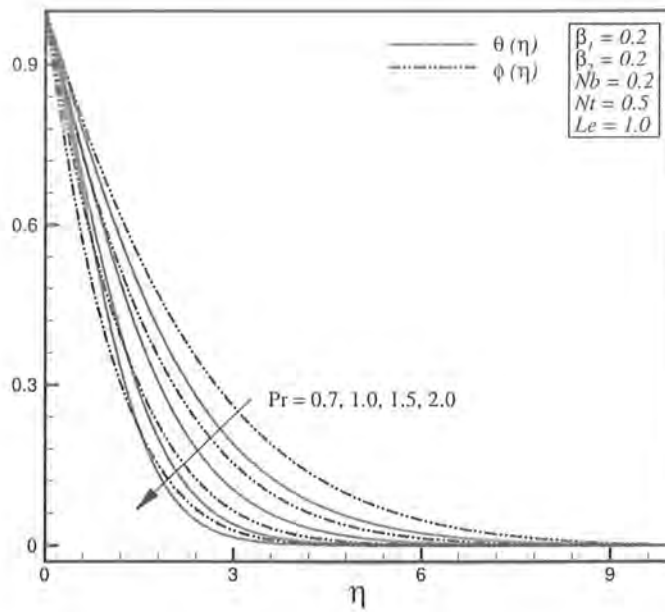


Fig 9.4: Variation of temperature and nanoparticle volume concentration for various values of Pr.

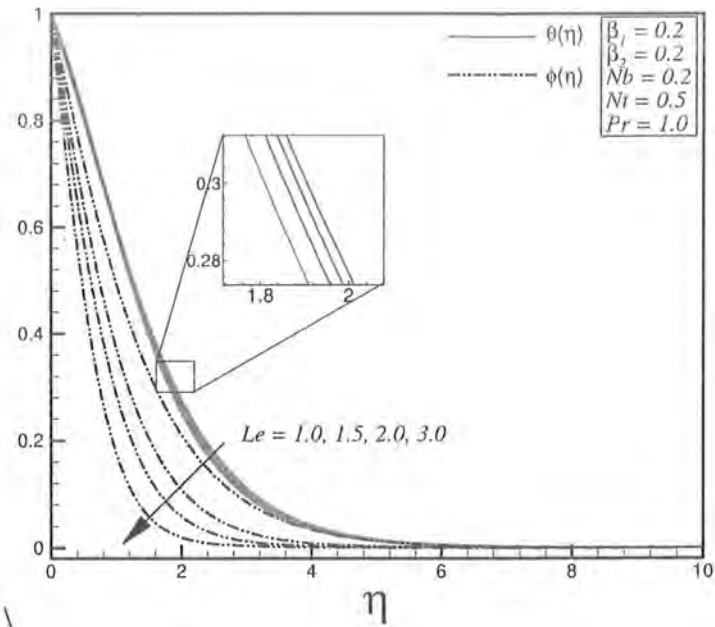


Fig 9.5: Variation of temperature and nanoparticle volume concentration for various values of  $Le$ .

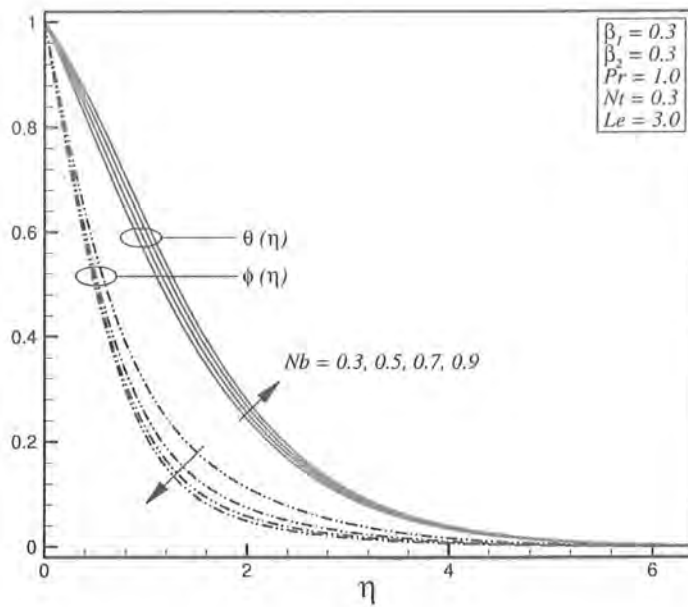


Fig 9.6: Variation of temperature and nanoparticle volume concentration for various values of  $Nb$ .

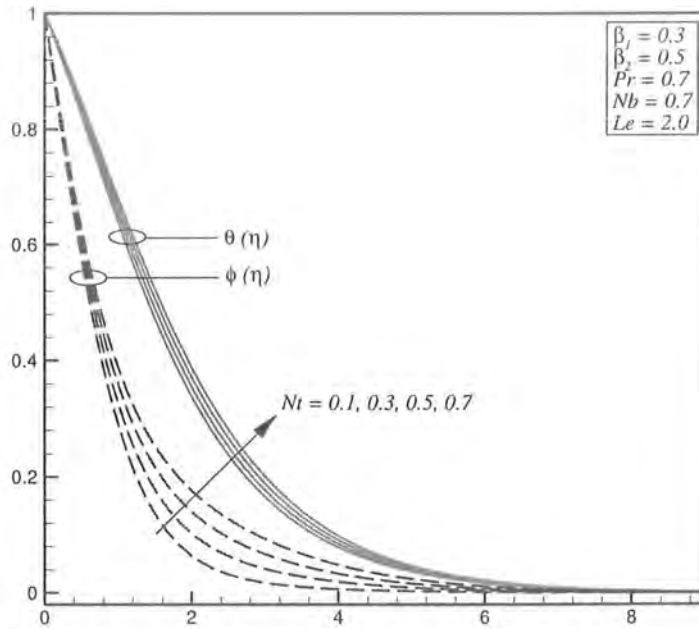


Fig 9.7: Variation of temperature and nanoparticle volume concentration for various values of  $Nt$ .

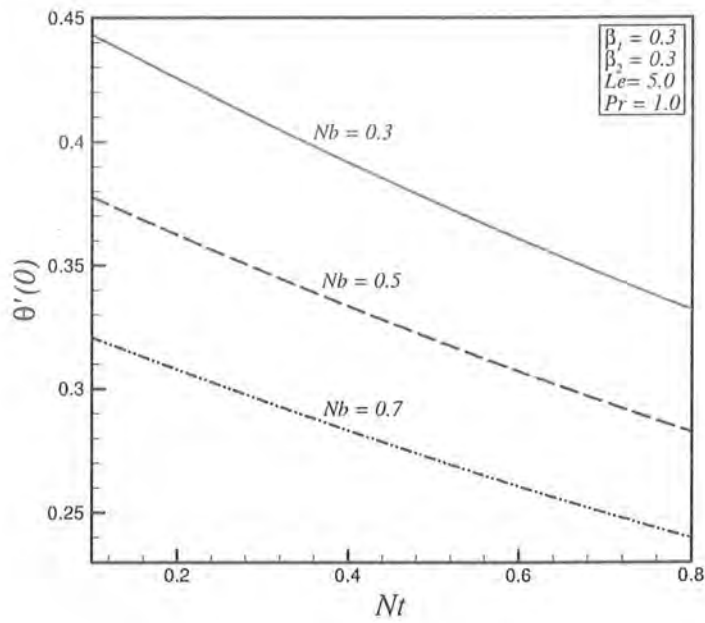


Fig 9.8: Variation of Nusselt number with  $Nt$  for various values of  $Nb$  when  $Pr < Le$ .

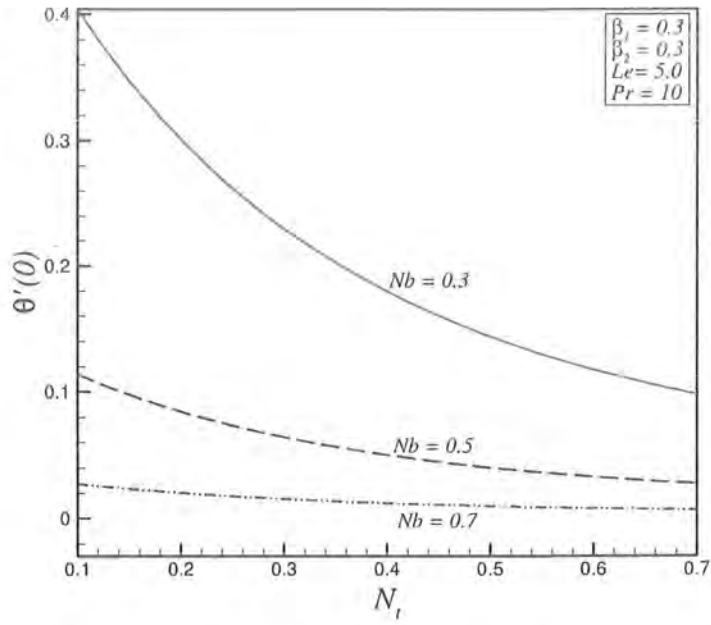


Fig 9.9: Variation of Nusselt number with  $Nt$  for various values of  $Nb$  when  $Pr > Le$ .

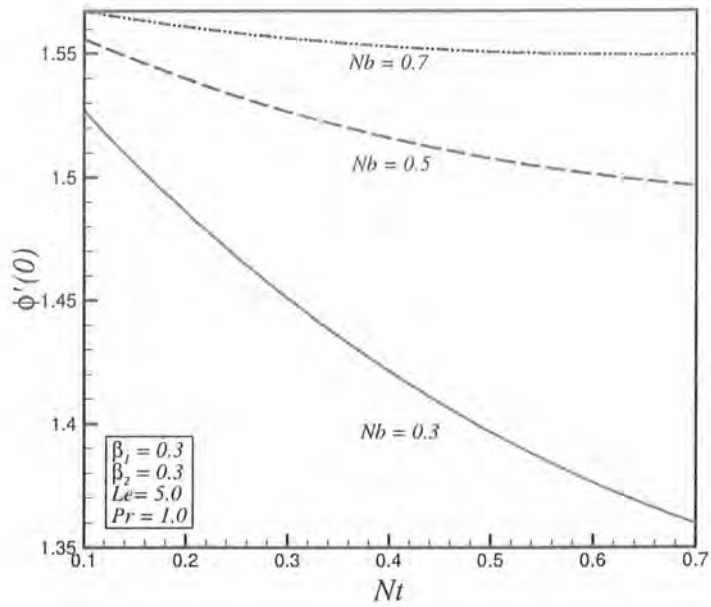


Fig 9.10: Variation of Sherwood number with  $Nt$  for various values of  $Nb$  when  $Pr < Le$ .

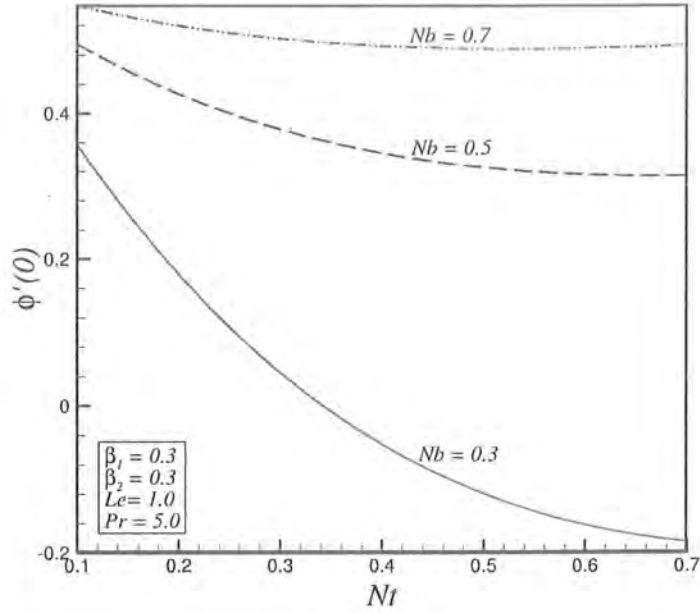


Fig 9.11: Variation of Sherwood number with  $Nt$  for various values of  $Nb$  when  $Pr > Le$ .

**Table 9.1:** Comparison of numerical values for local Nusselt number  $Re_x^{-1/2} Nu_x$  and the local Sherwood number  $Re_x^{-1/2} Sh$  in the absence of non-Newtonian parameters when  $Pr = 10$  and  $Le = 1$ .

Present results $\beta_1 = \beta_2 = 0$			Khan and Pop [34]	
$Nt$	$-\theta'(0)$	$-\phi'(0)$	$-\theta'(0)$	$-\phi'(0)$
0.1	0.9524	5.1294	0.9524	5.1294
0.2	0.6932	5.2732	0.6932	5.2740
0.3	0.5201	5.5286	0.5201	5.5286
0.4	0.4026	5.7952	0.4026	5.7952
0.5	0.3211	6.0351	0.3211	6.0351



**Table 9.2:** Comparison of numerical values for reduced Nusselt number  $Re_x^{-1/2} Nu_x$  in the absence of non-Newtonian parameters ( $\beta_1 = \beta_2 = 0$ ) and nanoparticle.

Pr	Present results for $-\theta'(0)$	Wang [15]
0.7	0.4582	0.4539
5.0	0.9114	0.9114
10	1.8954	1.8954
20	6.3539	6.3539
70	6.4622	6.4622

**Table 9.3:** Numerical Values for the reduced Nusselt number  $Re_x^{-1/2} Nu_x$  and the reduced Sherwood number  $Re_x^{-1/2} Sh$  in the presence of nanoparticle when  $\beta_1 = \beta_2 = 0.3$ .

$Nt \downarrow$	$Nb = 0.3$		$Nb = 0.5$		$Nb = 0.7$	
	$-\theta'(0)$	$-\phi'(0)$	$-\theta'(0)$	$-\phi'(0)$	$-\theta'(0)$	$-\phi'(0)$
0.3	0.33988	1.83935	0.14820	1.87035	0.06012	1.84885
0.5	0.24099	1.95862	0.10486	1.94572	0.04255	1.90081
0.7	0.17918	5.06659	0.07792	5.00568	0.03163	1.94018

## 9.4 Conclusions

In this study we have presented the Oldroyd-B fluid model for nanofluid over a stretching sheet. The effects of elastic parameter, Brownian motion and thermophoresis parameters on flow and heat transfer are discussed numerically. The main results of present analysis are listed below.

- Effects of  $\beta_1$  and  $\beta_2$  have opposite behavior for velocity, temperature and nanoparticle volume concentration. These phenomena only occur due to the effects of viscoelastic parameters  $\beta_1$  and  $\beta_2$ .
- Both temperature and nanoparticle volume concentration give same behavior for  $Pr$  and  $Le$ . Since  $Pr$  is the ratio of kinematic to dynamic viscosity, therefore for higher values of

$Pr$ , the temperature profile remains under control.

- Effects of  $Nb$  and  $Nt$  for temperature profile are similar where Both  $Nb$  and  $Nt$  enhance the temperature.
- Effects of  $Nb$  and  $Nt$  for nanoparticle volume concentration are opposite.
- The magnitude of the reduced Nusselt numbers decreases for higher values of  $Nb$ .
- The magnitude of the reduced Sherwood numbers increases for higher values of  $Nb$ .

## Bibliography

- [1] S.U.S. Choi, Nanofluids: from vision to reality through research, *J. Heat Transfer*, 131(033106), 1-9 (2009).
- [2] S.U.S. Choi, Enhancing thermal conductivity of fluids with nanoparticles, *International Mechanical Engineering Congress and Exposition*, San Francisco, USA, ASME, FED 231/MD, 66, 99-105 (1995).
- [3] L. Cheng, Nanofluid heat transfer technologies, *Recent Patents on Engineering*, 3, 1-7 (2009).
- [4] Elena V. Timofeeva, J. L. Routbort, D. Singh, Particle shape effects on Thermophysical properties of alumina nanofluids, *Journal of Applied Physics* , 106(1), 014304-10 (2009).
- [5] S. M. Sohel Murshed, C.A. Nieto de Castro, M.J.V. Lourenço, M.L.M. Lopes, F.J.V. Santos, A review of boiling and convective heat transfer with nanofluids, *Renewable and Sustainable Energy Reviews*, 15(5), 2342-2354 (2011).
- [6] J. C. Maxwell, *Electricity and magnetism*, 3rd edn. Clarendon, Oxford, (1904).
- [7] R. L. Hamilton, O. K. Crosser, Thermal conductivity of heterogeneous two-component systems. *Ind Eng Chem Fund*, 1(3), 187–191 (1962).
- [8] D. J. Jeffrey, Conduction through a random suspension of spheres. *Proc Roy Soc Lond Ser A Math Phys Sci* 335, 355–367 (1973).
- [9] R. Davis, The effective thermal conductivity of a composite material with spherical inclusions. *Inter J. Thermophys*, 7, 609–620 (1986).
- [10] Q. Xue, Model for thermal conductivity of carbon nanotube based composites. *Phys B: Condens Matter* 368, 302–307 (2005).

- [11] J. Buongiorno, Convective transport in nanofluids, *ASME J. Heat Transfer* 128, 240–250 (2006).
- [12] B. C. Sakiadis, Boundary-layer behavior on continuous solid surface: I Boundary-layer equations for two-dimensional and axisymmetric flow, *Journal American Institute of Chemical Engineers*, 7, 26-28 (1961).
- [13] F.K. Tsou, E.M. Sparrow, R.J. Goldstein, Flow and heat transfer in the boundary layer on a continuous moving surface, *Int. J. Heat Mass Transfer*, 10, 219-235 (1967).
- [14] L. Crane, Flow past a stretching plate, *Zeitschrift für Angewandte Mathematik und Physik*, 21, 645-647 (1970).
- [15] C. Y. Wang, The three-dimensional flow due to a stretching flat surface, *Physics of Fluids*, 27 (8), 1915–1917 (1984).
- [16] E. M. A. Elbasha, Heat transfer over an exponentially stretching continuous surface with suction, *Arch Mech*, 53, 643-651 (2001).
- [17] S. K. Khan, M. S. Abel and R. M. Sonth, Viscoelastic MHD flow heat and mass transfer over a stretching sheet with dissipation of energy and stress work. *Heat and Mass Transfer*, 40, 47-57 (2004).
- [18] K. Ahmad, R. Nazar, Magnetohydrodynamic three dimensional flow and heat transfer over a stretching surface in a viscoelastic fluid, *Journal of science and technology*, 3 (1), (2011).
- [19] E. Magyari, B. Keller, Heat and mass transfer in the boundary layers on an exponentially stretching continuous surface, *J. Phys. D: Appl. Phys.*, 32, 577-585 (1999).

- [20] C. Liu, Hung-H. Wang, Yih-F. Peng, Flow and heat transfer for three-Dimensional flow over an exponentially stretching surface, *Chemical Engineering Communications*, 200, 253-268 (2013).
- [21] M. Nakamura and T. Sawada, Numerical study on the flow of a non-Newtonian fluid through an axisymmetric stenosis, *ASME J. Biomechanical Eng*, 110, 137–143 (1988).
- [22] P.D. Weidman, D.G. Kubitschek, A.M.J. Davis, The effect of transpiration on self-similar boundary layer flow over moving surfaces, *Int. J. Eng. Sci.*, 44, 730-737 (2006).
- [23] A. Postelnicu, I. Pop, FalknerSkam boundary layer flow of a power-law fluid past a stretching wedge, *Appl. Math. Comp*, 217, 4359-4368 (2011).
- [24] B. Bidin, R. Nazar. Numerical solution of the boundary layer flow over an exponentially stretching sheet with thermal radiation, *Eurp. J. Scie.* 33, 710-717 (2009).
- [25] A. Aziz, Hydrodynamic and thermal slip flow boundary layers over a flat plate with constant heat flux boundary condition, *Commun. Nonlinear Sci. Numer. Simulat*, 15, 573-580 (2010).
- [26] A. Ishak, R. Nazar, I. Pop, Heat transfer over an unsteady stretching permeable surface with prescribed wall temperature, *Nonlinear Anal. RWA*, 10, 2909-2913 (2009).
- [27] S. Nadeem, Rizwan Ul Haq, Noreen Sher Akbar, Z.H. Khan, MHD three-dimensional Casson fluid flow past a porous linearly stretching sheet, *Alexandria Engineering Journal*, 52(4), 577-582 (2013).
- [28] N. F. M. Noor, Analysis for MHD flow of a Maxwell fluid past a vertical stretching sheet in the presence of thermophoresis and chemical reaction. *World Acad Sci Eng Technol*, 64, (2012).
- [29] C. Y. Wang, Free convection on a vertical stretching surface. *J Appl Math Mech (ZAMM)*, 69, 418–420 (1989).

- [30] P. D. Ariel, T. Hayat, S. Asghar, Homotopy Perturbation Method and Axisymmetric Flow over a Stretching Sheet, *International Journal of Nonlinear Sciences and Numerical Simulation*, 7(4), 399-406 (2006).
- [31] K. Khanafer, K. Vafai, M. Lightstone, Buoyancy-driven heat transfer enhancement in a two-dimensional enclosure utilizing nanofluids, *Int. J. of Heat and Mass Transfer*. 46, 3639-3653 (2003).
- [32] D.A. Nield and A.V. Kuznetsov, The Cheng--Minkowycz problem for natural convective boundary-layer flow in a porous medium saturated by a nanofluid, *Int. J. of Heat and Mass Transfer*. 52, 5792-5795 (2009).
- [33] A.V. Kuznetsov, D.A. Nield, Natural convective boundary-layer flow of a nanofluid past a vertical plate, *Int. J. of Therm. Sci.* 49, 243-247 (2010).
- [34] W. A. Khan, I. Pop, Boundary-layer flow of a nanofluid past a stretching sheet, *International Journal of Heat and Mass Transfer*, 53, 2477-2483 (2010).
- [35] O. D. Makinde, A. Aziz, Boundary layer flow of a nanofluid past a stretching sheet with a convective boundary condition, 50(7), 1326-1332 (2011).
- [36] S. Nadeem, C. Lee, Boundary layer flow of nanofluid over an exponentially stretching surface, *Nanoscale Research Letters*, 94, 7(1) (2012).
- [37] W. Khan, Z. Khan, M. Rahi, Fluid flow and heat transfer of carbon nanotubes along a flat plate with Navier slip boundary, *Applied Nano science*, 4(5), 633-641, (2014).
- [38] W. A. Khan, Aziz A, Natural convection flow of a nanofluid over a vertical plate with uniform surface heat flux, *Int. J. of Ther. Sci.* 50, 1207-1214 (2011).

- [39] W. Yu, D. M. France, J. L. Routbort, Stephen U. S. Choi, Review and Comparison of Nanofluid Thermal Conductivity and Heat Transfer Enhancements, *Heat Transfer Engineering*, 29(5), 432–460, (2008).
- [40] O. D. Makinde, Analysis of Sakiadis flow of nanofluids with viscous dissipation and Newtonian heating. *Appl Math and Mech, Eng Edi*, 33(12), 1545-1554 (2012).
- [41] T. G. Motsumi, O. D. Makinde, Effects of thermal radiation and viscous dissipation on boundary layer flow of nanofluids over a permeable moving flat plate. *Phy. Scr*, 86, 045003(8pp) (2012).
- [42] A. V. Kuznetsov, D. A. Nield, Double-diffusive natural convective boundary-layer flow of a nanofluid past a vertical plate, 50; 712-717 (2011).
- [43] N. Bachok, A. Ishak, I. Pop, Unsteady boundary-layer flow and heat transfer of a nanofluid over a permeable stretching/shrinking sheet, *International Journal of Heat and Mass Transfer*, 55(7–8), 2102-2109 (2012).
- [44] N. Bachok, A. Ishak, I. Pop, The boundary layers of an unsteady stagnation-point flow in a nanofluid, *International Journal of Heat and Mass Transfer*, 55(23–24), 6499-6505 (2012).
- [45] N. Bachok, A. Ishak, I. Pop, Boundary layer stagnation-point flow and heat transfer over an exponentially stretching /shrinking sheet in a nanofluid, *International Journal of Heat and Mass Transfer*, 55 (25-26), 8122-8128 (2012).
- [46] A. Malvandi, F. Hedayati, G. Domairry, Stagnation point flow of a nanofluid toward an exponentially stretching sheet with non-uniform heat generation/absorption, *Journal of Thermodynamics*, 2013, ID. 764827, 12 (2013).

- [47] K. Bhattacharyya, G. C. Layek, Magnetohydrodynamic Boundary Layer Flow of Nanofluid over an Exponentially Stretching Permeable Sheet, Volume 2014 (2014), Article ID 592536, pages 12.
- [48] X. Q. Wang, A. S. Mujumdar, Heat transfer characteristics of nanofluids: a review, *International Journal of Thermal Sciences*, 46(1), 1-19 (2007).
- [49] S. Kakaç, A. Pramuanjaroenkij, Review of convective heat transfer enhancement with nanofluids, *International Journal of Heat and Mass Transfer*, 52(13-14), 3187-3196 (2009).
- [50] D. Wen, G. Lin, S. Vafaei, K. Zhang, Review of nanofluids for heat transfer applications, *Particuology*, 7(2), 141-150 (2009).
- [51] T. Na, *Computational Methods in Engineering Boundary Value Problem*, Academic Press, (1974).
- [52] T. Cebeci, P. Bradshaw, *Physical and computational aspects of convective heat transfer*, Springer-Verlag, (1986).
- [53] T. Cebeci, J. Cousteix, *Modeling and Computation of Boundary-Layer Flows: Laminar, Turbulent and Transitional Boundary Layers in Incompressible and Compressible Flows*, Springer-Verlag, (2005).
- [54] H. Keller, T. Cebeci, Accurate numerical methods for boundary layer flows in two dimensional laminar flows, in: *Proceedings of the Second International Conference on Numerical Methods in Fluid Dynamics*, Vol. 8 of *Lecture Notes in Physics*, Springer Berlin Heidelberg, 92-100, (1971).
- [55] Shampine LF, Reichelt MW, Kierzenka J, Solving boundary value problems for ordinary differential equations in MATLAB using bvp4c. Available at <[http://www.mathworks.com/bvp\\_tutorial](http://www.mathworks.com/bvp_tutorial)>.



- [56] L. F. Shampine, I. Gladwell, S. Thompson, Solving ODEs with MATLAB, Cambridge: Cambridge University Press, (2003).
- [57] P. Amodio, J.R. Cash, G. Roussos, R.W. Wright, G. Fairweather, I. Gladwell, G.L. Kraut and M. Paprzycki, Almost block diagonal linear systems: sequential and parallel solution techniques, and applications, Numer. Lin. Algebra Applics. 7, 275-315 (2000).
- [58] U.M. Ascher, R.M.M. Mattheij, R.D. Russell, Numerical Solution of Boundary Value Problems for Ordinary Differential Equations, SIAM Classics in Applied Mathematics 13, SIAM, Philadelphia, PA, (1995).
- [59] U.M. Ascher and L.R. Petzold, Computer Methods for Ordinary Differential Equations and Differential Algebraic Equations, SIAM, Philadelphia, PA, (1996).
- [60] S.R. Bernfeld and V. Lakshmikantham, An Introduction to Nonlinear Boundary Value Problems, Mathematics in Science and Engineering 109, Academic Press, New York, NY, (1974).